Finite Element Analysis of Impregnated Diamond Drilling Bits

Jiayi Xu

Thesis submitted in fulfilment of the requirements for the degree of Doctor of Philosophy

School of Civil, Environmental and Mining Engineering
Faculty of Engineering, Computer and Mathematical Sciences
The University of Adelaide

Dedication

This work is dedicated to my beloved parents.

Finite Element Analysis of Impregnated Diamond Drilling Bits

By:

Jiayi Xu

Supervised by:

Associate Professor Abdul Sheikh, *Ph.D.,*
School of Civil, Environmental & Mining Engineering,
The University of Adelaide

Associate Professor Chaoshui Xu, *Ph.D.,*
School of Civil, Environmental & Mining Engineering,
The University of Adelaide

Thesis submitted in fulfilment of the requirements for the degree of
Doctor of Philosophy

School of Civil, Environmental & Mining Engineering
Faculty of Engineering, Computer and Mathematical Sciences
The University of Adelaide
North Terrace, Adelaide, SA 5005, Australia
Tel: +61(8) 8303 4323
Fax: +61(8) 8303 4359
Email: jiayi.xu@adelaide.edu.au, nicyxjy@hotmail.com

Abstract

Diamond, including its synthesis, is a unique material not just because of its rarity and decorative features. Some of its physical properties are exceptional, which can not easily be matched by other materials. It is the hardest material, measured at 10 Mohs on the Mohs scale of mineral hardness. It has the highest thermal conductivity at room temperature, the highest bulk modulus and the highest tensile strength for cleavage. It has low coefficients of friction and thermal expansion, and is relatively inert to chemical attack by common acids and bases. Due to these exceptional properties, synthetic diamond as an abrasive has been used as an advanced engineering material, in making tools for grinding, cutting and drilling purposes. Synthetic diamond is commonly used in impregnated drills for cutting purposes.

For bit design and manufacturing purposes, it is important to fully understand the complex interactions between rocks and diamond bits, as well as the mechanical behaviour of diamond particles within the impregnated bit during the drilling process. Major current issues of impregnated diamond tools include premature failure of diamonds, the ineffective wear rate of the matrix to continuously expose fresh diamonds and premature diamond fall out. Published researches to date include both experimental studies and numerical modellings for performance assessments and improvement. Some experimental studies have identified different failure mechanisms of the diamond particles and have studied the wear rate of the matrix under different drilling parameters, such as torque, reactive load and penetration rates. Others have tested suitable combinations of metals for the production of different matrix composites for different drilling purposes. It is well understood that in order to achieve optimal cutting efficiency during service, the matrix and diamond must wear simultaneously such that fresh diamonds will expose themselves after worn diamonds have fallen out of the matrix. It has been found that diamonds are mostly held by the matrix through mechanical interlocking, which in general has low interfacial bond strength. Some

research have been conducted to investigate the effects of metal-coating diamonds in an attempt to provide sufficiently high bond strength between diamond particles and the matrix and at the same time to ensure the bonds are weak enough so that the self-dressing capability of the drill bits can be achieved. Numerical models have been used to investigate the effects of the variation of stresses at the interface under different wear conditions. The local plastic deformation and residual stresses due to the sintering process have also been studied through numerical simulations.

In this research, the finite element method (FEM) is employed to investigate the interface failure mechanism of impregnated diamond bits, which is essentially an interface de-bonding process between diamond particles and the matrix, termed the diamond particle fallout. In particular, the cohesive zone modelling (CZM) technique is implemented to simulate the crack initiation and propagation along the interface. The extended finite element method (XFEM) is used to predict fractures in the matrix under certain loading conditions.

The thesis is divided into five chapters, which are described briefly below:

In Chapter 1, the general background together with the objectives and originality of the present research are introduced.

In Chapter 2, a two-dimensional micromechanical finite element model of diamond impregnated bits suitable for the simulation of interfacial failure between diamond particles and the metal matrix are presented. The surface based cohesive zone model (CZM) is an advanced and efficient technique that is able to adequately simulate and predict fracture initiation and propagation of an uncracked interface between two adhesive surfaces. Two numerical examples have been developed to validate the accuracy and adequacy of the presented model. The effects of different modelling parameters on the diamond particle retention capacity have also been thoroughly studied and compared in order to have a better understanding of the failure mechanism.

Chapter 3 describes the extension of the two-dimensional FE model to three-dimensional analysis. Similar to two-dimensional models, a model representing a single diamond particle partially embedded inside the matrix has been developed. A three-dimensional double cantilever beam (DCB) testing model has been created to simulate the crack propagation along the interface, and its results have been compared with the experimental results to validate the precision of the model. The effects of diamond particle shape, orientation, and protrusion, as well as interface properties on the diamond's retention ability, have also been studied.

Chapter 4 presents an efficient two-dimensional FE model incorporating both the cohesive zone method (CZM) and the extended finite element method (XFEM) for the prediction of de-bonding along interfaces and micro-cracking in the matrix. The effects of interface property, as well as the particle shape on failure modes, have also been investigated.

Finally, the conclusions of the present research are summarised in Chapter 5. The limitations of the present study and further research recommendations are also described in this chapter.

Statement of Originality

I, **Jiayi Xu**, hereby declare that this work contains no material which has been accepted for the award of any other degree or diploma in any university or other tertiary institution in my name and, to the best of my knowledge and belief, contains no material previously published or written by another person, except where due reference has been made in the text. In addition, I certify that no part of this work will, in the future, be used in a submission in my name, for any other degree or diploma in any university or other tertiary institution without the prior approval of the University of Adelaide and, where applicable, any partner institution responsible for the joint award of this degree.

I give consent to this copy of my thesis when deposited in the University Library, being made available for loan and photocopying, subject to the provisions of the Copyright Act 1968.

The author acknowledges that copyright of published works contained within this thesis resides with the copyright holder(s) of those works.

I also give permission for the digital version of my thesis being made available on the web, via the University's digital research repository, the Library catalogue, the Australian Digital Thesis Program (ADTP) and also through web search engines, unless permission has been granted by the University to restrict access for a period of time.

Signed: ……Date: ……..

Acknowledgments

This thesis marks a milestone on the road to research that was made possible via the collaboration and support of various persons, to whom I would like to express my gratitude. Many of them have accompanied and helped me in some way or the other when I was working on my project. Without their support and encouragement, the present thesis would not be possible.

First of all, I would like to express my gratitude to my principle supervisor Associate Professor Abdul Hamid Sheikh and my co-supervisor Associate Professor Chaoshui Xu who offered me the opportunity to obtain financial support from the Deep Exploration Technologies Cooperative Research Centre (DET CRC) at the University of Adelaide. My gratitude also goes to my supervisors for their supervision, comments and feedback throughout my period of study.

The financial support from the Deep Exploration Technologies CRC and the University of Adelaide are also greatly appreciated. The work has been supported by the Deep Exploration Technologies Cooperative Research Centre, whose activities are funded by the Australian Government's Cooperative Research Centre Programme. This is DET CRC Document 2016/897.

I am highly indebted to those, who have helped me in all aspects of this research and made my time in Adelaide unforgettable. I deeply and sincerely appreciate the help of Dr Chen Liang, Dr Liang Huang, Dr Xian Qun He and Dr Kiana Kashefiwho offered their ideas and showed patience when listening to my complaints during times of frustration. Their companionship was a memorable part of my life at the University of Adelaide.

Finally, I would like to express my sincerest gratitude to my beloved parents, Han Qin Xu and Yan Ping Gu, who have been trying their best to support my life and study in Adelaide all the time without requiring any return. I certainly

would not have been able to reach where I am standing now without their constant support and love throughout my life.

Table of Contents

List of Tables

List of Figures

Chapter 1

Introduction

1.1 Background

Diamonds are widely used in multiple divisions and have become one of the most valuable raw materials in the world, not only due to their rarity and decorative merit but also due to the material's exceptional physical characteristics, which are irreplaceable by any other materials. The most important and critical characteristic of a diamond is that it is the hardest natural material known to man: on the Mohs scale of mineral hardness it obtains 10 Mohs (the highest value), due to the strong sp3 directional bonding of diamonds. Apart from that, diamonds also have the highest thermal conductivity at room temperature, the highest bulk modulus and the highest critical tensile stress for cleavage (Robertson, 1992). Moreover, they have very low coefficients of friction and thermal expansion, and they are relatively inert to chemical attack by common acids and bases (Konstanty, 2005a). Due to the exceptional characteristics mentioned above and the latest progress in diamond synthesis, diamond abrasives have been used extensively as an advanced engineering material; in making tools for grinding, cutting and drilling purposes. It is always challenging and desirable work for designers and manufacturers to optimise the working efficiency and performance of diamond tools.

Although the first use of a diamond as a cutting or engraving tool can be traced back to 350 BC (Hughes, 1980), the first modern applications for diamond tools can be traced back about a century. The first milestone in the history of the development of diamond tools was the invention of a diamond

wire-drawing die by Brackendon in England. It was successfully fabricated and utilised by Milan and Balloffet in France (1980). Meanwhile, shaped diamond wheels were created by Pritchard and were used for grinding and polishing microscope lenses (Hughes, 1978; Tolansky, 1967). Later on, Hermann, a French engineer, started to use a single-crystal diamond tool for cutting, turning and shaping hard rocks and stones (Hughes, 1980). The idea of bonding diamond particles by means of metal powders can be traced back to 1883 when traditional abrasives, such as quartz or emery, were incorporated into a metal matrix (Jones, 1960). The earliest diamond grit impregnated tools, which are made with a mixture of diamond grits and powder metallurgy, were first introduced into the USA in the 1920s and 1930s, achieving further progress in the history of tool production (Jones, 1960). Consequently, diamond-impregnated tools were introduced into industrial application in the 1940s (Hughes, 1980). The developments in diamond tools were relatively slow before the early 1950s because only mined diamond crystals were available. Therefore the cost of the diamond tools was very high and it was impracticable for industry to process large quantity production at that time. However, since the invention of synthetic diamonds in the 1950s, industry has developed the capability to manufacture synthetic diamonds on an industrial scale, so developments in diamond tool manufacturing technology have grown at a faster rate than ever before. Thus, synthetic diamonds have been increasingly used as impregnated diamond tools for drilling, grinding, sawing and similar activities with hard materials such as rock, concrete, metal and glass. Nowadays, synthetic diamonds account for more than 95% of the diamond consumption in all industries (Konstanty, 2005a). Over the last five decades, due to the implementation of modern production techniques based on synthetic diamond tools, the cost of diamond-based industrial activities has become lower and the efficiency of the jobs has been improved significantly. Machinery and processing techniques in the stone and construction industries, road repair, petroleum and mining explorations, woodworking and the production of various parts and components made of glass, ceramics, metals and so forth, have also been revolutionized with the advent of low-cost, high-quality synthetic diamonds.

In the mining industry, one of the most significant challenges worldwide is to explore new underground resources that can be mined over the next few decades. Because of the previous mining developments and activities based on low-efficiency drilling techniques, the vast majority of existing mines are located where mineralised basement rocks are outcropping or shallow. Inevitably, however, those accessible surface resources and existing shallow mines have become depleted and therefore more cost-effective and more efficient drilling technologies are required to drill deeper holes to explore new, deeper mineral deposits. This investigation focuses on the diamond impregnated drilling bit, which is one type of the many diamond tools available that have been widely used in mining and geological exploration drilling.

Understanding the mechanics of the diamond drilling bit during its operation and developing a realistic modelling tool are extremely important for drilling bit design and drilling optimisation. When operations are forced to mine from deeper locations, the radical deterioration of drilling conditions due to the extreme depth gives rise to deficiencies in understanding of both the drilling mechanism itself and the optimisation of the drilling operation. The problem is further compounded by an inability to observe the drilling process meaningfully and the failures in the bits themselves, in real time. The key to the successful characterization of the drilling process for a whole diamond bit lies with a better understanding of bit failure under the bit-rock interaction mechanism.

In diamond core drilling, the bit rotates in a constant direction at a certain speed, with its active part remaining in contact with the workpiece material. The impregnated diamond bits, commonly used in the mineral exploration industry for drilling hard rocks, consist of large numbers of diamond grits, having a size of the order of 100 microns, which are thoroughly mixed with metal powders. The mixture is processed under high temperature and pressure, known as the sintering process, to form solid drill bits. The majority of previous efforts to understand the processes involved in using such bits have

focused on describing the interaction between the bits and the rocks, using theoretical analysis, experimental tests and numerical simulations.

Diamond impregnated bits are in practice made from a particulate composite material, where the metals act as the matrix for binding the diamond particles which are randomly distributed within the composite material. The basic functions of the metallic matrix are to hold the diamond particles firmly prior to them losing their cutting ability, in order to prevent premature diamond fall off and to induce wear at a rate compatible with the diamond loss. Moreover, the wear resistance of the matrix has to correspond with the abrasiveness of the workpiece material. If the matrix is too soft it will wear much faster than the diamond, which results in the premature fall out of the diamond. On the other hand, an extremely wear-resistant matrix could lead to the phenomenon called *glazing* which polishes the cutting segment surface until it eventually loses its cutting ability. To date, cobalt alloy has been the most widely used base matrix material for diamond impregnated bits due to its high yield strength, toughness and adequate resistance to abrasive wear, as well as its relatively low temperature and pressure requirements for consolidation (Konstanty & Bunsch, 1991; Konstanty, Bunsch, & Cias, 1991). Nevertheless, an extensive, market-oriented study on novel powders was triggered by the move to substitute cobalt with suitable alternatives due to its unstable price and high toxicity to the environment (Howkins, 2003; Spriano, Chen, Settineri, & Bugliosi, 2005). Therefore, other metal alloys began to be used as base matrix materials. The materials now commonly used for this metallic matrix include copper, tin, tungsten, and nickel due to their optimal mechanical and thermal properties (Hsieh & Lin, 2001; Lin, Yang, & Lin, 2008).

According to the previous research (Konstanty, 2005c), the matrix retention capacity of diamond particles is a complex, system-dependent property. The complexity of impregnated diamond drills become evident when designing the matrix as it must retain the diamond in such a way that they are neither pulled out, pushed in deeper, nor moved around while the tool is in operation (Sun, Pan, & Lin, 2002). In order to prevent the "glazing" phenomenon, it is

necessary to ensure that the metallic matrix wears relatively faster than the diamond grits in order to optimise the rate of diamond exposure (Sun et al., 2002). Moreover, diamonds are mostly held by the matrix through mechanical interlocking, which gives a low interfacial bonding strength (Hu, Chou, & Thompson, 2008). Consequently, therefore, insufficient retention capabilities could be introduced and which could result in the most undesirable failure mode, the premature fall out of the diamond. In order to improve the retention capacity of diamonds, a great deal of effort has been made to establish a strong bond between the matrix and diamonds by means of supportive chemical bonding. This can be achieved by using alloys that can react with the carbon atoms in the diamond to form metal-carbide elements at the interface (Scott, Nicholas, & Dewar, 1975). However, some of these alloys may melt at the hot pressing temperature, to wet and flow over the diamond particles and a continuous interfacial layer could be formed due to the concentration of the reactive elements. As the growth of carbide-forming elements reaches a critical point, the interface strength may become weak if it continues to increase in thickness and severe diamond surface degradation is often observed due to the formation of carbide layers which are too thick (Levin & Gutmanas, 1990). Due to the technical problems, the manufacturers cannot prevent surface degradation if they include the most strongly bonding alloys as matrix materials. Thus, for the above reasons, the recent trend is towards using metal-coated diamonds rather than chemically reactive matrices to improve the matrix retention ability of the diamond particles. A study conducted by Wang et al. (2002) indicates that the metal-coated diamond grits can not only protect the diamond from oxidisation, but also increase its retention ability after coating. Tungsten has been widely used as a coating material for diamond grits, and it leads to the formation of a thin film of tungsten carbide at the interface that acts as a strong chemical bond between the matrix and the diamonds (Konstanty, 2005b). Along with using tungsten as a coating metal, diamonds are also used with some other metals through systems such as Ti-coating, which significantly improves the interfacial bonding strength (Lin et al., 2008).

Initially, some experimental studies by Miller et al. (1990) and Xuefeng et al. (1994) on impregnated diamond bits have been conducted where the wear mechanisms of these bits have been thoroughly investigated. In these studies, the failure or wear modes have also been classified into four distinct types where the diamond pull out is one of these failure modes, which has made an importance contribution to improving the efficiency of these bits. At that time, the only way to determine the characteristics of local fractures at the contacting bit and rock surfaces was to use an optical microscope and a scanning electron microscope. However, the fracture status inside the bit could not be observed through the experimental tests. In terms of numerical simulations, preliminary studies of diamond impregnated bits using FEM were first attempted by Zhou et al. (1997) where two-dimensional linear/elastic material properties were assumed in the analysis of a single diamond, along with a portion of the surrounding matrix, taking perfect interfacial bonding between the matrix and diamond. This could be defined as the first micromechanical modelling of the bits, where the diamond is subjected to a horizontal cutting force at its tip. The researchers plotted the variations of normal stress distributions along the interface for different wear situations. A similar two-dimensional FE study was conducted by Suh et al. (2008) for a diamond impregnated grinding wheel, where they calculated the von Mises stress along the interface instead of normal stress. Moreover, different wear conditions, such as symmetrical, asymmetrical matrix wear and particle wear were also considered in Suh's study for comparison purposes. In a more updated but slightly different study, Li et al. (2010) tried to predict the permanent plastic deformation and residual stresses produced within the matrix near the diamond particle due to the sintering process, using three-dimensional plasticity-based finite element simulation of the micromechanical model. Another recent three-dimensional numerical simulation study conducted by Romanski (2010) has tried to explore the effects of principal factors which have an influence on potential diamond retention capacity in diamond impregnated tools. In that research (Romanski, 2010), the effects of Young's modulus and the yield strength of the matrix, as well as the friction between the diamond and the matrix on the energies of the plastic and elastic

deformation of the matrix, were analysed. The obtained results indicate that the yield strength is the dominant parameter for the diamond retention capability, whereas the other two factors are of secondary importance. As we can see from the previous FE modelling on diamond impregnated bits, to date, no one has investigated modelling of the interface failure of this system, which can predict the diamond pull out process more realistically. Most of the researches have been developed for pure stress and strain analysis of the impregnated diamond bits under specific loading conditions. In practice, this research, therefore, focuses on interfacial crack initiation and its propagation which is a complex process, however, a proper modelling of the full process is extremely important to have a better understanding of and designs for such diamond tools.

1.2 Research objectives

An extensive review of the literature allowed key areas of research on impregnated diamond tools to be identified. These include areas that have yet to be studied in-depth, or could be better analysed with the use of contemporary modelling techniques. The literature revealed a lack of comprehensive modelling on the wear mechanism of impregnated diamond drills. In order to overcome the difficulties with the design of impregnated diamond drilling bits, the underlying objective of the present study is to develop an effective and efficient numerical model to simulate the stress and strain behaviour in the diamond bits, and to predict the failure mechanism of the diamond impregnated tools. The developed model can also be refined further subsequently in order to analyse different diamond impregnated segments, such as different diamond shapes, sizes, protrusions and matrix properties. It is expected that the proposed numerical model could simulate the failure process of the diamond bits efficiently by incorporating the cohesive zone method and the extended finite element method in the finite element models. It is also expected that the numerical model for the diamond impregnated bits could fully consider the effects of all the design variables efficiently.

Micromechanical modelling of diamond particle debonding (fall out) in impregnated diamond segments was first achieved in two-dimensional models by incorporating the cohesive zone method in the FE analysis, identifying the key factors that influence the retention ability of diamond particles. Furthermore, a three-dimensional micromechanical model of a portion of the impregnated diamond bit has been developed to simulate diamond particle fallout failure under more realistic conditions. The factors that can affect the retention ability of diamond particles have been studied and identified. Lastly, the extended finite element method has been incorporated into the FE model to simulate crack initiation and propagation in the metal matrix under drilling conditions.

It should be noted that the proposed numerical model for the diamond impregnated drilling bits can be substantially consolidated to achieve more realistic and accurate results by incorporating the real operating parameters and material properties of diamond, matrix and interface of a specific drilling bit.

1.3 Thesis overview

This thesis consists of five chapters and is in the format of a thesis by publication. In addition to the Introduction in Chapter 1, Chapters 2, 3 and 4 are the kernel of this thesis and they present the research contributions and outcomes, which are reported and prepared for academic journals. The titles of these three papers and the corresponding brief summaries are as follows:

Paper 1 (Chapter 2): Interfacial failure modelling of diamond bits made of particulate composites

Chapter 2 develops an efficient and accurate failure mechanism analysis of a diamond impregnated drill bit using the finite element and cohesive zone methods to model the diamond particle embedded in the metal matrix and its

fall out failure under certain loading conditions. The numerical models developed in this paper are all in two-dimensional. 4-node bilinear plane strain quadrilateral elements have been used for the modelling of the diamond particle and metal matrix. The interface adhesion force is simulated by the incorporation of the cohesive zone method, which is the tool most commonly used to investigate the interfacial failure. Several numerical examples are first analysed by the proposed finite element model to assess its performance and this shows that the accuracy of proposed model is quite satisfactory. Parametric studies are presented to indicate the effect of the diamonds' shape, orientation, protrusion and interface parameters on the critical load to initiate interface failure (fall-out of the diamond particle) of diamond impregnated bit. The obtained results indicate that all these parameters have a significant influence on the particle retention capacity of the tool.

Paper 2 (Chapter 3): 3D-modelling of interfacial failure of diamond impregnated drill bits based on a micromechanical model

Chapter 3 presents numerical simulations of the diamond de-bonding analysis of diamond impregnated drill bits using the finite element method incorporated with the cohesive method in three dimensions. Two example experimental problems, double cantilever beam (DCB) and mixed-mode bending (MMB) tests have been taken and simulated to validate the finite element model by comparing the simulated results with the experimental results. Surface-based cohesive behaviour has been incorporated into the finite element model to simulate interface fracture initiation, as well as fracture propagation. The cohesive zone modelling (CZM) is based on linear softening traction-separation law. Parametric studies are undertaken to investigate the effect of various features that can influence the retention capacity of the diamond particles. These include the diamonds' shapes, orientations and load directions, as well as different interface properties. It is worth noting that the present model is capable of being further extended to help to simulate any type of diamond tool, thereby enabling manufacturers to improve the design of these tools also.

Paper 3 (Chapter 4): FE simulation of matrix crack and interface debonding of diamond impregnated drill bits - In two dimensions.

Chapter 4 proposes a novel computational methodology for predicting fractures in a metal matrix and interface delamination of impregnated diamond drill bits. A micromechanical finite element model (FEM), in two-dimensions, of a single diamond particle partially embedded inside a metal matrix is developed to simulate microcrack initiation and propagation in the metal matrix and diamond matrix interface, debonding simultaneously by using the extended finite element method (XFEM) and cohesive zone method (CZM) respectively. The developed model has been applied to examine the interface material property effect on the diamond particles' retention ability and failure modes during cutting and the diamond shape's effects on the critical load to initiate failure for different modes. The interface failure mode will always occur first when the property of the interface is assumed to be the same as the matrix property, irrespective of the shape of the diamond particle. Increasing the interface strength will raise the critical load for interface delamination, but the failure mode will be changed into *matrix crack* when the interface strength exceeds a certain value. For the interface failure mode, as can be seen from the studies of different diamond shapes, the hexagon shaped diamond has the highest retention ability, where the square and pentagon shaped particles have the lowest retention capacity. When the strength of the interface has been increased to a certain high value, the matrix crack starts to occur. Similar to the interface failure, the square shaped diamond requires the lowest load to initiate matrix failure, whereas the decagon shaped diamond requires the highest critical load.

Chapter 5 summarises the main contributions and conclusions of this thesis. Additionally, the limitations of this research are discussed, as well as potential future related work.

References for Chapter 1

HOWKINS, M. 2003. Trends in the supply and demand for cobalt. *Cobalt News*, 10-14.

HSIEH, Y.-Z. & LIN, S.-T. 2001. Diamond tool bits with iron alloys as the binding matrices. *Materials Chemistry and Physics,* 72, 121-125.

HU, J., CHOU, Y. K. & THOMPSON, R. G. 2008. Cohesive zone effects on coating failure evaluations of diamond-coated tools. *Surface and Coatings Technology,* 203, 730-735.

HUGHES, F. 1978. Diamond Grinding of Metals. *Industrial Diamond Information Bureau*, 1-3.

HUGHES, F. H. 1980. The early history of diamond tools. *Industrial Diamond Review,* 40, 405-407.

JONES, W. D. 1960. Fundamental Principles of Powder Metallurgy. *Edward Arnold Publishers Ltd.*, 807.

KONSTANTY, J. 2005a. Chapter 1 - Introduction. *In:* KONSTANTY, J. (ed.) *Powder Metallurgy Diamond Tools.* Amsterdam: Elsevier Science.

KONSTANTY, J. 2005b. Chapter 3 - Diamond tool design and composition. *In:* KONSTANTY, J. (ed.) *Powder Metallurgy Diamond Tools.* Amsterdam: Elsevier Science.

KONSTANTY, J. 2005c. Chapter 6 - Mechanical properties of the matrix. *In:* KONSTANTY, J. (ed.) *Powder Metallurgy Diamond Tools.* Amsterdam: Elsevier Science.

KONSTANTY, J. & BUNSCH, A. 1991. Hot pressing of cobalt powders. *Powder Metallurgy,* 34, 195-198.

KONSTANTY, J., BUNSCH, A. & CIAS, A. 1991. Factors affecting hardness and ductility of hot-pressed cobalt powders. *Powder Metallurgy,* 23**,** 345-356.

LEVIN, E. & GUTMANAS, E. Y. 1990. Solid-state bonding of diamond to Nichrome and Co-20wt% W alloys. *Journal of Materials Science Letters,* 9**,** 726-730.

LI, B., AMARAL, P. M., REIS, L., ANJINHO, C. A., ROSA, L. G. & FREITAS, M. D. 2010. 3D-modelling of the local plastic deformation and residual stresses of PM diamond–metal matrix composites. *Computational Materials Science,* 47**,** 1023-1030.

LIN, C.-S., YANG, Y.-L. & LIN, S.-T. 2008. Performances of metal-bond diamond tools in grinding alumina. *Journal of Materials Processing Technology,* 201**,** 612-617.

MILLER, D. & BALL, A. 1990. Rock drilling with impregnated diamond microbits—An experimental study. *International Journal of Rock Mechanics and Mining Sciences & Geomechanics Abstracts,* 27**,** 363-371.

MILLER, D. & BALL, A. 1991. The wear of diamonds in impregnated diamond bit drilling. *Wear,* 141**,** 311-320.

ROBERTSON, J. 1992. Properties of diamond-like carbon. *Surface and Coatings Technology,* 50**,** 185-203.

ROMANSKI, A. 2010. Factors affecting diamond retention in powder metallurgy diamond tools. *Archives of Metallurgy and Materials,* 55**,** 1073-1081.

SCOTT, P. M., NICHOLAS, M. & DEWAR, B. 1975. The wetting and bonding of diamonds by copper-base binary alloys. *Journal of Materials Science,* 10**,** 1833-1840.

SPRIANO, S., CHEN, Q., SETTINERI, L. & BUGLIOSI, S. 2005. Low content and free cobalt matrixes for diamond tools. *Wear,* 259**,** 1190-1196.

SUH, C.-M., BAE, K.-S. & SUH, M.-S. 2008. Wear behavior of diamond wheel for grinding optical connector ferrule — FEA and wear test —. *Journal of Mechanical Science and Technology,* 22**,** 2009-2015.

SUN, L., PAN, J. & LIN, C. 2002. A new approach to improve the performance of diamond sawblades. *Materials Letters,* 57**,** 1010-1014.

TOLANSKY, S. 1967. Early historical uses of diamond tools. *Industrial Diamond Information Bureau, London,* 2**,** 341-349.

WANG, Y. H., ZANG, J. B., WANG, M. Z., GUAN, Y. & ZHENG, Y. Z. 2002. Properties and applications of Ti-coated diamond grits. *Journal of Materials Processing Technology,* 129**,** 369-372.

XUEFENG, T. & SHIFENG, T. 1994. The wear mechanisms of impregnated diamond bits. *Wear,* 177**,** 81-91.

ZHOU, Y., FUNKENBUSCH, P. D. & QUESNEL, D. J. 1997. Stress distributions at the abrasive-matrix interface during tool wear in bound abrasive grinding—a finite element analysis. *Wear,* 209**,** 247-254.

Chapter 2

Interfacial failure modelling of diamond bits made of particulate composites

(Journal Paper 1)

J. Xu, A.H. Sheikh and C. Xu

School of Civil, Environmental and Mining Engineering, the University of Adelaide, Australia

Publication:

J. Xu, A.H. Sheikh, C. Xu. (2016). Interfacial failure modelling of diamond bits made of particulate composites. *Composite Structures*, http://dx.doi.org/10.1016/j.compstruct.2016.07.075.

Statement of Authorship

Title of Paper	Interfacial failure modelling of diamond bits made of particulate composites
Publication Status	☑ Published ☐ Accepted for Publication ☐ Submitted for Publication ☐ Unpublished and Unsubmitted w ork w ritten in manuscript style
Publication Details	J. Xu, A.H. Sheikh, C. Xu. (2016). Interfacial failure modelling of diamond bits made of particulate composites. *Composite Structures*, http://dx.doi.org/10.1016/j.compstruct.2016.07.075.

Principal Author

Name of Principal Author (Candidate)	Jiayi Xu
Contribution to the Paper	Undertook literature review, developed analytic procedure and numerical models, performed analysis on different parameters and prepared manuscript.
Overall percentage (%)	80%
Certification:	This paper reports on original research I conducted during the period of my Higher Degree by Research candidature and is not subject to any obligations or contractual agreements with a third party that would constrain its inclusion in this thesis. I am the primary author of this paper.
Signature	Date 30/08/2016

Co-Author Contributions

By signing the Statement of Authorship, each author certifies that:

i. the candidate's stated contribution to the publication is accurate (as detailed above);

ii. permission is granted for the candidate in include the publication in the thesis; and

iii. the sum of all co-author contributions is equal to 100% less the candidate's stated contribution.

Name of Co-Author	Abdul Hamid Sheikh
Contribution to the Paper	Supervised development of numerical models, helped manuscript preparation, reviewed and corrected draft of the manuscript.
Signature	Date 30/8/2016

Name of Co-Author	Chaoshui Xu
Contribution to the Paper	Supervised development of work, helped to evaluate and edit the manuscript.
Signature	Date 10-09-2016

Please cut and paste additional co-author panels here as required.

Abstract

The failure analysis of diamond impregnated bits, which are found as particulate composite materials consist of diamond particles randomly distributed within a metal matrix, is conducted to study the pull out the behaviour of diamond grits for an assessment of diamond retention capacity of these drilling bits. The finite element technique is used to model the diamond-matrix system where a zero thickness surface based cohesive zone modelling technique is used to simulate the failure at the interface between the matrix and the diamond particle. For the validation of the model, few numerical examples are initially solved and the results produced by the model are compared with the published results which show a good performance of the model. Finally, a parametric study is conducted to show the effects of shapes, orientations and protrusions of diamond particles as well as interface properties on the retention capacity of diamond particles.

***Keywords*:**

Diamond impregnated bits; Particulate composite materials; Diamond pull out; Interface debonding; Cohesive zone modelling; Finite element modelling

2.1 Introduction

Since the invention of synthetic diamonds dated back to 1950s, these diamonds have been increasingly used as impregnated diamond tools for drilling, grinding, sawing and similar activities of hard materials such as rock, concrete, metal and glass. The popularity of diamond impregnated tools is due to various advantages such as low friction coefficient, high stiffness and thermal conductivity as well as high bulk modulus exhibited by these tools (Busch and Hill, 1975, Paone and Madson, 1966). The impregnated diamond bits are commonly used in the mineral exploration industry for drilling hard rocks. A segment of these bits is made with particulate composite material consist of large numbers of diamond particles having a size of the order of 100 microns which are evenly distributed within a metal matrix. The diamond grits are thoroughly mixed with metal powders and the mixture is processed under high temperature and pressure, known as a sintering process, to form these solid bit segments. The materials commonly used for this metal matrix are cobalt, copper, tin, tungsten, and nickel due to their optimal mechanical and thermal properties (Hsieh and Lin, 2001, Lin et al., 2008, Tze-Pin et al., 1992). During the drilling operation, when the cutting surface of the bit slides over a rock due to rotation of the bit, the embedded diamond particles near the cutting surface are partially exposed due to gradual wear of the matrix material and these exposed diamonds do the cutting or drilling of the rock. The matrix is expected to hold the freshly exposed sharp diamonds firmly and at the same time, it should wear at a rate compatible with that of diamonds so that the worn diamond can fall out to allow new diamonds to expose continuously (Xuefeng and Shifeng, 1994). This is one of the major advantages of impregnated diamond bits, which is known as their self-sharpening ability. The de-bonding of diamonds prior to reaching their full-service life is one of the most undesirable failure modes of these bits. This premature loss of diamonds greatly impacts the tool's cutting efficiency and increase the cost of drilling operation (Konstanty, 2005a).

In order to study the mechanical properties of particulate composites, Huang et al. (1993) conducted an experimental test to evaluate the Elastic Moduli of

polyester resin matrix composites with hollow glass spheres inclusions as reinforcements and the results have been compared with the theoretically calculated elastic moduli. Tagliavia et al. (2010) have investigated the mechanical properties of syntactic forms reinforced with spherical hollow particles under tensile loading where the effect of particle-matrix de-bonding and particle wall thickness on the elastic modulus of the reinforced foam has been shown. Tagliavia et al. (2010) have developed a model which they used along with the finite element analysis to undertake this research. Shams et al. (2014) have developed another model which is very similar to Tagliavia et al. (2010). However, the behaviour of these particulate composite materials (Huang and Gibson, 1993, Tagliavia et al., 2010, Shams and Porfiri, 2014) will be quite different from the diamond impregnated bits as the most effective particles are partially exposed from the matrix in the present case whereas these are embedded within the matrix for these materials (Huang and Gibson, 1993, Tagliavia et al., 2010, Shams and Porfiri, 2014).

The retention of diamond grits by the matrix is a complex and system-dependent process which is affected by the properties of the matrix, interfacial materials as well as the size, shape and orientation of diamond particles (Chalkley and Thomas, 1969, Konstanty, 1999). A poor adhesion at the interface between the matrix and diamond particles leads to premature fall out of diamond grits while resisting the interfacial stresses developed during the operation of the bits. A majority of literature has identified that the premature interface failure is one of the major issues limiting the performance of diamond bits. In some cases, diamonds are mostly held by the matrix through mechanical interlocking which gives a low interfacial strength. In order to improve the retention capacity of diamonds, many attempts have been made to establish a strong bond between the matrix and diamonds by adding some alloy which reacts with carbons present in diamonds to form chemical bonding in the form of metal-carbide elements at the interface (Scott et al., 1975, Levin and Gutmanas, 1990). Initially, iron, tungsten and nickel alloys are added into the metal matrix formation which not only helps to improve the strength, toughness and hardness of the matrix but also enhances the

interfacial strength as these metals have a strong atomic bonding affinity for carbons. However, it has been proved that a severe diamond surface degradation is often observed by the formation of too thick carbide layers due to adding more chemically reactive materials into the metal matrix powder (Konstanty, 2005a). Also on an industrial scale of production, it is almost impracticable to prevent the graphitization of diamonds under high temperature which is required when the matrix material includes these reactive alloys. Consequently, the technique of metal-coated diamonds has been invented which not only protects the diamonds from oxidisation but also increases their retention capacity (Konstanty, 1999). Tungsten has been widely used as a coating material for diamond grits, and it helps to form a thin film of tungsten carbide at the interface that acts as a strong chemical bond between the matrix and diamonds (Konstanty, 2005a). Besides using tungsten as a coating material, some other metals such as Ti-coating are also used which improves the interfacial bonding strength significantly (Lin et al., 2008).

Initially, some experimental studies (Miller and Ball, 1990, Miller and Ball, 1991, Xuefeng and Shifeng, 1994) on impregnated diamond bits were conducted where the wear mechanisms of these bits were investigated. Also, the wear modes have also been classified into four distinct types where the pull out of diamonds is one of these failure modes, which has an importance influence on the efficiency of these bits. However, no one made any attempt to quantify these failure mechanisms in terms of displacements, forces or some other mechanical parameters so far. The first attempt towards modelling the behaviour of these diamond bits is due to Zhou et al. (1997) who conducted stress analysis of a single diamond particle along with a portion of the surrounding matrix as a representative part of these bits using a 2-dimensional finite element model without considering any failure or damage at the interface between the matrix and diamonds. This may be defined as a micromechanical modelling of the bits where the diamond is subjected to a horizontal cutting force only at its cutting tip (Miller and Ball, 1990). Zhou et al. (1997) plotted the variation of normal stress along the interface for different levels of matrix wear and these stress distributions were taken as the

measure of interface debonding failure. Suh et al. (2008) conducted a similar study on diamond impregnated grinding wheel where they calculated the von Mises stress along the interface where they also studied the effect of unsymmetrical matrix wear with respect to the diamond particle. In a slightly different study, Li et al. (2010) tried to predict the plastic deformation and residual stresses within the matrix near the diamond particle which is produced due to the sintering process where a 3-dimensional finite element simulation of the micro-mechanical model was used. It is interesting to note that no one has paid any attention so far on the modelling of interface failure of this system which can predict the diamond pull out process more realistically. This is a problem of interfacial crack propagation which is a complex process but a proper modelling of this process is necessary for a better understand of these diamond tools and their design.

A satisfactory solution of the above problem can be achieved by using the concept of fracture mechanics which can be implemented through finite element modelling. In this context, the Virtual Crack Closure Technique (VCCT) (Turon et al., 2007) became quite popular which is based on Linear Elastic Fracture Mechanics (LEFM). Although valuable information related to onset and stability of a crack can be obtained by using this technique (VCCT), it is not convenient for modelling crack propagation as VCCT requires re-meshing to advance the crack front when the energy release rate reaches its critical value (Rinderknecht and Kröplin, 1997). Moreover, the VCCT requires the information of a pre-defined initial crack. These problems can be eliminated by using the cohesive zone modelling (CZM) technique which is becoming very popular in recent years for modelling automatic crack propagation in many engineering problems. However, this technique needs the information of the crack propagation direction in advance. Incidentally, this is predefined in the present problem which is simply the interface between the matrix and diamonds. Similarly, there are many other problems such as delamination in multi-layered composite laminates, bond failure of reinforcing bars or externally bonded plates in concrete structures, delamination in adhesively bonded joints, matrix-inclusions de-bonding in any composite

materials and similar situations where the direction of crack propagation is known (Grassi and Zhang, 2003, M. Alfano, 2007, de Morais et al., 2002).

Actually, the delamination problem in multilayered composite structures has drawn a significant attention in recent past which has helped to develop this modelling technique (CZM) so well that it can be used with full confidence. The fundamental idea of the CZM technique is based on the concept of fracture process zone which is characterised by the cohesive law or traction separation law for de-cohesion of atomic lattices as proposed by Barenblatt (1962). According to this model, the traction across the interface between the two materials is increased elastically at the beginning with the separation of these two materials until the traction reaches its critical value. This traction is then decreased with further increase of the separation and eventually disappears according to some principles of damage mechanics.

The CZM technique, which has been successfully applied to various problems, should be most suitable for the present problem but it has not been exploited so far. Thus the matrix diamond interface failure is modelled by finite element and CZM techniques in combination for the first time in this study. This will help to understand the wear mechanism of impregnated diamond bits due to diamond pull out more accurately that can benefit the design of these bits. Moreover, there is a need for investigating the effect of different parameters such as protrusions, shapes and orientations of the diamond particle on its retention capacity which is undertaken in this research as this has not been studied previously.

2.2 Numerical Model

2.2.1 Geometry of the model and its finite element meshing

Similar to the previous investigations (Suh et al., 2008, Zhou et al., 1997), the failure of diamond impregnated bits is modelled by taking a single diamond particle which is partially embedded within the matrix and cuts the rock with its exposed part during the drilling operation (Fig. 2.1a). The model also includes a portion of the surrounding matrix that holds the diamond particle (Fig. 2.1a) where the dimension of this portion of the matrix (within the dotted lines) is adequate to dissipate the stresses produced by the forces acting on the diamond particle. For the justification of the above model, it is assumed that diamond particles are evenly distributed within the matrix and having adequate gaps between them so that stresses around these particles do not affect each other. This is true for most of the diamond bits as they are designed to have adequate service lives by avoiding non-uniform distribution of diamond grits which is responsible for localised stress concentration leading to premature failure of these bits. In order to predict the failure and stresses within the representative portion of the diamond bit mentioned above (Fig. 2.1a), a 2-dimensional finite element modelling of this portion (Fig. 2.1b) is undertaken. For the convenience of representing the problem, the finite element model (Fig. 2.1b) is drawn as a mirror image (upside down) of the actual object. Although the model considered both horizontal and vertical forces to simulate cutting force (Fx) and vertical thrust force (Fy) on the bit, the results indicate that the fall-out of the diamond particle due to interfacial debonding are primarily facilitated by tangential cutting force and the additional vertical force do not affect the result much. Moreover, the magnitude of the cutting force is unknown and it changes during the cutting process. This problem is addressed by the displacement control technique where the displacement is imposed at the tip of the protruded (exposed) part of the diamond particle. The finite element model has predicted the cutting in the form of resisting force with respect to the imposed displacement. This has

also determined the critical load for the interfacial debonding of the diamond particle.

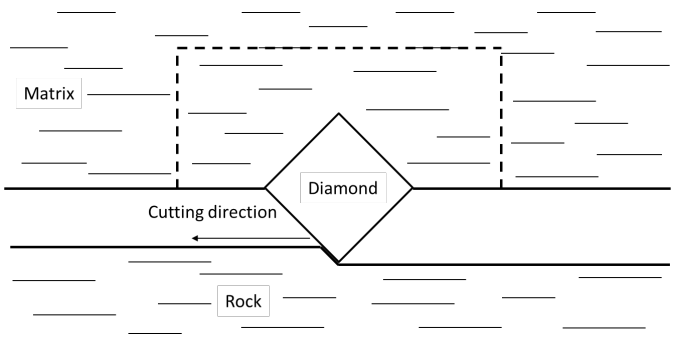

(a) Schematic draw of the drilling operation of a diamond impregnated bit

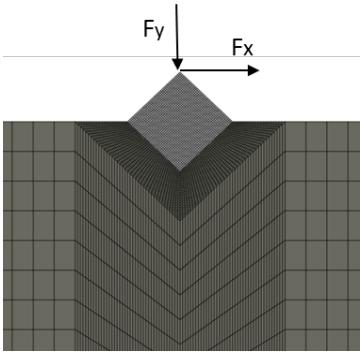

(b) Finite element model of the representative part of the diamond impregnated bit

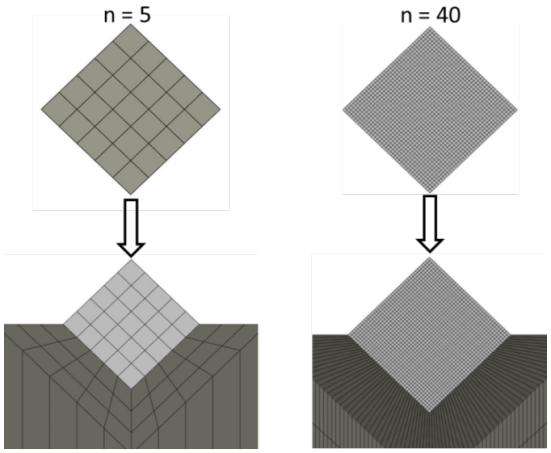

(c) Two different sample mesh densities of a diamond particle and its surround matrix

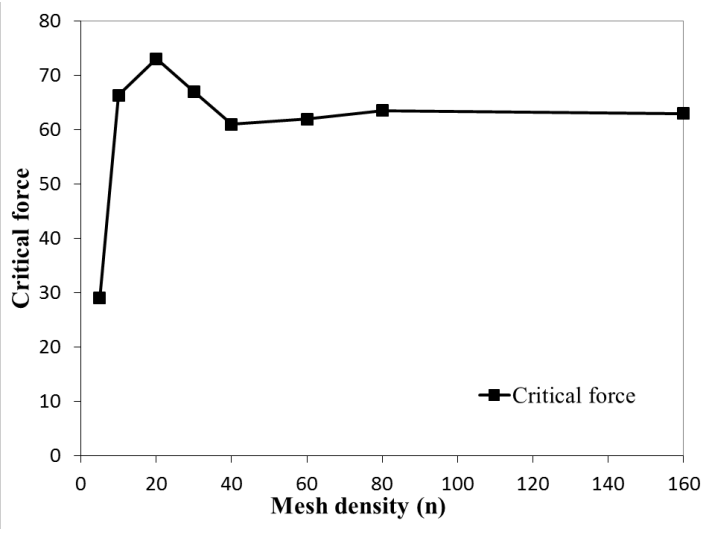

(d)Critical force versus n (mesh size)

Fig. 2.1 Finite element model of a diamond impregnated drill bit.

Although the natural diamond particles are highly irregular in shape (either round and/or few sharp edges and corners), the shape of synthetic diamond grits, used in impregnated diamond bits, are controlled and these can be treated as regular polygons (2D model) in most cases. A square geometry has typically been used by different investigator for simplicity which is also used in most of the cases of the present study. The typical size of synthetic diamond particles varies from 0.01 to 0.5 mm (Xuefeng and Shifeng, 1994, Li et al., 2010) and this is taken as 0.5 mm in the present simulation. The size taken for the surrounding matrix is about 20 times larger than that of the diamond which is large enough to ensure that the stresses are zero near the boundaries (dotted lines in Fig. 2.1a) of the matrix. In the present study, a well-regarded finite element code ABAQUS 6.12 is used for a reliable numerical modelling of the diamond-matrix system. Four nodes bilinear plane strain quadrilateral elements are used to model both diamond and matrix. The mesh convergence study is performed for all examples to ensure a converged solution but the details are not shown. A sample representative case of the finite element model of the system with meshing is shown in Fig. 2.1b. A finer mesh is used for the regions of interest, which is the diamond particle and the portion of the matrix in the vicinity of the interface, while a coarse mesh is used for the portion of matrix away from the interface with a gradual

transition in order to improve the computational efficiency. The detail of the mesh convergence study of this problem is illustrated by taking 8 different mesh densities. The mesh divisions used for the diamond particle is defined as n¡Án and the value of n is taken as 5, 10, 20, 30, 40, 60, 80 and 160 in the present study. Fig. 2.1c shows two sample cases corresponding to n=5 and n=40. The values of the critical load obtained from these eight mesh densities are plotted in Fig. 2.1d, which shows that the results converged well as the mesh density increased. It can be seen that a mesh density corresponding to n=40 is adequate to obtain accuracy result in this case.

2.2.2 Material model of the matrix and diamonds and their properties

Since diamonds behaves like a brittle material, they are treated as elastic and isotropic materials. In the present study, the modulus of the elasticity is taken as E = 1100 GPa whereas the Poisson's ratio ¡Í = 0.1 for these diamond particles (Zhou et al., 1997, Li et al., 2010, Suh et al., 2008). The Tungsten carbide cobalt (WC-Co) alloy is used as the matrix material which is having high wear resistance and hardness characteristics. The mechanical properties of WC-Co are significantly influenced by the content of cobalt as well as the tungsten carbide grain size before sintering (Andrew, 1998). The modulus of elasticity and Poisson's ratio of WC-Co alloy are taken as 600 GPa and 0.2 respectively which were experimentally determined by Jaensson et al. (1972) for low cobalt contained alloy. It is worth to note that WC-Co alloy is a kind of cemented carbide material and due to the high proportion of tungsten carbide content, the matrix behaves as a hard metal and it is treated as elastic material in the present study. In order to ensure that, elastic-plastic material properties are used to model the matrix in some sample test cases where no significant effect of plasticity is observed.

2.2.3 Failure model for the diamond-matrix interface

The traditional continuum-based approach is not computationally attractive for modelling the interfacial failure in the present study as the thickness of the interface is very small which needs a very fine mesh to capture the sudden variation of displacements and stresses within this small distance. In this situation, the concept of cohesive zone modelling approach (Elices et al., 2002, M. Alfano, 2007) is most appropriate which is adopted in the present study. This modelling approach assumes that the interface has no thickness and the formulation is based on traction-separation relationship instead of stress-strain relationship. A typical traction-separation ($\tau - \delta$) relationship is shown in Fig. 2.2 where OA shows the elastic response of the interface having a high stiffness of K and AB represents the interfacial damage in the form of a linear softening law. The damage is characterised by the damage parameter (d) as shown in Fig. 2.2 which helps to represent the irrecoverable damage of the interface through pure elastic unloading with reduced stiffness. The separation at failure δ^f is obtained from the ultimate stress τ^0 (a material property of the interface) and the interfacial fracture toughness G_c (another material property) which is the area of the triangle OAB. The use of fracture energy helps to make the analyses mesh-insensitive.

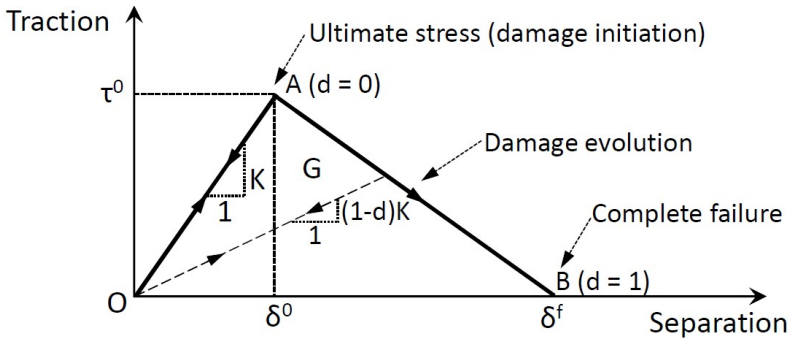

Fig. 2.2 A typical bilinear traction-separation relationship.

As the present problem is based on 2D analysis, an interface may have two possible modes of failure: 1) Mode I or opening mode due to the tensile stress acting normal to the interface and 2) Mode II or sliding mode due to shear stress parallel to the interface. Thus the traction separation law (Fig. 2.2)

mentioned above will be used for both these modes of failure which will have a coupling that will be discussed later. In the present case, the separation indicates the relative displacements between the diamond and the matrix at their interface whereas the tractions are simply the interfacial stresses. These relative displacements $\{\Delta\}$ at any point of the interface may be expressed as:

$$\{\Delta\}=\begin{Bmatrix}\bar{u}\\ \bar{v}\end{Bmatrix}=\begin{Bmatrix}u^{+}\\ v^{+}\end{Bmatrix}-\begin{Bmatrix}u^{-}\\ v^{-}\end{Bmatrix}=\sum_{i=1}^{4}N_i(\xi=-1,\eta)\begin{Bmatrix}u_i^{+}\\ v_i^{+}\end{Bmatrix}-\sum_{i=1}^{4}N_i(\xi=1,\eta)\begin{Bmatrix}u_i^{-}\\ v_i^{-}\end{Bmatrix} \quad (2.1)$$

where u^{+} and u^{-} are the displacement components at the two sides of an interfacial point in the global *x*-direction whereas u_i^{+} and u_i^{-} are the corresponding displacements at the *i*-th node of the elements (Fig. 2.3) used to model the materials on the two sides of this interfacial point and N_i are the shape functions of these elements. This is similarly applicable to v^{+} and v^{-} which are the displacement components in the global *y*-direction. The normal and tangential components of these relative displacements $\{\delta\}$ are in local coordinate system *n*-s (Fig. 2.3) which can be obtained from their global counterparts $\{\Delta\}$ using the coordinate transformation.

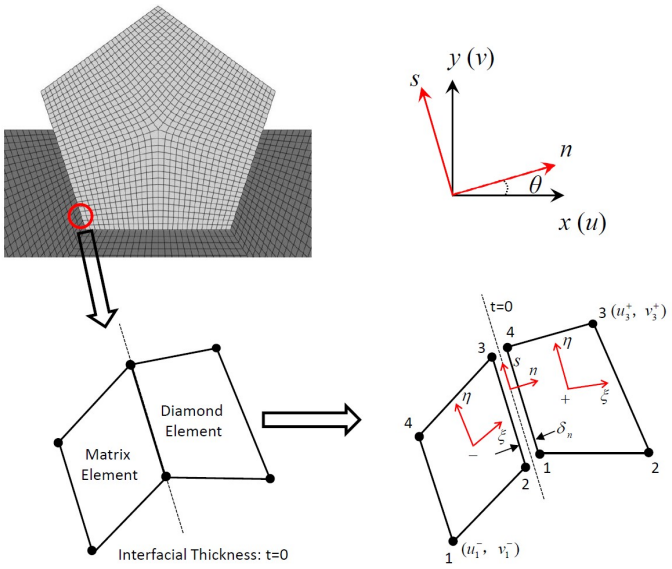

Fig. 2.3 Detail of an interface for cohesive zone modelling.

According to the isoparametric formulation, the coordinates of an element can be written as $x=\sum_{i=1}^{4}N_i x_i$ and $y=\sum_{i=1}^{4}N_i y_i$ where x_i and y_i are the nodal coordinates of the element. With these, the vectors along the curvilinear coordinate system ξ and η can be obtained as:

$$\{V\}_\xi=\begin{Bmatrix}\frac{\partial x}{\partial \xi}\\ \frac{\partial y}{\partial \xi}\end{Bmatrix}=\sum_{i=1}^{4}\frac{\partial N_i}{\partial \xi}\begin{Bmatrix}x_i\\ y_i\end{Bmatrix} \tag{2.2}$$

$$\{V\}_\eta=\begin{Bmatrix}\frac{\partial x}{\partial \eta}\\ \frac{\partial y}{\partial \eta}\end{Bmatrix}=\sum_{i=1}^{4}\frac{\partial N_i}{\partial \eta}\begin{Bmatrix}x_i\\ y_i\end{Bmatrix} \tag{2.3}$$

The above vectors may be taken at any point on the interface after substituting as $\xi=+1$ or $\xi=-1$ depending on the location of the element (i.e., negative or positive side of the interface). In order to keep the presentation simple, the + or – superscripts are avoided in this section. It should be noted that the vectors $\{V\}_\xi$ and $\{V\}_\eta$ may not be orthogonal to each other in all cases as the elements will not always have a rectangular shape (Fig. 2.3). However, the vector $\{V\}_\eta$ will always follow the interfacial direction which aligns with the mode II or shear failure. In order to get the vector $\{V\}_n$ along the normal direction of the interfacial and laying in $\xi-\eta$ plane for the modelling of mode I failure, it is convenient to have the vector perpendicular to the $\xi-\eta$ (or *x*-*y*) plane first and it can simply be obtained as:

$$\{V\}_t=\frac{\left(\{V\}_\xi\times\{V\}_\eta\right)}{\left\|\{V\}_\xi\times\{V\}_\eta\right\|}. \tag{2.4}$$

As the above equation gives a normalised unit vector $\{V\}_t$ perpendicular to the $\xi-\eta$ plane, $\{V\}_\eta$ can be normalised to have the tangential unit vector $\{V\}_s$ which may be utilised to get the unit normal vector $\{V\}_n$ as follows:

$$\{V\}_s = \frac{\{V\}_\eta}{\left\|\{V\}_\eta\right\|} \tag{2.5}$$

$$\{V\}_n = \{V\}_s \times \{V\}_t \tag{2.6}$$

Once $\{V\}_n$ and $\{V\}_s$ are obtained, the transformation matrix $[Q]$, which correlates the local coordinate system *s*-*n* of the interface (Fig. 2.3) with the global coordinate system *x*-*y*, can be simply formed as:

$$[Q] = \begin{bmatrix} \{V\}_n^T \\ \{V\}_s^T \end{bmatrix} = \begin{bmatrix} \cos\theta & \sin\theta \\ -\sin\theta & \cos\theta \end{bmatrix} \tag{2.7}$$

where θ is the orientation of the normal to the interface as shown in Fig. 2.3. By using the above transformation matrix $[Q]$ and the interfacial relative displacements $\{\Delta\}$ expressed in global coordinates in Eqs. (1), these relative displacements can be expressed in local coordinates as:

$$\{\delta\} = \begin{Bmatrix} \delta_n \\ \delta_s \end{Bmatrix} = [Q]\{\Delta\} \tag{2.8}$$

The damage introduces nonlinearity in the system that requires an incremental/ iterative procedure for solving the governing equations. As the damage is an irreversible process, the solution technique dependent on the loading history. Thus there is a need for storing the maximum values of these relative displacements ($\delta_n^{\max}$, $\delta_s^{\max}$) which occurred before any increment/iteration and they are updated in that increment/iteration as follows:

$$\text{If } \delta_n > \delta_n^{\max} \Rightarrow \delta_n^{\max} = \delta_n \text{ otherwise } \delta_n^{\max} = \delta_n^{\max} \tag{2.9}$$

$$\text{If } |\delta_s| > \delta_s^{\max} \Rightarrow \delta_s^{\max} = |\delta_s| \text{ otherwise} \delta_s^{\max} = \delta_s^{\max} \tag{2.10}$$

The interfacial normal and shear tractions (τ_n and τ_s) can be related to the maximum value of these relative displacements using the interfacial constitutive properties in the form of traction-separation laws (Fig. 2.2) as:

$$\begin{gathered} \tau_n = K_n \delta_n \text{ if } \delta_n^{\max} \le \delta_n^0 \\ \tau_n = (1 - d_n) K_n \delta_n \text{ if } \delta_n^0 < \delta_n^{\max} < \delta_n^f \\ \tau_n = 0 \text{ if } \delta_n^{\max} \ge \delta_n^f \end{gathered} \tag{2.11}$$

$$\begin{gathered} \tau_s = K_s \delta_s \text{ if } \delta_s^{\max} \le \delta_s^0 \\ \tau_s = (1 - d_s) K_s \delta_s \text{ if } \delta_s^0 < \delta_s^{\max} < \delta_s^f \\ \tau_s = 0 \text{ if } \delta_s^{\max} \ge \delta_s^f \end{gathered} \tag{2.12}$$

For the bilinear traction separation law (Fig. 2.2), the damage parameters for these two modes of fracture may be written as:

$$d_n = \frac{\delta_n^f \left(\delta_n^{\max} - \delta_n^o\right)}{\delta_n^{\max} \left(\delta_n^f - \delta_n^o\right)}, \; d_s = \frac{\delta_s^f \left(\delta_s^{\max} - \delta_s^o\right)}{\delta_s^{\max} \left(\delta_s^f - \delta_s^o\right)} \tag{2.13}$$

The above equations (11) and (12) can be used if the two modes of failure are independent having no coupling between them. However, due to the varying drilling conditions of the impregnated diamond bits, the matrix diamond interface is more likely to have a mixed-mod fracture where the two modes of failure will be coupled as mentioned earlier. In that situation, the damage onset and its propagation may occur before reaching the ultimate stress of mode I (τ_n^0) and mode II (τ_s^0). Under mixed mode failure scenario, a quadratic failure criterion proposed by Cui et al. (1993) for the prediction of damage initiation seems to be most suitable which is used in the present study and it is expressed as:

$$\left(\frac{\langle \tau_n \rangle}{\tau_n^0}\right)^2 + \left(\frac{\tau_s}{\tau_s^0}\right)^2 = 1 \tag{2.14}$$

Similarly, the power law (Zhai and Zhou, 2000) is used for the mixed mode damage evolution of the interface which is expressed in terms of energy release rates (G_I and G_{II}) and their critical values (i.e., fracture toughness for these two modes) as:

$$\left(\frac{G_I}{G_{IC}}\right)^2 + \left(\frac{G_{II}}{G_{IIC}}\right)^2 = 1 \tag{2.15}$$

where $G_I = \int_0^{\delta_n^{\max}} \tau_n d\delta_n$ and $G_{II} = \int_0^{\delta_s^{\max}} \tau_s d\delta_s$. In a mixed mode failure analysis, the traction separation relationship (Fig. 2.2) for the two modes are combined and expressed in terms of an equivalent traction-separation relationship having a similar bilinear shape which helps to implement the mixed-mode damage model conveniently. This combined traction-separation relationship will have a same initial stiffness (*K*) whereas the separation at the onset of damage initiation δ_m^0 and the separation at complete failure δ_m^f (subscript *m* indicates mixed-mode fracture) can be obtained from Equations (14) and (15) respectively (Camanho et al., 2003). In that case, the two components of the separation obtained in any incremental/iterative are to be combined to have single resultant component δ_m as:

$$\delta_m = \sqrt{\delta_n^{\,2} + \delta_s^2} \tag{2.16}$$

With the above equations, the stiffness matrix of the interface can be derived using Virtual Work Principles following the unusual steps of finite element technique. It should be noted that the Newton-Cotes integration technique is used to evaluate the interfacial stiffness matrix following the full integration scheme in order to have better results as recommended by Borst et al. (1989)

and Goncalves et al. (2000). Thus the material properties required for defining the interfacial behaviour in the present study are the fracture toughness values G_{IC} and G_{IIC} for the two modes and the corresponding ultimate stresses τ_n^0 and τ_s^0. It has been proved experimentally as well as theoretically (Zhai and Zhou, 2000, Cavalli, 2003) that these material parameters should be taken for the weaker material which is the metal matrix in the present case if the matrix is adequately connected to the diamond. Thus, the material properties of tungsten carbide cobalt (matrix) are taken as the interfacial material parameters which are:

τ_n^0 = 543 MPa, τ_s^0 = 314 MPa, G_{IC} = 0.14 mJ/mm^2 and G_{IIC} = 0.33 mJ/mm^2.

2.3 Validation of the numerical examples

Although some researchers studied the behaviour of diamond impregnated bits experimentally (Liao and Luo, 1992, Tze-Pin et al., 1992, Miller and Ball, 1991) as well as numerically (Zhou et al., 1997, Suh et al., 2008) but there is no experimental test data available for validation of the present model as no one attempted to quantify the failure mechanism as mentioned earlier. On the other hand, the available numerical results (Zhou et al., 1997, Suh et al., 2008) cannot be used for a complete validation of the present models because these studies did not consider the interfacial damage. These studies (Zhou et al., 1997, Suh et al., 2008) used a linear finite element model to evaluate the diamond-matrix interfacial stresses which were taken as a simple measure of interfacial debonding. . However, these numerical results (Zhou et al., 1997, Suh et al., 2008) are utilised for a partial validation of the present model taking a perfect diamond-matrix interface. The interface damage model used in the present analysis is indirectly validated with the test data of a double cantilever beam (DCB) (de Morais et al., 2002).

2.3.1 Validation of the model with perfect diamond-matrix interface considering different levels of matrix and diamond wear

This problem is picked up from the published paper (Zhou et al., 1997) who applied a constant cutting force (P = 2.5N) on the diamond particle having a square geometry with 0.015mm sides (Fig. 2.4a) and the analysis was carried out taking the modulus of elasticity as 1141 GPa and 110 GPa for the diamond and the matrix (bronze) respectively. The problem seems to be hypothetical in regards to the particle size and the magnitude of cutting force but this is used only for the purpose of validation. The same loading, material properties and geometric dimensions are used in the present finite element model and the analysis is carried out for different levels of matrix wear (Fig. 2.4a). For the representation of results with respect to the meshing used in the present analysis (diamond has a regular/structured meshing with a division of 12x12), the matrix wear is defined as "0" (initial condition or basic case) when one-fourth of the diamond height is exposed or protruded out of the matrix whereas this is "6" when six layers of matrix elements of the basic case are removed to have half protrusion of the diamond particle (Fig. 2.4a). These elements are removed incrementally at the rate of two layers at a time that has simulated seven different levels of matrix wear ranging from "0" to "12" with an increment of 2. The finite element mesh used for three sample cases of matrix wear is shown in Fig. 2.4a, where the entire portion of the matrix considered in the present model, is not shown for the convenience of presentation.

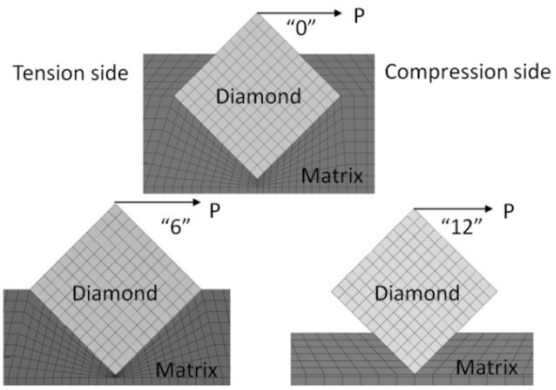

(a) Finite element meshing of the model geometry.

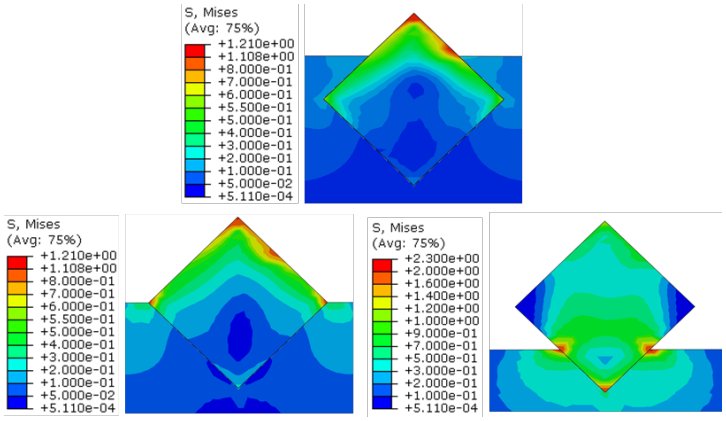

(b) Distribution of the Von-Mises stress over the entire body found in the present FE analysis.

Fig. 2.4 Finite element analysis for a different level of matrix wear.

Similar to Zhou's study, the cutting force is applied on the left side of the diamond particle's exposed edge where total force (2.5 N) is equally distributed at the six nodes starting from the top corner of the diamond. The variations of Von-Mises stress over the entire system predicted by the present finite element model are illustrated as stress contours in Fig. 2.4b. It could be noted that higher values of this stress component are concentrated at the tension side of the diamond-matrix interface near the exposed surface of the matrix. As Zhou et al. (1997) presented their results in the form of distribution of the normal stress (σ_n) along the diamond-matrix interface; the normal stress (σ_n) at any point of the interface, which acts perpendicular to the interfacial plane, is computed by transforming the stresses (σ_x, σ_y, σ_{xy}) at that point obtained in the present analysis. For this purpose, the elements of the interface,

which are within the diamond particle, are selected and the stresses at their gauss points are utilised. It should be noted that the number of gauss point of an element is one which is at its centroid for the type of element used in the present model. Based on these calculations, the variation of normal stress (σ_n) found along the interface on the tensile side of the diamond particle is plotted in Fig. 2.5. For the convenience of presentation, the distance along the interface, which is the horizontal axis of Fig. 2.5, is shown in terms of element numbers of the diamond particle where the number assigned to the lower corner element is 0 and the number incremented by one while moving along the interface on the tensile side following the direction of the arrow as shown. The figure shows that the matrix wear has a significant effect on the variation of interfacial normal stress. For the initial condition of the matrix wear ("0"), the maximum value of the normal stress is about 0.8 MPa which is found at element #17. For the highest level of matrix wear ("12"), the maximum/peak normal stress is found to be 1.25 MPa which indicates that it increases with the increase of the level of matrix wear. The figure shows the occurrence of a second peak stress when matrix wear is severe (e.g., second peak stress at element #7 and element #5 for matrix wear corresponding to "10" and "12" respectively). It also illustrates a significant variation of the stress distribution at the exposed surface of the matrix. Moreover, the present results are found to have a very good agreement with those reported by Zhou et al. (1997).

In order to study the effect of plastic deformation of the matrix (metal) on the final results, a typical elastic-plastic material model based on von Mises yield criterion with isotropic hardening and associated flow rule is used to the matrix (bronze). A bilinear stress-strain curve with a yield stress of 70 MPa, the ultimate stress of 220 MPa and maximum plastic strain of 5% is used for the material. The comparison of the results obtained from these two models (one with an elastic material model for the matrix and the other with elastic-plastic material model) has not shown any significant difference. Thus the elastic material model for representing the behaviour of matrix seems to be adequate for the present problem and it is followed in this paper.

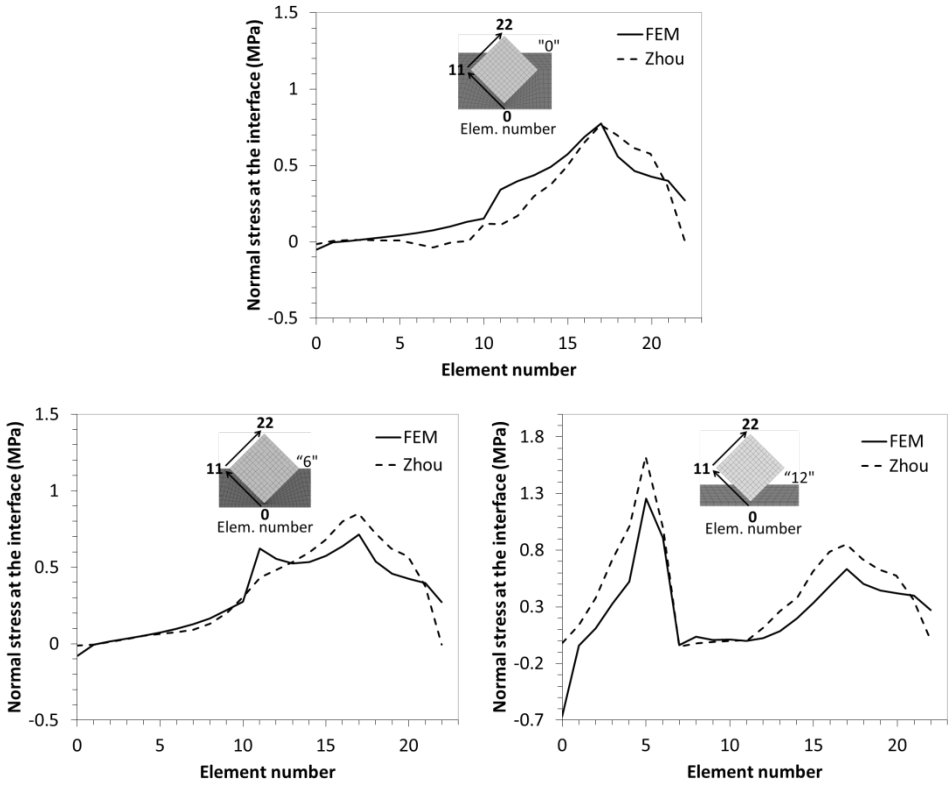

Fig. 2.5 Variation of normal stress along the interface as element centre stress in the diamond.

A similar investigation was carried out by Suh et al. (2008) who used 0.000231 N for the cutting force and 0.02 mm for the diameter of the square shaped diamond particle. The elastic modulus used for the matrix and diamond are 7 GPa and 1171 GPa respectively. Moreover, they have presented their results in the form of von Mises stress instead of normal stress along the tension side of the diamond matrix interface. Using these geometric and material properties, the present finite element models are developed for two different levels of diamond wear which are defined as “1” and “9”. Fig. 2.6a shows these two sample cases where a number (e.g., “1”) indicates the number of elements from the unworn top corner to the worn horizontal plane of the diamond particle along one of its exposed edges. This numbering system is based on the meshing used in the present analysis (diamond has a mesh with the division of 15x15). Since the value of the normal force has not been mentioned in the paper, it is assumed a value of 0.00231 N of normal force (ten times larger than the horizontal cutting force) is applied to the

horizontally worn surface of the diamond. The variation of the von Mises stress over the entire diamond-matrix system predicted by the present model is shown in Fig. 2.6b for these two cases of diamond wear.

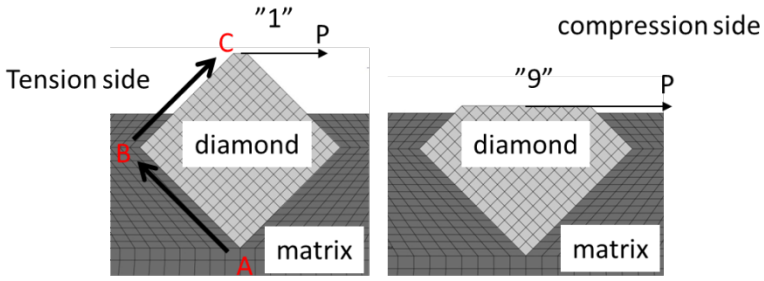

(a) Finite element meshing of the model geometry

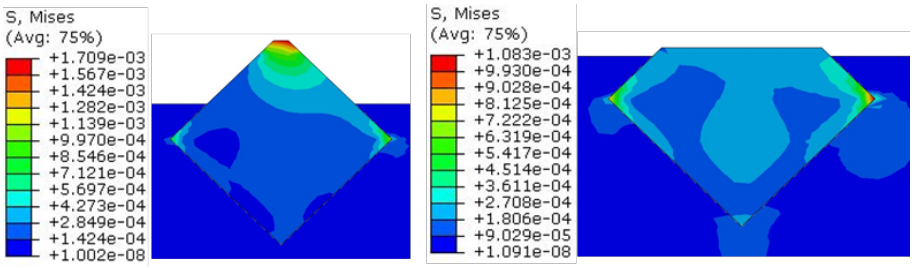

(b) Distribution of the Von-Mises stress over the entire body found in the present FE analysis

Fig. 2.6 Finite element analysis for different level of diamond wear.

For both cases of diamond wear as mentioned above, the variation of von Mises stress along the diamond-matrix interface obtained in the present analysis is plotted in Fig. 2.7. In this case, the von Mises stress is calculated at the nodes along the interface of the tension side of the diamond where these nodes are taken from the bottom corner "A" of the diamond to the top corner "C" (Fig. 2.6 (a)). With respect to the meshing used in the present analysis (mesh division of diamond: 15x15), "A" is defined as 0, "C" is defined as 30 (no wear) and the diamond left corner "B" is defined as "15". Fig. 2.7 shows that there are some discrepancies between the present results and those reported by Suh et al. (2008). One of the probable reasons for the discrepancy between these results is the magnitude of the applied normal force which is not reported by Suh et al. (2008) and a value of this force is guessed in the present analysis. Assuming a value of the friction coefficient in the range of 0.1, the value of the normal force is taken in the range of 10 times of the

cutting force. Moreover, Suh et al. (2008) obtained a higher stress near the root (Point A, Fig. 2.6a) compared to that at the left corner (Point B, Fig. 2.6a) which is not expected physically. The left corner of the diamond particle is most vulnerable and it should capture more stresses compared to other parts which are experience consistently in all cases of the present study.

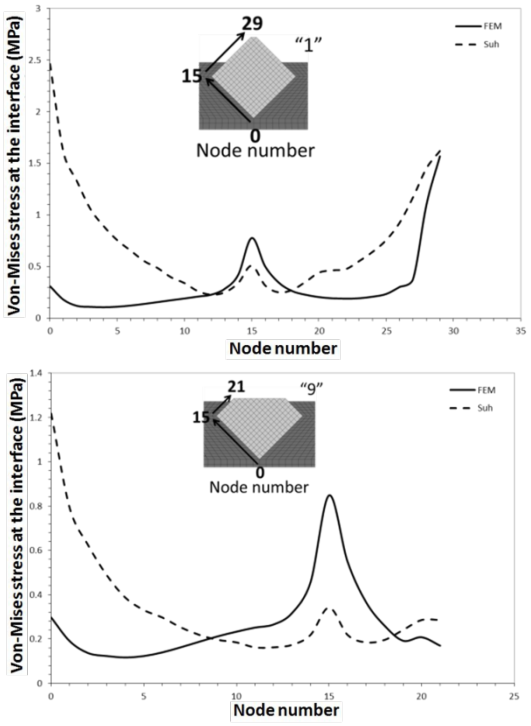

Fig. 2.7 Variation of Von-Mises stresses along the interface node as a function of particle wear.

2.3.2 Validation of the interfacial damage model with a double cantilever beam

As there is no data available for the validation of diamond-matrix interfacial damage as mentioned earlier, the problem of a double cantilever beam (DCB) as shown in Fig. 2.8 is used in this section for an indirect validation of the interfacial damage model. This problem (DCB) is commonly used in laminated composite structures and some other areas for the same purpose. The experimental test data reported by Morais et al. (2002) for a DCB made

of T300/977-2 carbon fibre reinforced epoxy laminate is used for the present analysis. The laminate (3.96 mm) consists of 24 identical layers having 0^0 orientation and the following material properties: E_1 = 150.0 GPa, E_2 = 11.0 GPa, G_{12} = 6.0 GPa, ν_{12} = 0.25. Similar to the diamond-matrix system, a two dimensioned finite element model is developed for the DCB (Fig. 2.8) with the damage model based on cohesive zone modelling technique at the interface (BC) between the two cantilever beams. The load-displacement (P-δ) curve obtained in the present analysis is plotted in Fig. 2.9 along with that reported by Morais et al. (2002) which shows that the numerical result has a reasonable correlation with the experimental results.

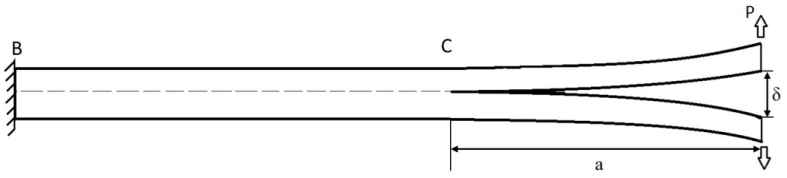

Fig. 2.8 Schematic drawing of double-cantilever beam test.

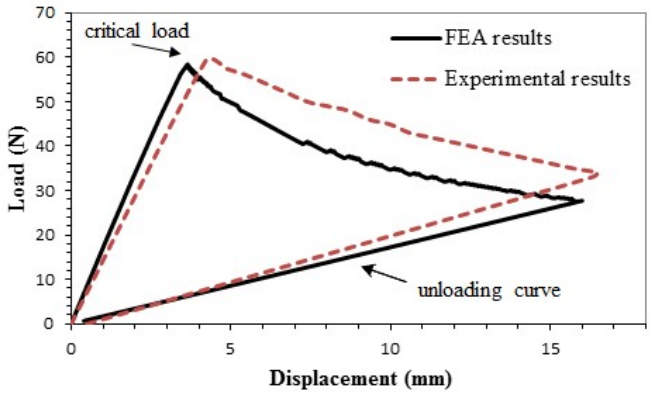

Fig. 2.9 Load-deflection curve of the double cantilever beam with delamination.

In order to validate the crack propagation under mixed–mode loading condition of the developed model, the experimental test data reported by Crews et al. (1998) for a mixed-mode bending (MMB) test apparatuses (Fig. 2.10) made of AS4/PEEK carbon-fibre reinforced composite is used for the

present analysis. Table 2.1 shows the dimension and material properties of the MMB specimens.

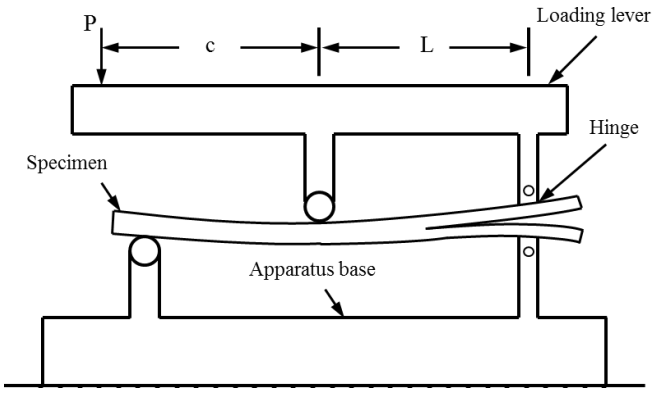

Fig. 2.10 Illustration of mixed-mode bending test.

Table 2.1 Dimension and properties for MMB test specimen.

Specimen Dimension				
L (Length)		W (Width)		T (Thickness of one arm)
102 mm		25.4 mm		1.56 mm
Mechanical Material Properties				
E_{11}	$E_{22} = E_{33}$	$G_{12} = G_{13}$	G_{23}	$\nu_{12} = \nu_{13}$
122.7 GPa	10.1 GPa	5.5 GPa	3.7 GPa	0.25
ν_{23}	G_{IC}	G_{IIC}	T	S
0.45	0.969kJ/m^2	1.719 kJ/m^2	80 MPa	100 MPa

In this study, five different G_{II}/G_T ratios have been simulated and compared with the experimental results, which are shown in Table 2.2. It can be seen that a good agreement between the numerical predictions and the experimental results is obtained.

Table 2.2 Numerical and experimental comparison of maximum loads of MMB Test.

G_{II}/G_T	P_{max} (numerical, N)	P_{max} (experimental, N)	Error (%)
0% (DCB)	165.83	147.11	12.7
20%	106.75	108.09	1.2
50%	298.64	275.35	8.4
80%	483.06	518.66	6.9
100% (ENF)	845.75	733.96	15.2

2.4 Parametric study

With initial confidence gained from the validation of the proposed modelling technique carried out in the previous section, the method is applied for the interfacial failure modelling of diamond-matrix system in this section. As there is no published result available for this problem, a large number of cases are investigated in the form of parametric study. The specific parameters used in this study include diamond shapes, diamond orientations, diamond protrusion levels and interface material properties. In order to have an understanding of the effect of an individual parameter, the value of that parameter is varied while the values of other parameters are kept unchanged.

2.4.1 Effect of diamond shapes

The previous studies (Konstanty, 2005b, Romanski, 2010) have observed experimentally that the shape of diamond grits has a significant effect on their retention capacity or pull out rate. Thus the diamond shape is an important parameter which is investigated in this section. As mentioned earlier, the diamond bits use synthetic diamond particles which are produced by the chemical vapor deposition (CVD) technique (Chou and Liu, 2005). This mechanized process (CVD) helps to produce regular shaped diamonds that can be conveniently represented as polygons as shown in Fig. 2.11. In this study, seven regular polygonal shapes having different number of sides

ranging from 4 to 18 are used to show their effects on diamond retention capacity. The finite element meshing used for modelling all these diamond-matrix system is also shown in Fig. 2.11a. A size of r = 0.25 mm (radius of the circle circumscribing the polygons) is taken for all these polygonal shapes. The portion of these diamonds above the exposed surface of the matrix is defined as protrusion height which is taken as 0.25 mm for all these cases (i.e., the centre of the particles lies along the exposed surface of the matrix). The material properties used are same as those provided in Section 2. The force is applied to these systems by imposing a gradual horizontal displacement at the tip (top corner) of the diamond towards right side. The distribution of equivalent von Mises stress over the entire system obtained at the onset of interface failure is presented in Fig. 2.11b. The figure shows the occurrence of stress concentration near the tip point (loading point) and the upper most point of the diamond-matrix interface on the compression side (right side) in all cases. The stress concentration at this interfacial point is observed as the diamond is still having contact with the matrix at this point. As the interface has completely debonded at this stage, the chemical bond between the diamond and matrix is lost which should lead to the fall out of diamonds. However, it is observed that stress concentrations are still present around one corner of the left (or tension) side of the interfaces for hexagon, decagon and octadecagon shaped diamonds. This ensures a contact between the matrix and diamonds at these corners, which prove additional restrain in the form of mechanical interlocking to have better retention ability. Thus the diamond particles having hexagon, decagon and octadecagon shapes are supposed to have relatively higher retention capacity.

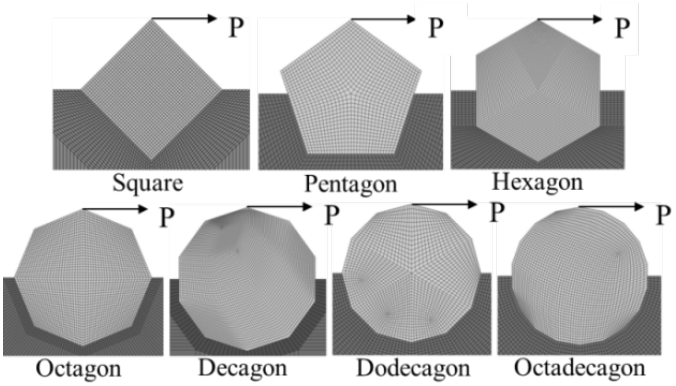

(a) Finite element meshing of the model geometry for different diamond shapes – same circumcircle radius.

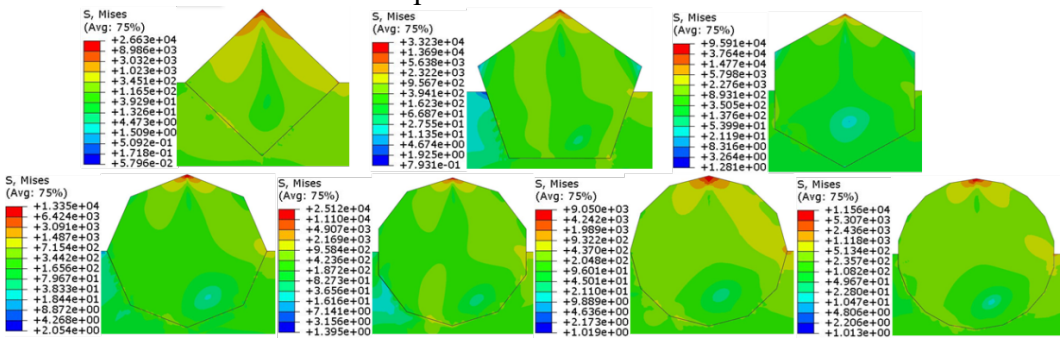

(b) Von-Mises stress distributions of different diamond shapes

Fig. 2.11 Models for different diamond particle shapes with same radius and protrusion height.

The forces produced at the diamond tip points due to the displacement imposed at these points are captured. The force-displacement variation for two representative cases (square and hexagon-shaped particles) is plotted in Fig. 2.12. It shows that the force is increased up to its peak value linearly and dropped down sharply for both cases where this pick force may be defined as the critical load of the initiation of interfacial debonding. The interfacial cracks are observed after reaching this critical load which cased this sudden reduction of the cutting force. For the square particle, the force is dropped to zero steadily after reaching its critical value of 61N, which indicates that the particle has completely lost its retention capacity. In contrast, a relatively higher value of the peak force (86.5N) is produced for the hexagonal particle which is due to its additional mechanical interlocking with the matrix. Moreover, the force started increasing again after reaching a value of 14.6N

and this is also due to the mechanical interlocking which didn't allow the particle to move out from the matrix freely. This is similarly observed in the case of decagon and octadecagon shaped particles. The orientation of the interface near the exposed surface of the matrix on the left (tension) side plays an important role on this addition mechanical interlocking found in the abovementioned cases. The critical load of interface failure is an important parameter to a designer as it indicates the retention capacity provided by the interface which is the primary focus of the present study.

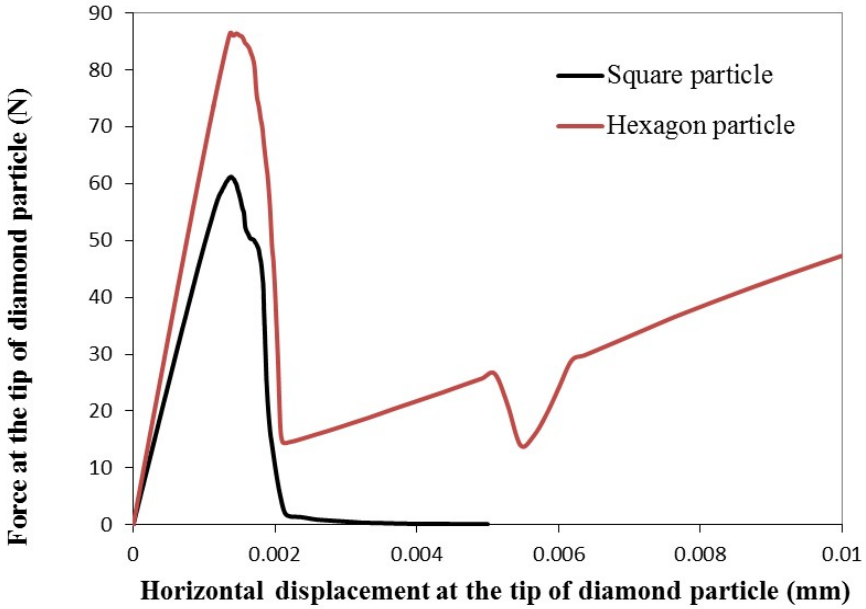

Fig. 2.12 Force-displacement variation at the tip of diamond particles.

The critical values of the cutting force corresponding to the initiation of the interface failure for each of the case studies are plotted in Fig. 2.13. The results have an anticipated trend where the hexagon, decagon and octadecagon particles have relatively higher retention ability due to the additional mechanical bonding as explained above. Among the different shapes studied here, the hexagon particle is found to have the highest retention capacity (86.5 N). For the particles, predominantly hold by the interfacial adhesion bonding with minimum mechanical interlocking, the critical force is found to increase with the increase of number of sides. For such cases, the square particle has the lowest value of critical force (61.2 N) whereas the dodecagon shaped particle has the highest value (85 N). It seems the orientation of the particles

will play an important role on the mechanical interlocking which will influence the diamond retention capacity.

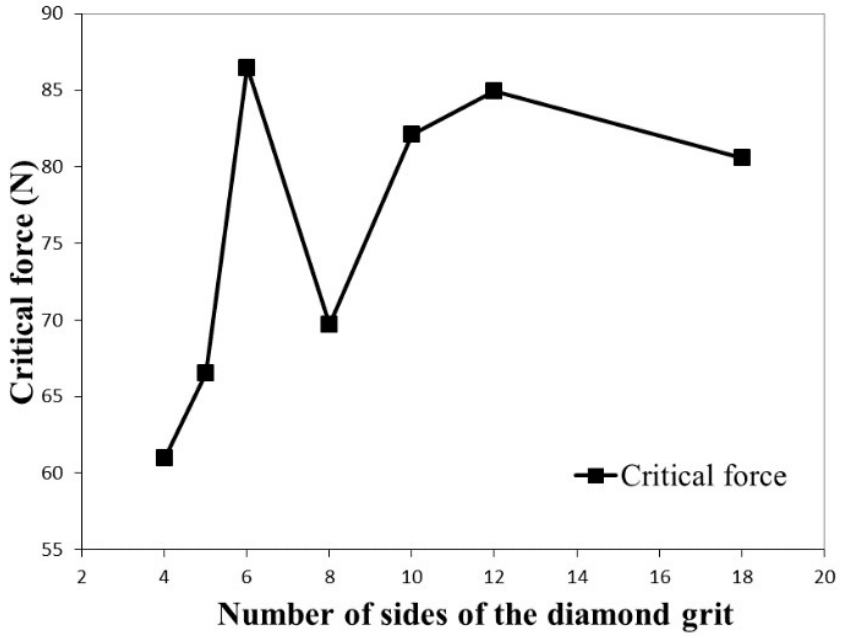

Fig. 2.13 Effect of the diamonds' shape on its retention capacity with the same circumcircle radius.

In order to show the variation of crack opening at the critical point with respect to the cutting force, one of the cases considered in the above study (Fig. 2.11) is taken as the sample example, which is shown in Fig. 2.14a. It is observed that the left corner (point B, Fig. 2.14a) is the critical point having a maximum crack opening. This result is plotted in Fig. 2.14b, which shows that the cutting force reached its maximum value (61N) when the crack opening at the critical point became 0.00026 mm.

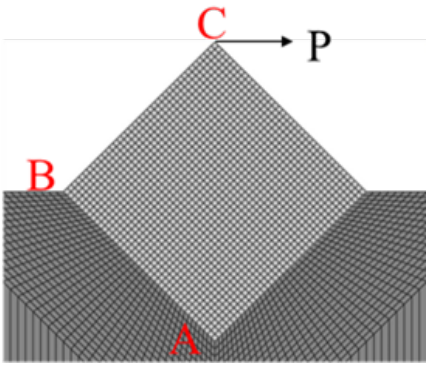

(a) Square shaped diamond particle

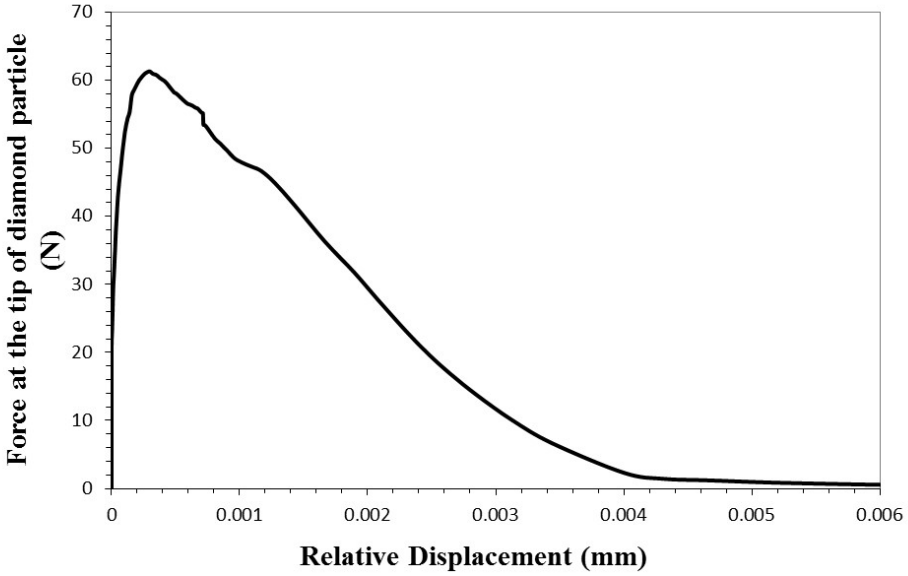

(b) Relative displacement jump versus load.

Fig. 2.14 Results of displacement jump with respect to the cutting force for square shaped diamond particle at point B.

Although it is more realistic to apply distributed load on the cutting edge of the diamond particle to simulate the real drilling process, it is observed in the present study that the load distribution has no effect on the retention capacity of the diamond particle when compared with the point load. In order to demonstrate this, one of the cases of the problem considered in Fig. 2.11 (square shaped diamond particle) is taken as a sample case which is reanalysed with a distributed loading as shown in Fig. 2.15 where other parameters (used in Section 4.1) are kept unchanged. The maximum force to cause the diamond debonding failure is about 62N for the case of distributed load whereas this is 61N for the case of point load. Therefore, a concentrated

load is applied for the purpose of simplicity. This cutting force is induced by imposed a horizontal displacement in order to mimic the actual drilling scenario.

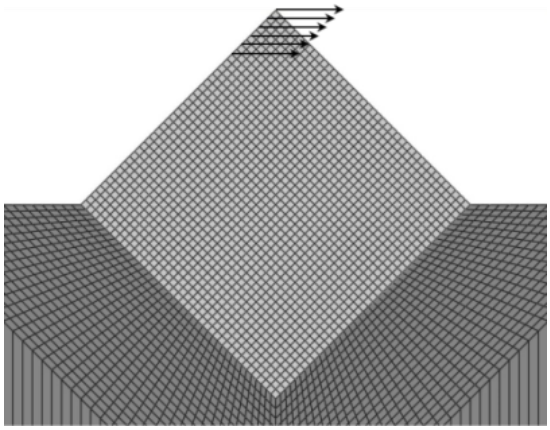

Fig. 2.15 Distributed load applied on the diamond of the model.

The problem studied above (Fig. 2.13) with a constant circumcircle radius of diamond particles (Fig. 2.11) is reinvestigated with a constant volume fraction taking same area (0.125 mm^2) for all diamond particle shapes (Fig. 2.11). In this situation, the circumcircle radius of regular polygons is decreased with the increase of the number of their sides. Keeping other parameters unchanged, the problem is reanalysed and the critical values of the cutting force corresponding to the initiation of the interface failure obtained for the different shapes are plotted in Fig. 2.16. It shows that the values of this critical load found in the present scenario (Fig. 2.16) are reduced for all diamond shapes except the first case (square shape) compared to those obtained earlier (Fig. 2.13). Similar to the previous scenario, the hexagon shaped diamond particle has the highest retention capacity in the present situation (constant volume fraction) and it is 80.8 N now. However, the octagon shaped particle has the lowest retention capacity in the present scenario and it is 49 N.

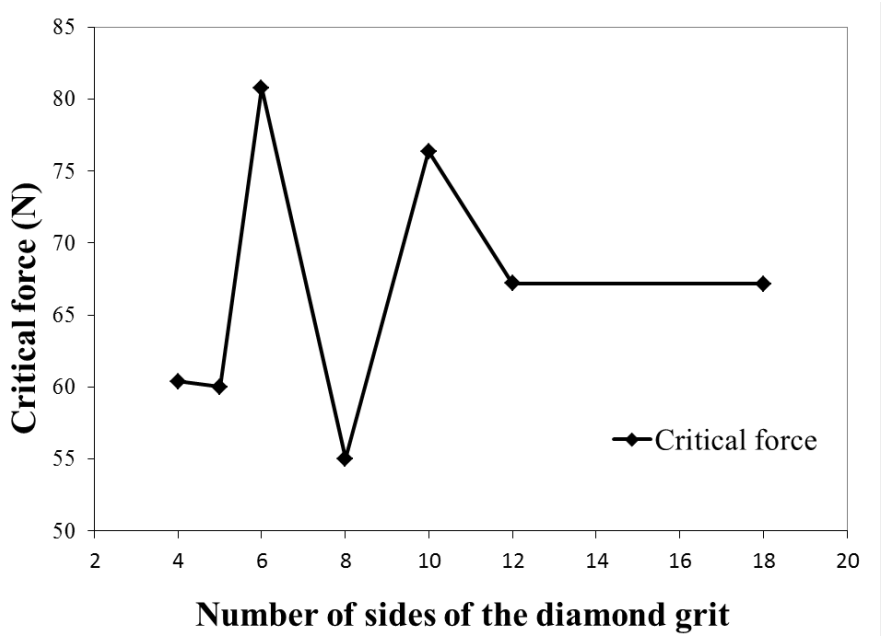

Fig. 2.16 Effect of diamond shape on its retention capacity with the same volume fraction.

2.4.2 Effect of diamond orientations

The effect of orientation of the diamond particles on their retention capacity is studied in this section for all seven particle shapes shown in Fig. 2.11a. The diamond particle size and material properties are same as those used in the previous section. For all these particle shapes, four different orientations are studied which are obtained by rotating the particles about their centres which are held at their initial position. In order to get the four orientations, the particles are rotated with an equal increment which is one-fourth of the angle between the radial lines passing through two adjacent corners as shown in Fig. 2.17a. It should be noted that this angle is different for the different shapes (e.g., $90^0/4 = 22.5^0$ for the square particle whereas $60^0/4 = 15^0$ for the hexagonal particle) and its value decreases with the increase of the number of sides of the particles. Fig. 2.17a also shows the position of all these cases where the force or rather the horizontal displacement is imposed gradually. The finite element meshing of the diamond-matrix system for a sample particle shape (square) is shown in Fig. 2.17b for its four different orientations.

Similarly, the results are shown as equivalent von-Mises stress in Fig. 2.17c which is obtained at the instant of interface failure (at the onset of the peak value of the cutting force).

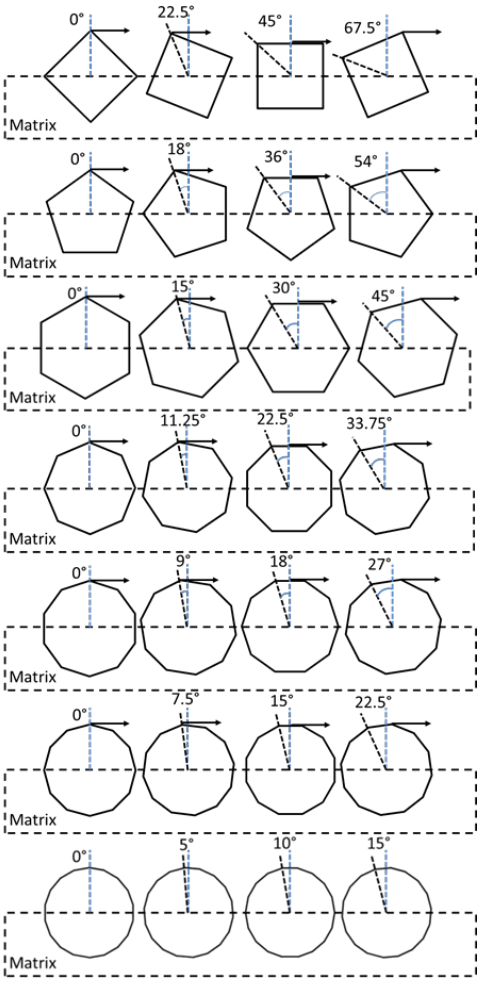

(a) Orientations of the diamond particles having different shapes

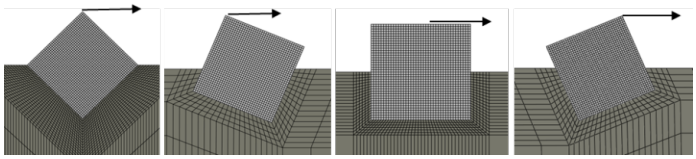

(b). Finite element meshing of the square shaped particle for different orientations

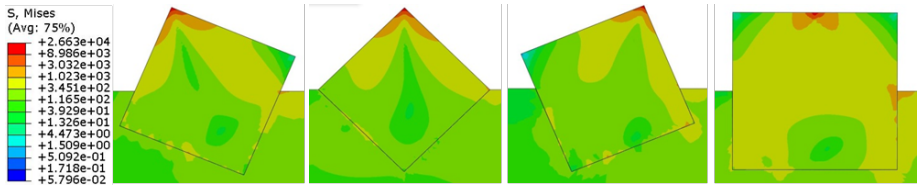

(c) Von-Mises stress distribution of the system having the square particle

Fig. 2.17 Diamond particles with different orientations.

The critical forces corresponding to the interface failure of all these cases obtained from the present analysis are reported in Table 2.3. The table shows that the retention capacity of diamonds is greatly affected by the orientation of diamond grits. For the different particle shapes, the variation of retention capacities of these grits due to their orientations is shown in terms of its highest and lowest values in Fig. 2.18. It can be seen from this figure that the square and decagon shaped particles achieved their highest retention capacities when they are having an orientation of 45° and 18° respectively which correspond to a situation of wear flat when a flat edge is utilised for cutting. The orientation has the highest influence for the square shaped diamond whereas this is lowest for the dodecagon shaped particle. However, the enhancement of diamond retention capacity with a wear flat situation is not desirable as the efficiency of the entire drilling process is also dependent on the sharpness of the cutting surface. Thus the four orientations are divided into two categories entitled as sharp and blunt where the blunt category (last column) corresponds to wear flat scenario which is not acceptable even it gives a higher diamond retention capacity. It is interesting to note that the hexagon shaped diamond particle has a relatively higher retention capacity when it has an orientation of 0° (sharp cutting surface) and a lower retention capacity for an orientation that makes the cutting surface blunt.

Table 2.3 Critical forces for the onset of interfacial failure.

Cutting surface	Sharp			Blunt
Orientation (Square)	0°	22.5°	67.5°	45°
Interfacial Failure Force (N)	61.2	60.1	44.9	100
Orientation (Pentagon)	0°	18°	54°	36°
Interfacial Failure Force (N)	66.5	42	70.1	67.8
Orientation (Hexagon)	0°	15°	45°	30°
Interfacial Failure Force (N)	86.5	48.1	66.7	72.9
Orientation (Octagon)	0°	11.25°	33.75°	22.5°
Interfacial Failure Force (N)	68.4	63.6	60.5	89.8
Orientation (Decagon)	0°	9°	27°	18°
Interfacial Failure Force (N)	88.3	81.9	64.6	100.8
Orientation (Dodecagon)	0°	7.5°	22.5°	15°
Interfacial Failure Force (N)	82.3	79.1	81.6	84.4
Orientation (Octadecagon)	0°	5°	15°	10°
Interfacial Failure Force (N)	80.6	56.2	60.7	62.3

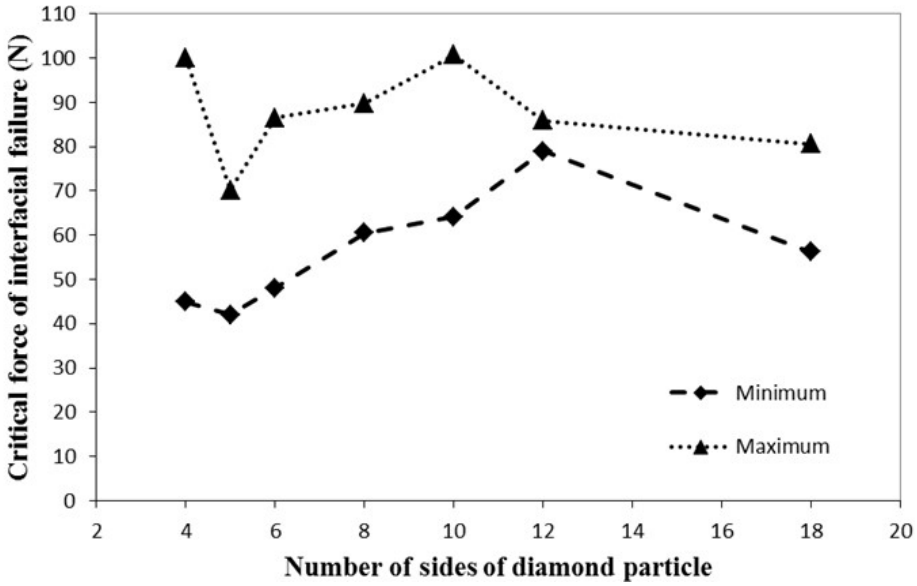

Fig. 2.18 Effect of orientations and shapes of diamonds on their retention capacity.

2.4.3 Effect of diamond protrusion (particle wear and matrix wear)

The wear of diamond bits is a complex process and it depends on a number of parameters associated with different operating conditions encountered while cutting different types of rocks. The material properties of diamond and matrix used in this section are same as those provided in section 2. The metal matrix is likely to wear faster while cutting soft rocks consists of coarser loosely cemented particles. In contrast, it would wear slower while cutting hard rocks consist of finer particles. As a result of these, different protrusion levels of diamond grits (heights of the exposed part of the particles) can be obtained during the cutting operation. Since the protrusion of diamond grits depends on the diamond wear as well as the matrix wear, the effect of both these wear mechanisms is studied. In order to assess the contribution of the individual mechanisms, they are incorporated in the present numerical model separately as shown in Fig. 2.19. A regular quadrilateral shaped diamond particle with a symmetric orientation and symmetric matrix/diamond wear are taken to avoid the influence of other parameters on the effect of diamond protrusions.

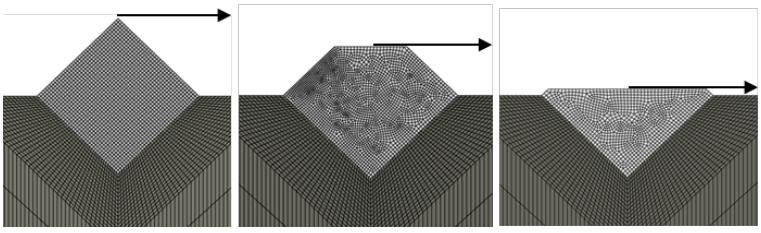

(a) Different protrusions due to particle wear (symmetric)

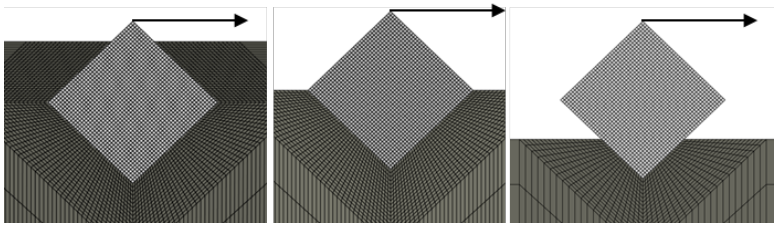

(b) Different protrusions due to matrix wear (symmetric)

Fig. 2.19 Interface failure influenced by (a) diamond wear and (b) matrix wear.

In the present study, thirteen different cases of protrusion levels are considered where seven cases are due to the diamond wear (from 0.0197mm to 0.25mm of protrusion height) and six cases are due to matrix wear (from 0.0625mm to 0.375mm of protrusion height). The critical forces corresponding to the initiation of interface debonding for all these cases predicted by the present numerical model are shown in Fig. 2.20. The results indicate that the critical force decreases with the increase of protrusion height in all cases as expected. In most of these cases, the critical force is same as the ultimate force required for the complete pull out of the diamond grit except the cases of the lower level of matrix wear (up to 0.25mm) where the load carrying capacity of the particle increases steadily after the initiation of interface debonding. This is due to a strong mechanical interlocking provided the matrix which holds the particle in its position and does not allow a complete pull out of the particle. Moreover, Fig. 2.20 shows that the critical force for the matrix wear is relatively higher than that of diamond wear when protrusion level is up to 0.25mm and same for both types of wear. The numerical results are reasonably intuitive which indicates that if the matrix wear rate is too high compared with the diamond wear rate, the diamond will have premature fall out before utilising the full capacity of the diamond which will significantly affect the efficiency of the diamond bit.

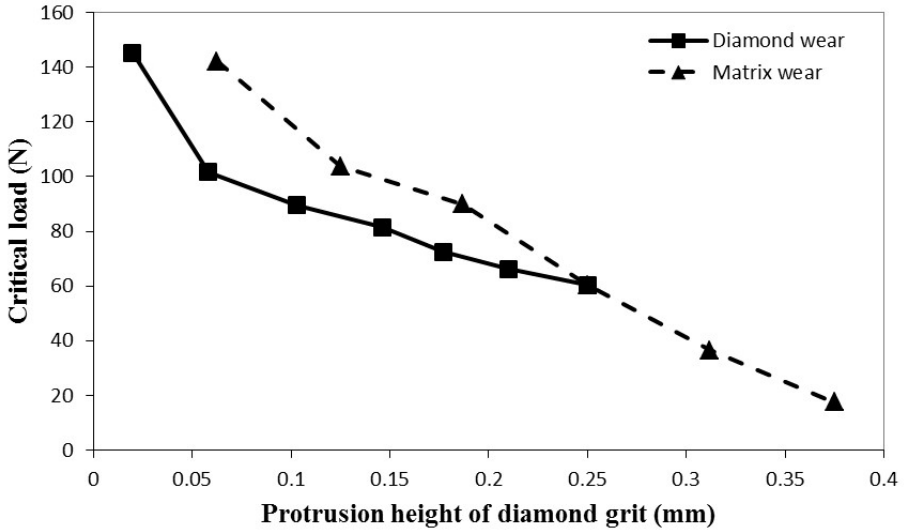

Fig. 2.20 Effect of diamond/matrix wear on critical load for interface failure.

2.4.4 Multiple diamond particles and their interactions

In order to study the interaction of neighbouring particles, a typical example of a diamond bit consists of five diamond particles having identical shapes and protrusions as shown in Fig. 2.21 is considered in this section. The material properties of the matrix as well as diamonds, and their sizes and loading are same as those used in Section 4.3. The diamonds are having an equal spacing (S) which is varied from 1mm to 8mm to show the effect of this spacing on the retention capacity of these diamond particles. The critical loads corresponding to the interface failure of these diamond particles (Fig. 2.21) obtained for four different values of their spacing (S) are presented in Table 2.4. The results clearly show that the interaction between the particles is reduced once the spacing between the particles is increased.

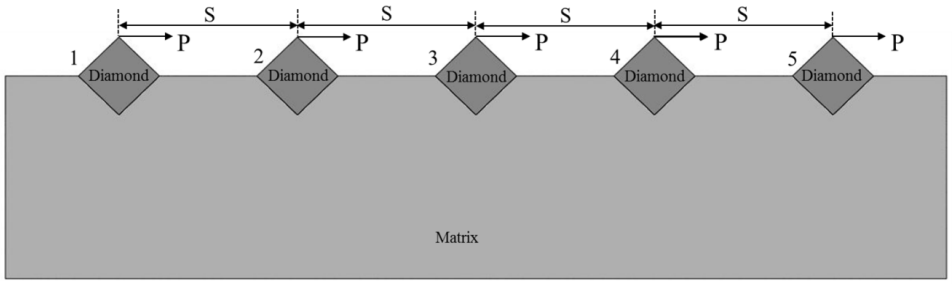

Fig. 2.21 Multiple diamond particles with equal spacing (S).

Table 2.4 Variation of critical load with respect to spacing between diamonds.

	Critical Load P (N)				
	Diamond 1	Diamond 2	Diamond 3	Diamond 4	Diamond 5
Case 1 (S=1mm)	42.8	65.1	63.7	62.2	75.9
Case 2 (S=2mm)	50.4	49.3	60.5	66.1	66.2
Case 3 (S=4mm)	62.3	62.2	61	63.1	66
Case 4 (S=8mm)	59.5	60.2	60.8	61.4	61.2

2.4.5 Effect of interface properties

The interface properties can be affected by several reasons associated with the sintering process and type of metal matrix. As discussed earlier, the cohesive zone model is used for simulating the interface failure and the cohesive model is characterised by four parameters. In order to investigate the effect of these interface parameters, four different cases having different values of these parameters (Table 2.5) are considered in the present study. For this purpose, four different shapes of the diamond particle are used which are square, pentagon, hexagon and decagon (Fig. 2.11a).

Table 2.5 Four case studies of different interfacial parameters.

	Mode I		Mode II	
	Ultimate stress (τ_n^0)	Fracture stress (G_{IC})	Ultimate stress (τ_n^0)	Fracture stress (G_{IIC})
Case 1	543 MPa	0.14 mJ/mm^2	314 MPa	0.33 mJ/mm^2
Case 2	271.5 MPa	0.07 mJ/mm^2	314 MPa	0.33 mJ/mm^2
Case 3	543 MPa	0.14 mJ/mm^2	157 MPa	0.165 mJ/mm^2
Case 4	271.5 MPa	0.07 mJ/mm^2	157 MPa	0.165 mJ/mm^2

The variation of critical force corresponding to the initiation of interface failure with respect to the number of sides of the diamond particles is plotted in Fig. 2.22 for the four different combinations of the interfacial properties (Table 2.5). It can be seen from the figure that the value of critical force decreases steadily with the decrease of interfacial strength as well as the fracture toughness values. However, the contribution of the Mode I properties is more than that of the Mode II properties. This difference is specifically quite big for square and pentagonal shape of the diamond grit. The figure shows that a highest critical force is found for all the particle shapes when the value of all interface properties is higher (Case 1, Table 2.5) whereas a lowest critical force is found when the value of all interface properties is lower (Case 4, Table 2.5). Thus, the interface properties are dominant parameters for the retention ability of diamond particles.

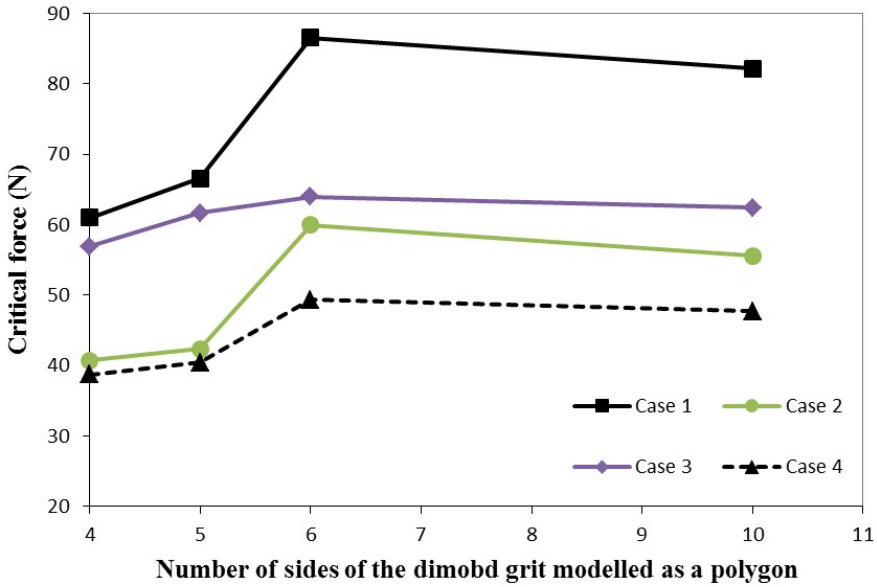

Fig. 2.22 Effect of interface properties on the critical load for interface failure.

2.5 Conclusions

In this paper, a failure analysis of diamond impregnated bits found in the form of particle composite materials is attempted for the first time. The present study has a focus on the interfacial failure mechanism between the matrix and diamond particles. This provides the vital understanding of diamond pull out mechanism which is one of the significant failure modes of diamond bits. For this purpose, a single diamond particle along with a portion of the surrounding matrix is used as a representative part of diamond bits. The diamond is subjected to a tangential force at its tip which simulates the cutting force whereas the matrix is restrained at its far ends. The finite element modelling is used to simulate the diamond matrix system where 4 node plane strain quadrilateral elements are used for the diamond and matrix materials. A zero thickness surface based cohesive zone modelling technique is used to simulate the failure at the interface between the matrix and the diamond.

In order to validate the finite element model and investigate its performance, numerical examples are solved and the results produced by the finite element

model are compared with the results available in the literature. The performance of the model is found to be good in the majority of these test problems which include interfacial stress analysis of diamond impregnated bits, and de-bonding simulations of a double cantilever beam and mixed-mode bending tests. Based on the confidence gained from the observation, the present model is used to conduct a parametric study for the critical force prediction of the interface failure initiation of diamond impregnated bits.

It has been observed that the shapes, orientations and protrusions of diamond particles, and interfacial properties have a significant influence on the retention capacity of diamond particles. As the efficiency of the entire drilling process is also dependent on the sharpness of the cutting surface, the hexagon shaped diamond particle is found to have a better performance for drilling because it has a relatively higher retention capacity when it is under sharp cutting face. The results also indicate that the critical force decreases with the increase of protrusion height in all cases. It is also observed that the interface properties are the dominant parameters for the retention ability of diamond particles as the value of critical force decreases steadily with the decrease of interfacial strength as well as the fracture toughness values, and the contribution of the Mode I properties is more than that of the Mode II properties.

Acknowledgement

The work has been supported by the Deep Exploration Technologies Cooperative Research Centre whose activities are funded by the Australian Government's Cooperative Research Centre Programme. This is DET CRC Document 2016/890.

References for Chapter 2

ANDREW, W. 1998. *Cemented Tungsten Carbides: Production, Properties and Testing; 1998,* Norwich, NY, USA.

BARENBLATT, G. I. 1962. Advances in Applied Mechanics. *Academic Press, New York***,** pp. 55.

BUSCH, D. M. & HILL, B. S. 1975. *Concrete Drilling with Diamond Impregnated Bits*, De Beers Industrial Diamond Division.

CAMANHO, P. P., DÁVILA, C. G. & DE MOURA, M. F. 2003. Numerical simulation of mixed-mode progressive delamination in composite materials. *Journal of Composite Materials,* 37**,** 1415-1438.

CAVALLI, M. N. 2003. Cohesive Zone Modelling of Structural Joint Failure. *Ph.D. Thesis, University of Michigan*.

CHALKLEY, J. R. & THOMAS, D. M. 1969. The tribological aspects of metal bonded diamond grinding wheels. *Powder Metallurgy,* 12(24)**,** 582-597.

CHOU, Y. K. & LIU, J. 2005. CVD diamond tool performance in metal matrix composite machining. *Surface and Coatings Technology,* 200**,** 1872-1878.

CREWS, J. J. H. & R., R. J. 1998. A Mixed-Mode Bending Apparatus for Delamination Testing. NASA Langley Technical Report Server.

CUI, W. & WISNOM, M. R. 1993. A combined stress-based and fracture-mechanics-based model for predicting delamination in composites. *Composites,* 24**,** 467-474.

DE BORST, R. & ROTS, J. G. 1989. Occurence of Spurious Mechanisms in Computation of Strain-Softening Solids. *Engineering Computations,* 6**,** 272-280.

DE MORAIS, A. B., DE MOURA, M. F., MARQUES, A. T. & DE CASTRO, P. T. 2002. Mode-I interlaminar fracture of carbon/epoxy cross-ply composites. *Composites Science and Technology,* 62**,** 679-686.

ELICES, M., GUINEA, G. V., GÓMEZ, J. & PLANAS, J. 2002. The cohesive zone model: advantages, limitations and challenges. *Engineering Fracture Mechanics,* 69**,** 137-163.

GONÇALVES, J. P. M., MOURA, M. F. S. F. D., CASTRO, P. M. S. T. D. & MARQUES, A. T. 2000. Interface element including point-to-surface constraints for three-dimensional problems with damage propagation. *Engineering Computations,* 17**,** 28-47.

GRASSI, M. & ZHANG, X. 2003. Finite element analyses of mode I interlaminar delamination in z-fibre reinforced composite laminates. *Composites Science and Technology,* 63**,** 1815-1832.

HSIEH, Y.-Z. & LIN, S.-T. 2001. Diamond tool bits with iron alloys as the binding matrices. *Materials Chemistry and Physics,* 72**,** 121-125.

HUANG, J. S. & GIBSON, L. J. 1993. Elastic moduli of a composite of hollow spheres in a matrix. *Journal of the Mechanics and Physics of Solids,* 41**,** 55-75.

JAENSSON, B. O. & SUNDSTRÖM, B. O. 1972. Determination of Young's modulus and poisson's ratio for WC Co alloys by the finite element method. *Materials Science and Engineering,* 9**,** 217-222.

KONSTANTY, J. 1999. Developing a better understanding of the bonding and wear mechanisms involved in using diamond impregnated tools. *In Proceedings of International Workshop on Diamond Tool Production, Turin, Italy***,** pp. 97-106.

KONSTANTY, J. 2005a. Chapter 3 - Diamond tool design and composition. *In:* KONSTANTY, J. (ed.) *Powder Metallurgy Diamond Tools.* Amsterdam: Elsevier Science.

KONSTANTY, J. 2005b. *Powder Metallurgy Diamond Tools*, Elsevier Science & Technology Books.

LEVIN, E. & GUTMANAS, E. Y. 1990. Solid-state bonding of diamond to Nichrome and Co-20wt% W alloys. *Journal of Materials Science Letters,* 9**,** 726-730.

LI, B., AMARAL, P. M., REIS, L., ANJINHO, C. A., ROSA, L. G. & FREITAS, M. D. 2010. 3D-modelling of the local plastic deformation and residual stresses of PM diamond–metal matrix composites. *Computational Materials Science,* 47**,** 1023-1030.

LIAO, Y. S. & LUO, S. Y. 1992. Wear characteristics of sintered diamond composite during circular sawing. *Wear,* 157**,** 325-337.

LIN, C.-S., YANG, Y.-L. & LIN, S.-T. 2008. Performances of metal-bond diamond tools in grinding alumina. *Journal of Materials Processing Technology,* 201**,** 612-617.

M. ALFANO, F. F., A. LEONARDI, C. MALETTA AND G. H. PAULINO 2007. Cohesive Zone Modeling of Mode I Fracture in Adhesive Bonded Joints. *Key Engineering Materials,* 348-349**,** 13-16.

MILLER, D. & BALL, A. 1990. Rock drilling with impregnated diamond microbits—An experimental study. *International Journal of Rock Mechanics and Mining Sciences & Geomechanics Abstracts,* 27**,** 363-371.

MILLER, D. & BALL, A. 1991. The wear of diamonds in impregnated diamond bit drilling. *Wear,* 141**,** 311-320.

PAONE, J. & MADSON, D. 1966. *Drillability Studies: Impregnated Diamond Bits*, Department of the Interior, Bureau of Mines.

RINDERKNECHT, S. & KRÖPLIN, B. 1997. A computational method for the analysis of delamination growth in composite plates. *Computers & Structures,* 64**,** 359-374.

ROMANSKI, A. 2010. Factors affecting diamond retention in powder metallurgy diamond tools. *Archives of Metallurgy and Materials,* 55**,** 1073-1081.

SCOTT, P. M., NICHOLAS, M. & DEWAR, B. 1975. The wetting and bonding of diamonds by copper-base binary alloys. *Journal of Materials Science,* 10**,** 1833-1840.

SHAMS, A. & PORFIRI, M. 2014. Analysis of particle–matrix interfacial debonding using the proper generalized decomposition. *Composite Structures,* 111**,** 602-618.

SUH, C.-M., BAE, K.-S. & SUH, M.-S. 2008. Wear behavior of diamond wheel for grinding optical connector ferrule — FEA and wear test —. *Journal of Mechanical Science and Technology,* 22**,** 2009-2015.

TAGLIAVIA, G., PORFIRI, M. & GUPTA, N. 2010. Analysis of hollow inclusion–matrix debonding in particulate composites. *International Journal of Solids and Structures,* 47**,** 2164-2177.

TURON, A., DÁVILA, C. G., CAMANHO, P. P. & COSTA, J. 2007. An engineering solution for mesh size effects in the simulation of delamination using cohesive zone models. *Engineering Fracture Mechanics,* 74**,** 1665-1682.

TZE-PIN, L., HOOD, M., COOPER, G. A. & XIAOHONG, L. 1992. Wear and failure mechanisms of polycrystalline diamond compact bits. *Wear,* 156**,** 133-150.

XUEFENG, T. & SHIFENG, T. 1994. The wear mechanisms of impregnated diamond bits. *Wear,* 177**,** 81-91.

ZHAI, J. & ZHOU, M. 2000. Finite element analysis of micromechanical failure modes in a heterogeneous ceramic material system. *International Journal of Fracture,* 101**,** 161-180.

ZHOU, Y., FUNKENBUSCH, P. D. & QUESNEL, D. J. 1997. Stress distributions at the abrasive-matrix interface during tool wear in bound abrasive grinding—a finite element analysis. *Wear,* 209**,** 247-254.

Chapter 3

3-D Finite element modelling of diamond pull-out failure in impregnated diamond bits

(Journal Paper 2)

J. Xu, A.H. Sheikh and C. Xu

School of Civil, Environmental and Mining Engineering, the University of Adelaide, Australia

Publication:

J. Xu, A.H. Sheikh, C. Xu. (2016). 3-D Finite element modelling of diamond pull-out failure in impregnated diamond bits. *Diamond and Related Materials*, http://dx.doi.org/10.1016/j.diamond.2016.11.006

Statement of Authorship

Title of Paper	3-D Finite element modelling of diamond pull-out failure in impregnated diamond bits
Publication Status	☑ Published ☐ Accepted for Publication ☐ Submitted for Publication ☐ Unpublished and Unsubmitted w ork w ritten in manuscript style
Publication Details	J. Xu, A.H. Sheikh, C. Xu. (2016). 3-D Finite element modelling of diamond pull-out failure in impregnated diamond bits. *Diamond and Related Materials*, http://dx.doi.org/10.1016/j.diamond.2016.11.006

Principal Author

Name of Principal Author (Candidate)	Jiayi Xu
Contribution to the Paper	Undertook literature review, developed analytic procedure and numerical models, performed analysis on different parameters and prepared manuscript.
Overall percentage (%)	80%
Certification:	This paper reports on original research I conducted during the period of my Higher Degree by Research candidature and is not subject to any obligations or contractual agreements with a third party that would constrain its inclusion in this thesis. I am the primary author of this paper.
Signature	Date 30/11/2016

Co-Author Contributions

By signing the Statement of Authorship, each author certifies that:

i. the candidate's stated contribution to the publication is accurate (as detailed above);

ii. permission is granted for the candidate in include the publication in the thesis; and

iii. the sum of all co-author contributions is equal to 100% less the candidate's stated contribution.

Name of Co-Author	Abdul Hamid Sheikh
Contribution to the Paper	Supervised development of numerical models, helped manuscript preparation, reviewed and corrected draft of the manuscript.
Signature	Date 30/11/2016

Name of Co-Author	Chaoshui Xu
Contribution to the Paper	Supervised development of work, helped to evaluate and edit the manuscript.
Signature	Date 30/11/2016

Please cut and paste additional co-author panels here as required.

Abstract

In this study, the finite element technique is used to analyse the failure mechanisms of impregnated diamond bits. The diamond bit is established as particulate composites consist of diamond particles, with variant sizes and shapes, randomly distributed within a metal matrix for hard rock drilling. Investigations are carried out using a 3-D numerical model of diamond particles embedded in a metal matrix. This study mainly focuses on the interfacial debonding behaviour between diamond particles and the matrix for the assessment of diamond retention capacity of the drill bit. A zero thickness surface based on cohesive zone modelling technique is used to simulate the failure at the interface. In order to validate the present model, several example problems are solved by the method. The solutions are compared with published results and a good agreement is observed. The effects of the shape and orientation of diamond particles as well as the interface properties on the retention capacity of diamond particles in the drill bit are investigated with the help of a parametric study.

***Keywords*:**

Interface debonding; Impregnated diamond tools; Rock cutting; Cohesive zone modelling; Finite element analysis; Fracture simulation

3.1 Introduction

Impregnated diamond core (IDC) bits have been widely employed for rock cutting and drilling in the area of mining for mineral exploration over the last few decades (Miller and Ball, 1991). It is due to the unique characteristics of synthetic diamonds such as the extremely high hardness (Paone and Madson, 1966), as well as the high thermal conductivity, bulk modulus, critical tensile stress (Wang et al., 2002) and the low coefficient of friction and thermal expansion rate (Konstanty, 2005a). A typical IDC bit is composed of several segments that are made of large numbers of synthetic diamond particles having a size of the order of 100 microns which are thoroughly mixed with metal powders through the sintering process. During the drilling operation, the embedded diamond particles near the cutting surface are partially exposed due to gradual wear of the matrix material when the cutting surface of the bit slides over a rock due to rotation of the bit, and these exposed diamonds do the cutting or drilling of the rock. The matrix is expected to hold the freshly exposed sharp diamonds firmly and at the same time, it should wear at a rate compatible with that of diamonds so that the worn diamond can fall out to allow new diamonds to expose continuously (Scott et al., 1975), which is also known as their self-sharpening ability. Despite the success of IDC bits, their drilling efficiency is still low under some conditions due to the lack of fundamental understanding of the failure mechanisms inside the bit.

Xuefeng and Shifeng (1994), Miller and Ball (1990) conducted some experimental studies on IDC bits to investigate the wear mechanisms of those bits in the 1990s, and four distinct types of wear modes have been classified where the pull out of diamonds prior to reaching their full-service life is the most undesirable failure mode which can greatly impact the tool's cutting efficiency and increase the cost of drilling operation (Konstanty, 2005b). The retention ability of diamond grits is mainly affected by the mechanical and chemical bonding at the interface between the diamond and the surrounding matrix. In some cases, diamonds are mostly held by the matrix through mechanical interlocking which gives a low interfacial strength. Therefore,

many attempts have been made by researchers, (Scott et al., 1975) and (Levin and Gutmanas, 1990), to establish a strong bond between the matrix and diamonds by adding some alloys which react with carbons present in diamonds to form chemical bonding in the form of metal-carbide elements at the interface to improve the retention ability of diamonds. However, it has been found that the added chemically reactive materials in the metal matrix powder can cause severe surface degradation of diamonds and it is impracticable to prevent the graphitization of diamonds under sintering process (Konstanty, 2005b). Consequently, the technique of metal-coated diamonds has been invented and used which not only protects the diamonds from oxidisation but also increases their retention capacity (Wang et al., 2002). Tungsten and titanium have been widely used as coating materials for diamond grits, and it helps to form a thin film of metal-carbide at the interface that acts as a strong chemical bond between the matrix and diamonds (Konstanty, 2005, Lin et al., 2008).

Zhou et al. (1997) attempted to model the behaviour of diamond bits under drilling condition by conducting stress analysis at the diamond-matrix interface of a 2-dimensional finite element model without considering any failure or damage in the bit. This may be defined as a micromechanical modelling of the bits where the diamond is subjected to a horizontal cutting force only at its cutting tip. Zhou et al. (1997) plotted the variation of normal stress along the interface for different levels of matrix wear and these stress distributions were taken as the measure of interfacial debonding failure. Suh et al. (2008) conducted a similar study on diamond impregnated grinding wheel where they calculated the von Mises stress along the interface where they also studied the effect of unsymmetrical matrix wear with respect to the diamond particle. A 3-dimensional finite element model was presented by Li et al. (2010) who tried to predict the plastic deformation and residual stresses within the matrix near the diamond particle which is produced due to the sintering process. The main limitation of these models is that no one has paid any attention so far on the modelling of interfacial failure of this system. Although the interfacial crack propagation is a complex process for simulation,

it is necessary to conduct a proper model to analyse the interfacial debonding behaviour.

The concept of fracture mechanics, which can be implemented through finite element modelling, can be used to characterise the onset and growth of delamination. Based on that, the Virtual Crack Closure Technique (VCCT) has been incorporated into finite element codes for analysing composite delamination (Turon et al., 2007). However, it is not convenient for modelling crack propagation of IDC bits as VCCT requires pre-defining initial crack and re-meshing to advance the crack front when the energy release rate reaches its critical value (Rinderknecht and Kröplin, 1997). The cohesive zone modelling (CZM) technique became very popular in recent years for modelling crack onset and growth using traction-separation law that relates the opening displacement in the process zone to the resisting tractions. This technique needs the information of the crack propagation direction in advance which is the interface between the matrix and diamond in present problem. The traction-separation law is defined in each fracture mode by the initial elastic stiffness, the interfacial strength and the critical energy release rate or fracture energy (Barenblatt, 1962a).

This paper develops a three-dimensional finite element model incorporated with CZM technique to simulate the matrix diamond interfacial failure. This will help to understand the wear mechanism of impregnated diamond bits due to diamond pull out more accurately that can benefit the design of these bits. Moreover, there is a need for investigating the effect of different parameters such as protrusions, shapes and orientations of the diamond particle on its retention capacity which is undertaken in this research as this has not been studied previously

3.2 Finite element model

3.2.1 Failure model for the diamond-matrix interface

The concept of cohesive zone model (CZM) was proposed by Barenblatt (Barenblatt, 1962b) which is aiming to eliminate the crack tip stress singularity in the classical linear elastic fracture mechanics (LEFM). On the other hand, the LEFM is not computationally attractive for modelling the interfacial failure in the present study as the thickness of the interface is very small which needs a very fine mesh to capture the sudden variation of displacements and stresses within this small distance. Previous papers (Sørensen, 2002) and (B.F. Sørensen and Jacobsen, 2003) indicated that cohesive zone models can provide quantitatively predictive analyses for interfacial fracture of adhesively bonded composite joints. Thus, the CZM approach (Elices et al., 2002, M. Alfano, 2007) is the most appropriate technique to be adopted in the present study. In three-dimensional analysis, an interface has three possible modes of failure: 1) Mode I (opening mode) due to tensile stress acting normal to the interface, 2) Mode II (sliding mode) due to shear stress parallel to the interface and perpendicular to the crack front, and 3) Mode III (tearing mode) due to shear stress parallel to the interface and parallel to the crack front. Fig. 3.1 shows two elements connected with the cohesive surface under undeformed and deformed configurations where the top element represents the diamond part and the bottom element represents the matrix part. Four nodes linear tetrahedron elements are used to model both diamond and matrix in this study.

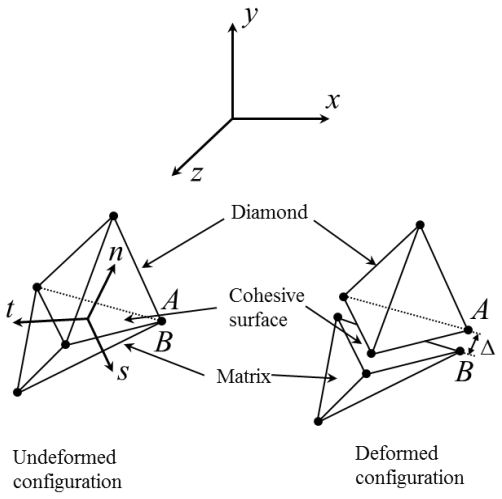

Fig. 3.1 Cohesive fracture separation (a) undeformed configuration and (b) deformed configuration.

The relative displacement vector $\{\Delta\}$ in global coordinates (x-y-z) at any point in the interface of deformed configuration can be expressed as:

$$\{\Delta\}=\begin{Bmatrix}\bar{x}\\ \bar{y}\\ \bar{z}\end{Bmatrix}=\begin{Bmatrix}x^{+}\\ y^{+}\\ z^{+}\end{Bmatrix}-\begin{Bmatrix}x^{-}\\ y^{-}\\ z^{-}\end{Bmatrix}=\sum_{i=1}^{4}N_i\begin{Bmatrix}x_i^{+}\\ y_i^{+}\\ z_i^{+}\end{Bmatrix}-\sum_{i=1}^{4}N_i\begin{Bmatrix}x_i^{-}\\ y_i^{-}\\ z_i^{-}\end{Bmatrix} \tag{3.1}$$

where x^{+} and x^{-} are the displacement components at the two sides of an interfacial point in the global x-direction whereas x_i^{+} and x_i^{-} are the corresponding displacements at the i-th node of the elements (Fig. 3.2) used to model the materials on the two sides of this interfacial point and N_i are the shape functions of these elements. This is similarly applicable to the displacement components in the global y-direction and z-direction. The components of $\boldsymbol{n}$, $\boldsymbol{s}$ and $\boldsymbol{t}$ (Fig. 3.2) represent the vectors in local coordinate system. Thus, the normal and tangential components of $\{\Delta\}$ with respect to the relative displacements in local coordinate system $\{\delta\}$ (Liao and Luo, 1992) can be obtained as:

$$\{\delta\} = \begin{Bmatrix} \delta_n \\ \delta_s \\ \delta_t \end{Bmatrix} = [Q]\{\Delta\} \tag{3.2}$$

where $[Q]$ is the transformation matrix from the global to a local coordinate system. The CZM approach assumes that the interface has no thickness and the formulation is based on traction-separation relationship, shown in Fig. 3.2. Fig. 3.2 shows the traction-separation ($\tau - \delta$) law where OA denotes the elastic response of the interface having a high stiffness of K and AB represents the interfacial damage in the form of a linear softening law. The ultimate stress τ^0 represents the damage initiation point where the area under of the triangle OAB illustrates the fracture toughness G_c. The separations indicate the relative displacements between the diamond and the matrix (Fig. 3.1) at their interface whereas the tractions are simply the interfacial stresses.

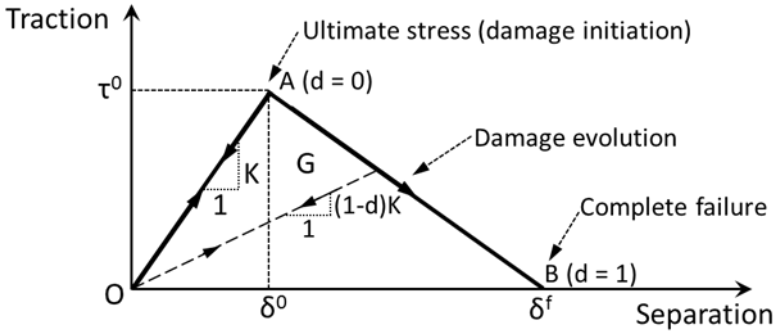

Fig. 3.2 A typical bilinear traction-separation relationship.

The CZM approach requires an incremental (iterative) procedure for solving the governing equations. As the damage is an irreversible process, the solution technique dependent on the loading history. Thus, it is needed to store the maximum values of these relative displacements (δ_n^{max}, δ_s^{max} and δ_t^{max}) which calculated before in any increment (iteration) and they are updated in that increment as follows:

$$\text{If } \delta_n > \delta_n^{\max} \Rightarrow \delta_n^{\max} = \delta_n \text{ otherwise } \delta_n^{\max} = \delta_n^{\max} \tag{3.3}$$

$$\text{If } |\delta_s| > \delta_s^{\max} \Rightarrow \delta_s^{\max} = |\delta_s| \text{ otherwise } \delta_s^{\max} = \delta_s^{\max} \tag{3.4}$$

$$\text{If } |\delta_t| > \delta_t^{\max} \Rightarrow \delta_t^{\max} = |\delta_t| \text{ otherwise } \delta_t^{\max} = \delta_t^{\max} \tag{3.5}$$

For pure Mode I and pure Mode II or Mode III the tangential and normal components of the interfacial traction vector (τ_n , τ_s and τ_t) can be related to the maximum value of these relative displacements using the interfacial constitutive properties in the form of traction-separation law (Fig. 3.2) as:

$$\begin{aligned} \tau_n &= K_n \delta_n \text{ if } \delta_n^{\max} \le \delta_n^0 \\ \tau_n &= (1-d_n) K_n \delta_n \text{ if } \delta_n^0 < \delta_n^{\max} < \delta_n^f \\ \tau_n &= 0 \text{ if } \delta_n^{\max} \ge \delta_n^f \end{aligned} \tag{3.6}$$

$$\begin{aligned} \tau_s &= K_s \delta_s \text{ if } \delta_s^{\max} \le \delta_s^0 \\ \tau_s &= (1-d_s) K_s \delta_s \text{ if } \delta_s^0 < \delta_s^{\max} < \delta_s^f \\ \tau_s &= 0 \text{ if } \delta_s^{\max} \ge \delta_s^f \end{aligned} \tag{3.7}$$

$$\begin{aligned} \tau_t &= K_t \delta_t \text{ if } \delta_t^{\max} \le \delta_t^0 \\ \tau_t &= (1-d_t) K_t \delta_t \text{ if } \delta_t^0 < \delta_t^{\max} < \delta_t^f \\ \tau_t &= 0 \text{ if } \delta_t^{\max} \ge \delta_t^f \end{aligned} \tag{3.8}$$

For the bilinear softening law (Fig. 3.2), the damage parameters for these three modes of fracture may be written as:

$$d_n = \frac{\delta_n^f \left(\delta_n^{\max} - \delta_n^o\right)}{\delta_n^{\max} \left(\delta_n^f - \delta_n^o\right)},\ d_s = \frac{\delta_s^f \left(\delta_s^{\max} - \delta_s^o\right)}{\delta_s^{\max} \left(\delta_s^f - \delta_s^o\right)},\ d_t = \frac{\delta_t^f \left(\delta_t^{\max} - \delta_t^o\right)}{\delta_t^{\max} \left(\delta_t^f - \delta_t^o\right)} \tag{3.9}$$

The above equations (6), (7) and (8) can be used if the three modes of failure are independent having no coupling between them. However, due to the varying drilling conditions of the impregnated diamond bits, the matrix diamond interface is more likely to have a mixed-mode fracture where the

three modes of failure will be coupled as mentioned earlier. In that situation, the damage onset and its propagation may occur before reaching the ultimate stress of Mode I (τ_n^0), Mode II (τ_s^0) and Mode III (τ_t^0). Under mixed-mode failure scenario, a quadratic failure criterion proposed by Cui et al. (Cui and Wisnom, 1993) for the prediction of damage initiation is used in the present study and it is expressed as:

$$\left(\frac{\langle \tau_n \rangle}{\tau_n^0}\right)^2 + \left(\frac{\tau_s}{\tau_s^0}\right)^2 + \left(\frac{\tau_t}{\tau_t^0}\right)^2 = 1 \tag{3.10}$$

The power law [33] is used for the mixed-mode damage evolution of the interface which is expressed in terms of energy release rates (G_I, G_{II} and G_{III}) and their critical values (fracture toughness for these three modes) as:

$$\left(\frac{G_I}{G_{IC}}\right)^2 + \left(\frac{G_{II}}{G_{IIC}}\right)^2 + \left(\frac{G_{III}}{G_{IIIC}}\right)^2 = 1 \tag{3.11}$$

where $G_I = \int_0^{\delta_n^{\max}} \tau_n d\delta_n$, $G_{II} = \int_0^{\delta_s^{\max}} \tau_s d\delta_s$, $G_{III} = \int_0^{\delta_t^{\max}} \tau_t d\delta_t$ and $G_{IC} = \int_0^{\delta_n^f} \tau_n d\delta_n$, $G_{IIC} = \int_0^{\delta_s^f} \tau_s d\delta_s$, $G_{IIIC} = \int_0^{\delta_t^f} \tau_t d\delta_t$. In a mixed-mode failure analysis, the traction-separation relationship (Fig. 3.2) for the three modes are combined and expressed in terms of an equivalent traction-separation relationship having a similar bilinear shape which helps to implement the mixed-mode damage model conveniently. This combined traction-separation relationship will have a same initial stiffness (K) whereas the separation at the onset of damage initiation δ_m^0 and the separation at complete failure δ_m^f (subscript m indicates mixed-mode fracture) can be obtained from Equations (10) and (11) respectively (Camanho et al., 2003). In that case, the two components of the separation obtained in any incremental are to be combined to have single resultant component δ_m as:

$$\delta_m = \sqrt{\delta_n{}^2 + \delta_s^2 + \delta_t^2} \tag{3.12}$$

With the above equations, the stiffness matrix of the interface can be derived using Virtual Work Principles following the unusual steps of finite element technique.

3.2.2 Material model of the matrix, diamond and interface

In this study, diamonds are treated as elastic and isotropic materials due to their fragility. The Tungsten carbide cobalt (WC-Co) alloy is used as the matrix material which is having high wear resistance and hardness characteristics, as well as the strong bonding. The mechanical properties of diamond and matrix used in this study are shown in table 3.1, which are taken from experimental tests done by Field et al. (1986) and Jaensson et al. (1972) respectively. By assuming that toughnesses and strengths in Mode II and III are equal to each other and a high default value of the stiffness *K* is used, it is shown that the mixed-mode constitutive equations of the cohesive interface are defined by four material properties: G_{IC}, G_{IIC}, τ_n^0, and τ_s^0. Since there is no experimental method available to directly determine the interfacial parameters of diamond bits (Zhai and Zhou, 2000, Cavalli, 2003), the material properties of the matrix are taken as the interfacial material parameters which are illustrated in table 3.1. Elastic-plastic material properties of the matrix are used in some sample test cases where no significant effect of plasticity is observed.

Table 3.1 Mechanical properties of diamond, matrix and interface.

		E (GPa)		v
Diamond		1100		0.1
Matrix		600		0.2
	τ_n^0 (MPa)	τ_s^0 & τ_t^0 (MPa)	G_{IC} (mJ/mm^2)	G_{IIC} & G_{IIIC} (mJ/mm^2)
Interface	543	314	0.14	0.33

3.2.3 Material model of the matrix, diamond and interface

It is assumed that diamond particles are evenly distributed within the matrix and having adequate gaps between them so that stresses around these particles do not affect each other. This is true for most of the diamond bits as they are designed to have adequate service lives by avoiding non-uniform distribution of diamond grits which is responsible for localised stress concentration leading to premature failure of these bits. Similar to the previous researches (Zhou et al., 1997, Suh et al., 2008), the failure of diamond impregnated bits is modelled by taking a single diamond particle which is partially embedded within a portion of the matrix and cuts the rock with its exposed part during the drilling operation (Fig. 3.3). Fig. 3.3 illustrates different views of a typical IDC bit as well as its operational variables. Fig. 3.4 shows the developed three-dimensional micromechanical model of the IDC bit as well as its mesh and the shape of the diamond particle. This model has been used to predict the failure and stresses within the representative portion of the diamond bit mentioned above (Fig. 3.3d). For the convenience of representing and analysing the problem, the finite element model is drawn as a mirror image (upside down, Fig. 3.4) of the actual object (Fig. 3.3d) and a displacement load is imposed at the tip of the exposed part of the diamond particle to simulate the contact load between diamond and rock. As the fall-out of the diamond particle due to interfacial debonding are primarily facilitated by tangential cutting force, the model has predicted the cutting in the form of resisting force with respect to the imposed horizontal displacement.

According to previous researches (Xuefeng and Shifeng, 1994, Li et al., 2010), the typical size (in diameter) of synthetic diamond particles varies from 0.01 to 0.5 mm and this is taken as 0.5 mm in the present simulation. A regular octahedron shaped diamond particle (Fig. 3.4) has been assumed and used as a typical shape of the diamond in this study, and the radius of a circumscribed sphere of this octahedron particle is equal to 0.25 mm. Finer meshes are applied in the region of interest, which is in the vicinity of the interface between the diamond and matrix as shown in Fig. 3.4 as the stress intensity will occur at the interface area. The mesh convergence studies are performed for all models in this study to ensure a converged solution.

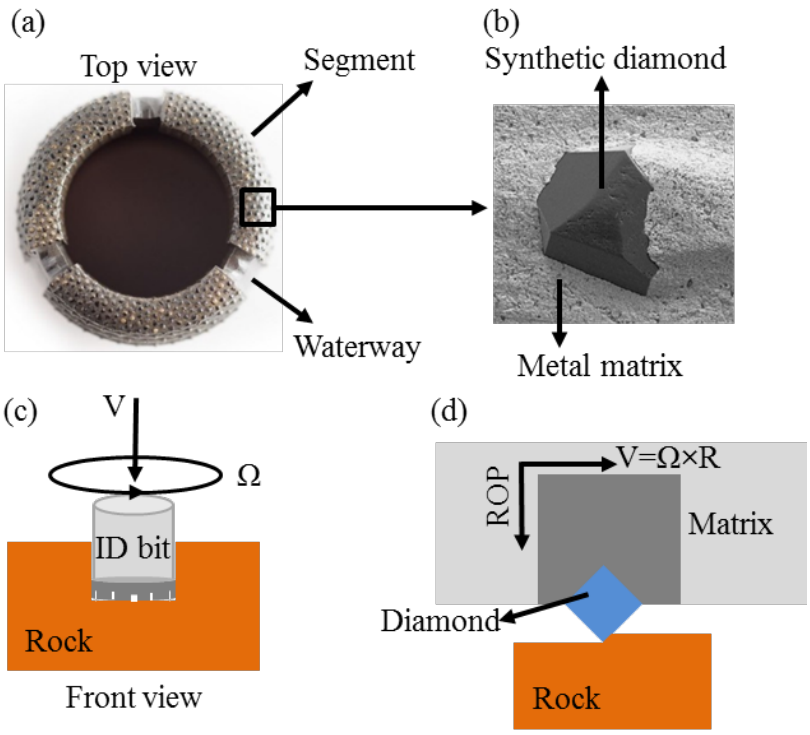

Fig. 3.3 Impregnated diamond core bit and its variables: (a) Top view, (b) SEM view of exposed diamond, (c) side view and (d) bit-rock interface view (2-D).

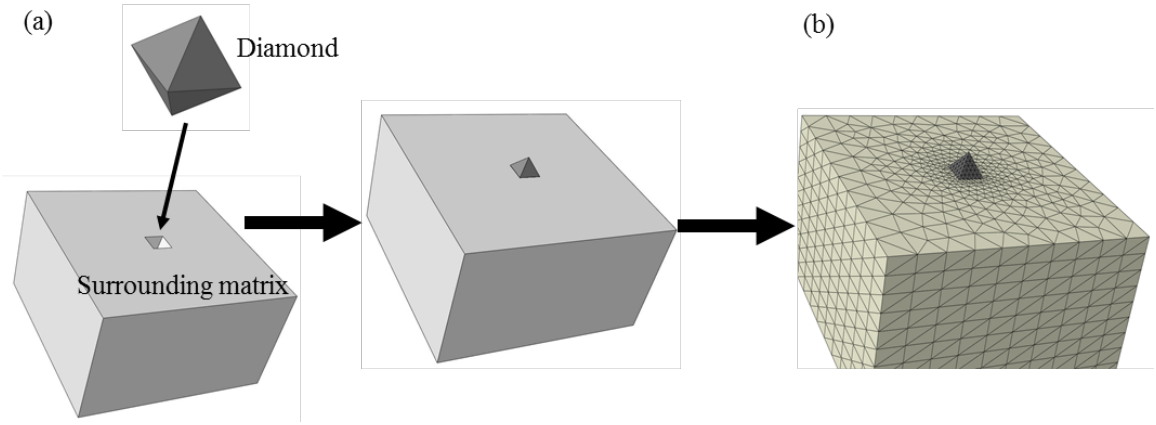

Fig. 3.4 3-D finite element model of the representative part of the IDC bit: (a) Diamond & Matrix parts and (b) mesh configuration of the model.

3.3 Validation of the numerical examples

Despite the behaviour of IDC bits have been studied by various researchers using both experimental tests (Miller and Ball, 1990, Liao and Luo, 1992) as well as numerical simulations (Zhou et al., 1997, Suh et al., 2008, Romanski, 2010), there is no experimental test data available for validation of the present model as no one attempted to determine the interfacial strength between diamond and matrix for any type of IDC bit. Thus, the available numerical results (Zhou et al., 1997, Suh et al., 2008) are utilised for a partial validation of the present model by taking a perfect diamond-matrix interface. The cohesive zone damage model used in the present analysis is indirectly validated with the experimental test results of a double cantilever beam (DCB) test and a mixed mode bending test (MMB).

3.3.1 Validation with available numerical researches

The first numerical example is taken from the paper of Zhou et al. (1997) who conducted a two-dimensional model of diamond-matrix system, shown in Fig. 3.5a, to analyse the stress distribution in the system with a constant cutting force (P = 2.5N) applied on the diamond particle. The diamond was

assumed as a square geometry with 0.015mm side length. The material properties used in the present finite element model are taken from the paper where the moduli of elasticity are 1141 GPa and 110 GPa for the diamond and the matrix (bronze) respectively, and the corresponding Poisson's ratios are 0.1 and 0.3. Three different levels of matrix wear are taken from the research (Zhou et al., 1997) (Fig. 3.5a) and they are denoted as case 1, case 2 and case 3. The finite element mesh used for three sample cases of matrix wear is shown in Fig. 3.5a, where a small part of the portion of the matrix considered in the present model is illustrated.

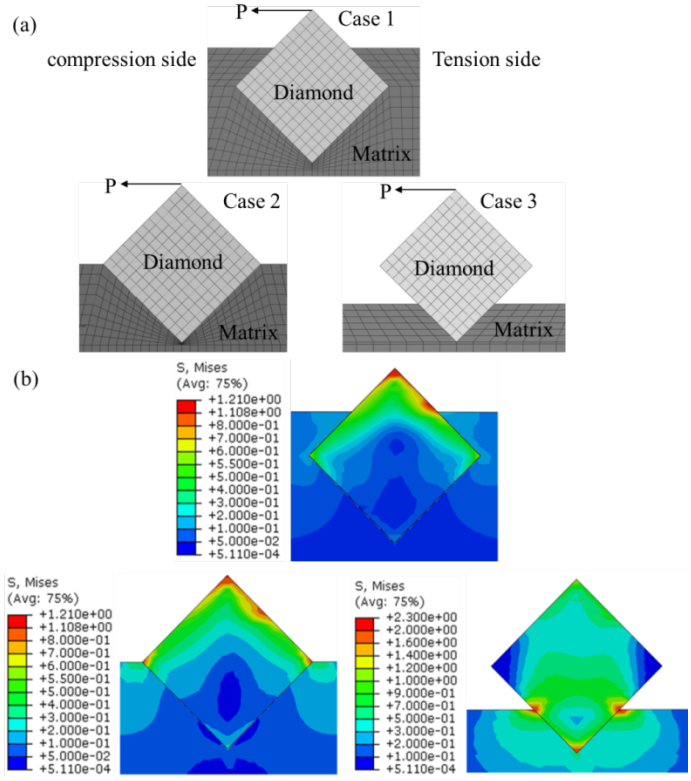

Fig. 3.5 Finite element model for different level of matrix wear: (a) Finite element meshing of the model geometry, (b) Distribution of the Von-Mises stress over the entire body.

Fig. 3.5b shows the variations of Von-Mises stress over the entire system predicted by the present finite element model. It could be noted that higher values of this stress component are concentrated at the tension and compression sides of the diamond-matrix interface near the exposed surface

of the matrix. According to the study by Zhou et al (1997). The normal stress (σ_n) at the centre of those elements, which are located on the tension side of the interface within the diamond particle, is computed by the stresses (σ_x, σ_y, σ_{xy}) at that point obtained in the present analysis. Based on these calculations, the variation of normal stress (σ_n) found along the interface on the tensile side of the diamond particle is plotted in Fig. 3.6. For the convenience of presentation, the distance along the interface, which is the horizontal axis in Fig. 3.6, is shown in terms of element numbers of the diamond particle where the number assigned to the lower corner element is 0 and the number incremented by one while moving along the interface on the tensile side following the direction of the arrow as shown. The figure shows that the matrix wear has a significant effect on the variation of interfacial normal stress. For the first case (Fig. 3.6), the maximum value of the normal stress is about 0.8 MPa which is found at element #17. For the third case study, the maximum/peak normal stress is found to be 1.25 MPa which indicates that it increases with the increase of the level of matrix wear. To conclude, the present results are found to have a very good agreement with those reported by Zhou et al. (1997). In order to study the effect of elastic-plastic effect of the metal matrix on the final result, a typical elastic-plastic material property (bronze) is used for the matrix, which the yield stress of 70 MPa, the ultimate stress of 220 MPa and the maximum plastic strain of 5% is used. The results indicate that there is no significant influence caused by introducing the elastic-plastic material properties of the matrix. Thus, the elastic material model for representing the behaviour of matrix seems to be adequate for the present problem and it is followed in this paper.

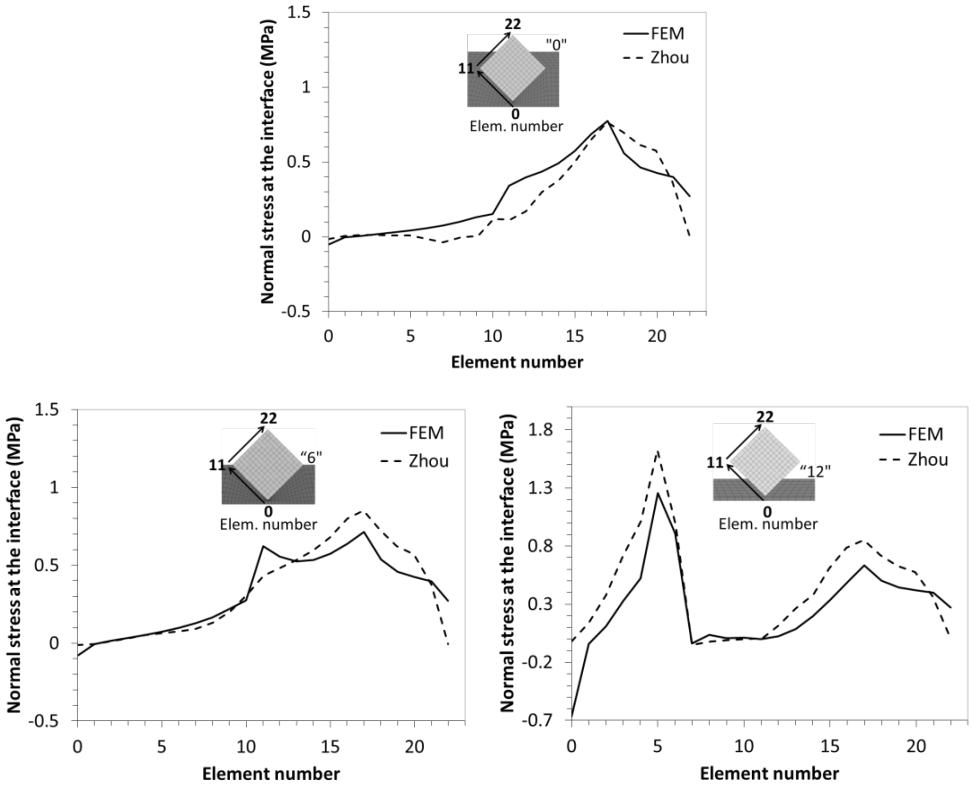

Fig. 3.6 Variation of normal stress along the interface as element centre stress in the diamond.

3.3.2 Validation of the interfacial damage model with a DCB test

The problem of a double cantilever beam (DCB) as shown in Fig. 3.7a is used in this section for an indirect validation of the interfacial damage model. It is well known that the DCB test is commonly used for evaluating the delamination resistance in Mode I direction of laminated composite materials. In present study, a DCB made of carbon-epoxy polymer that consists of the following material properties: $E_1 = E_2 = E_3 = 8E10^6$ MPa, $G_{12} = G_{13} = G_{23} = 4E10^6$ MPa, $\nu_{12} = \nu_{13} = \nu_{23} = 0$, 800 MPa, $G_{IC} = 1.2$ N/mm, $G_{IIC} = G_{IIIC} = 6$ N/mm, are used and a three-dimensional finite element model is developed for the DCB (Fig. 3.7b) with the damage model of surface based cohesive zone modelling at the interface between the two cantilever beams. The load-displacement (P-δ) curve obtained in the present analysis is plotted in Fig. 3.8

along with that calculated by Tada et al. (1985). The results indicate that the numerical result has a reasonable correlation with the result predicted by theory.

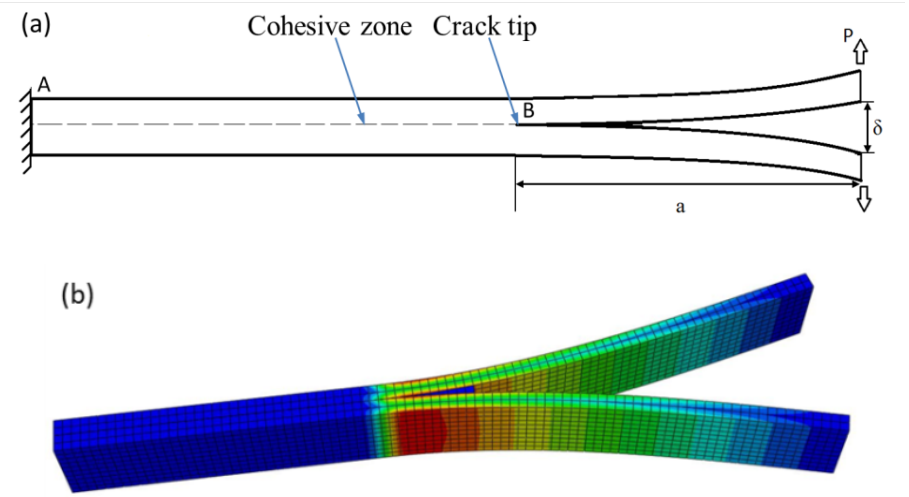

Fig. 3.7 Finite element model of DCB test: (a) Illustration of DCB test specimen and (b) 3-D model DCB.

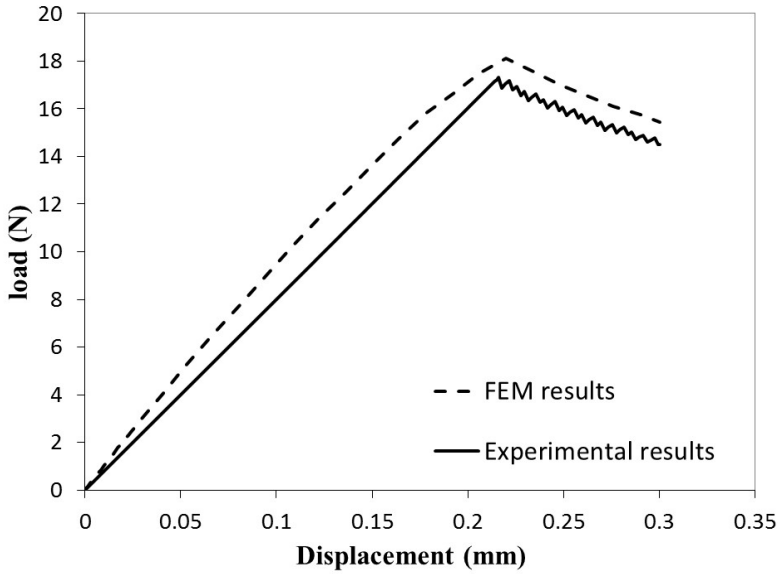

Fig. 3.8 Experimental and numerical results comparison for the three-dimensional DCB debonding.

3.3.3 Validation of the interfacial damage model with an MMB test

The experimental test reported by Crews et al. (1998) for a mixed-mode bending (MMB) test apparatus (Fig. 3.9a) made of AS4/PEEK carbon-fibre reinforced composite is used in the present study for the validation of the developed model. Table 3.2 shows the values of the dimensions as well as the material properties of the MMB test specimen. The different G_{II}/G_T ratios could be obtained by adjusting the loading position P (Fig. 3.9a) during the experimental test. A 3-D finite element model (Fig. 3.9b) of the MMB test is developed to simulate the failure mechanisms of the beam under various loading conditions (mixed-mode failure).

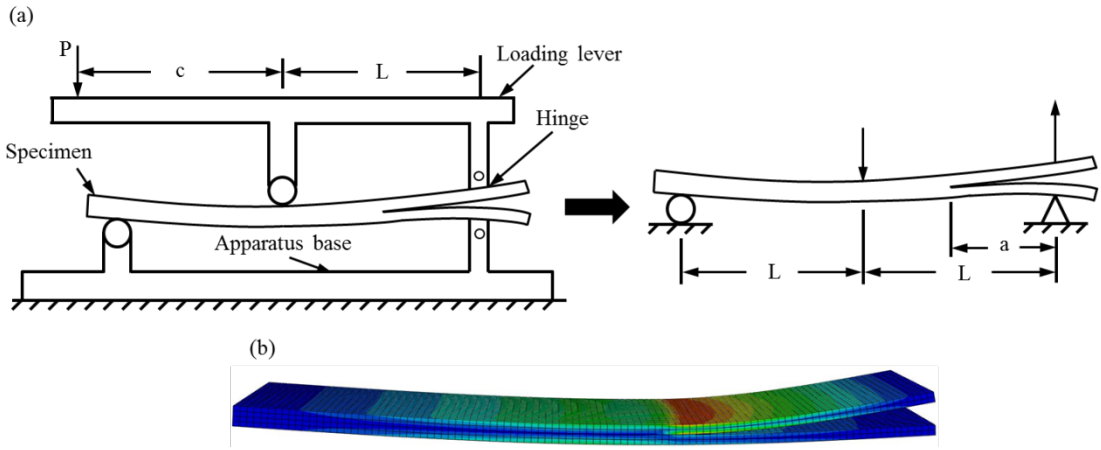

Fig. 3.9 Finite element model of MMB test: (a) Illustration of MMB apparatus and (b) 3-D model of MMB specimen.

Table 3.2 Mechanical properties of diamond, matrix and interface.

Specimen Dimension				
L (Length)	W (Width)	T (Thickness of one arm)		
102 mm	25.4 mm	1.56 mm		
Mechanical Material Properties				
E_{11}	$E_{22} = E_{33}$	$G_{12} = G_{13}$	G_{23}	$\nu_{12} = \nu_{13}$
122.7 GPa	10.1 GPa	5.5 GPa	3.7 GPa	0.25
ν_{23}	G_{IC}	G_{IIC}	T	S
0.45	0.969kJ/m^2	1.719 kJ/m^2	80 MPa	100 MPa

In this study, three different G_{II}/G_T ratios are simulated and compared with the experimental results, which are shown in Fig. 3.10. It can be seen that a good agreement between the numerical predictions and the experimental results is obtained.

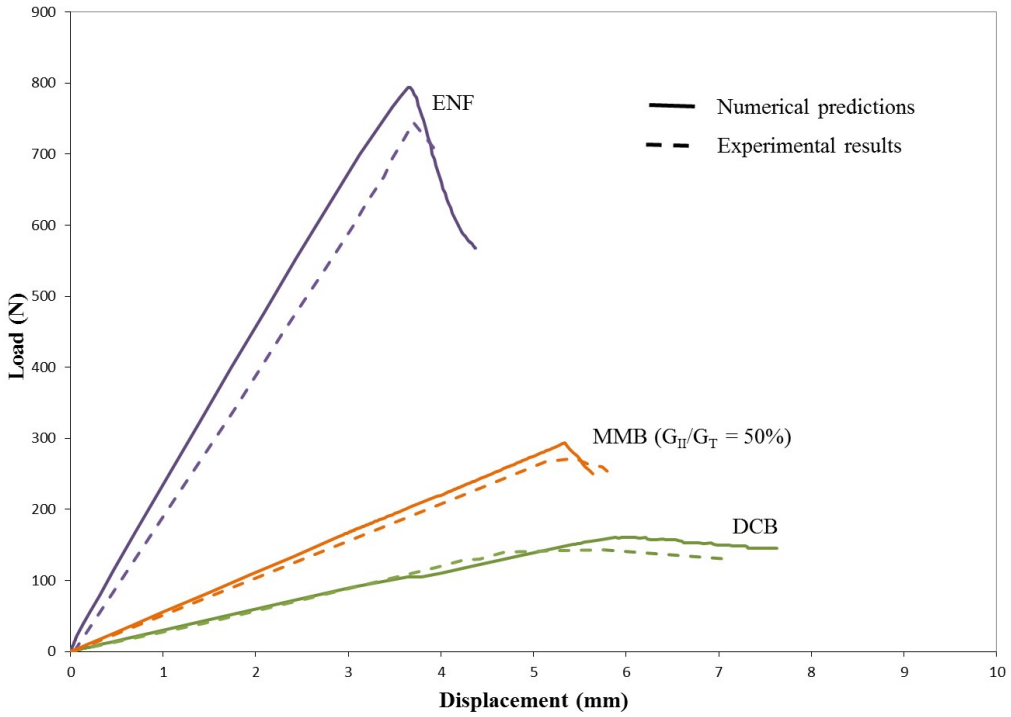

Fig. 3.10 Numerical and experimental comparison of the load-displacement response of MMB test.

3.4 Results and discussions of parametric study

The CZM is applied for the interfacial failure modelling of diamond-matrix system in this section, and a number of cases are investigated in the form of parametric study which including diamond shapes, diamond orientations, load directions and interfacial material properties. In order to have an understanding of the effect of an individual parameter, the value of that parameter is varied while the values of other parameters are kept unchanged.

3.4.1 Effect of diamond shapes with different load directions

The effect of diamond shapes on the retention capacity of diamond particles in ID bits is investigated in this section. Three different diamond shapes (Cube, Octahedron and Dodecahedron), shown in Fig. 3.11a, are built in the developed model and they are all regular polyhedrons with the same radius, r = 0.25 mm (radius of the circumscribed sphere), and same protrusion height, h = 0.25 mm (the portion of these diamonds above the exposed surface of the matrix). The material properties used are same as those provided in Table 3.1. The force is applied to these systems by imposing a gradual horizontal displacement at the tip (top corner) of the diamond, shown in Fig. 3.11a. However, the direction of the applied load can vary in the horizontal plane as the current model is in three-dimensional. Therefore, three different loading directions are applied for each diamond shape in this study to determine its effect on the retention ability of the diamond particles, shown in Fig. 3.11b. The finite element meshing used for modelling all these diamond-matrix systems is also shown in Fig. 3.11c. The distributions of von Mises stress (before interfacial failure) over the entire system of different diamond shapes are obtained and illustrated in Fig. 3.11d. As the stress distributions are taken before the complete debonding of the interface, the stress is concentrated at

the tipping point (loading point) of the diamond particle as well as the area around the interface.

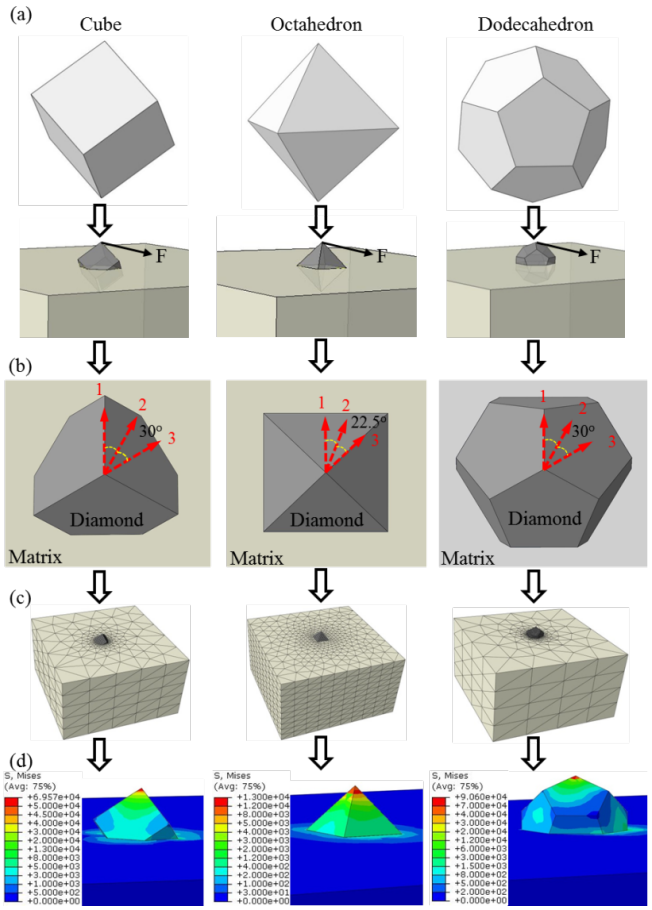

Fig. 3.11 Models for diamond particles with vertex-face toward upward: (a) different diamond shapes, (b) different horizontal loads from a top view, (c) finite element meshing and (d) Von-Mises stress distributions.

The force-displacement variations for three diamond shapes with three different loading directions are plotted in Fig. 3.12. The results indicate that the different load directions have only slight effects on the force-displacement response for all the three different diamond shapes shown in Fig. 3.11. For the cube-shaped particle, the results show that the forces are increased linearly at the start and the force-displacement ratio is dropped slightly after the failure of interfacial debonding, eventually, the force continues to increase without a drop. For the octahedron shaped particle, the forces drop to zero steadily after reaching its critical value. For the dodecahedron shaped particle, the forces

start increasing again after a brief decline. The critical force for interfacial failure is an important parameter to a designer as it indicates the retention capacity provided by the interface which is the primary focus of the present study.

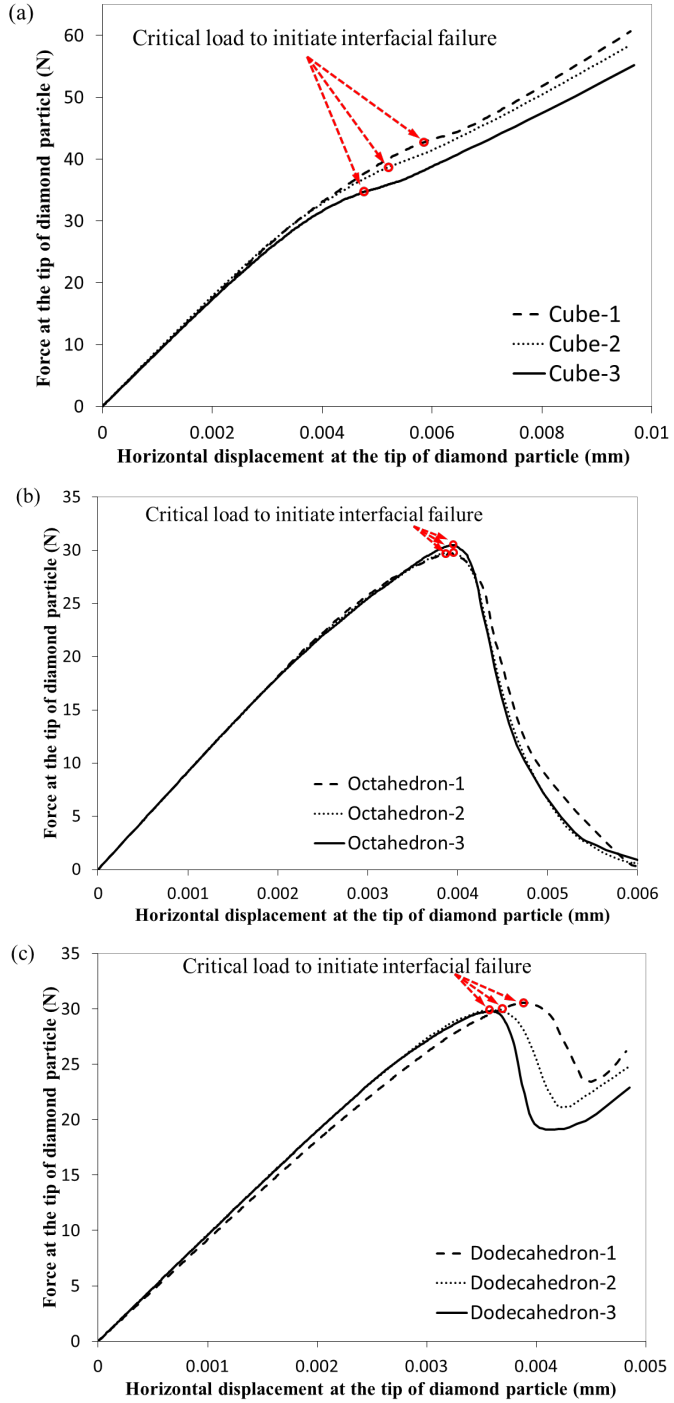

Fig. 3.12 Force-displacement variation at the tip of diamond particles with different load directions: (a) cube, (b) octahedron and (c) dodecahedron.

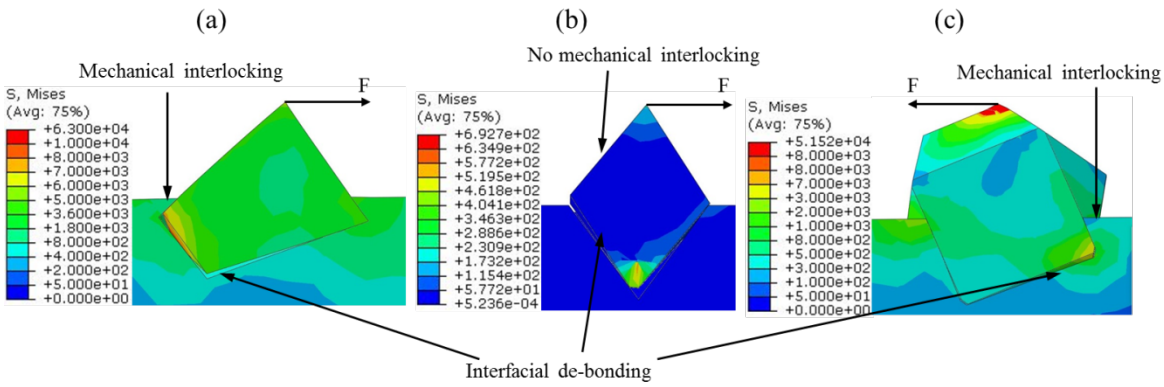

Fig. 3.13 Cut-out views of Von-Mises stress distribution of different diamond shapes: (a) Cube, (b) Octahedron and (c) Dodecahedron.

The critical forces corresponding to the initiation of the interfacial failure for all the cases from the present study are shown in Table 3.3.3. It can be seen that the cube-shaped diamond particle has the highest retention capacity (37.6 N) due to its stronger interfacial adhesion. The octahedron and dodecahedron shaped particles have similar critical values, which are 30 N and 30.9 N respectively. From the cut-out view of Von-Mises stress distribution presented in Fig. 3.13, the octahedron particle has been pulled out after the occurrence of interfacial debonding, which means there is no mechanical interlock for this particle after the occurrence of the interface debonding, and it has much lower stress distribution when compared with the other two shapes. For the octahedron and dodecahedron particles, they are still held steadily by the matrix even they have lost the interfacial adhesion.

Table 3.3 Force to initiate interfacial failure for different case studies.

Diamond shapes	Load for diamond fall-out (N)			Average value (N)
	Direction 1	Direction 2	Direction 3	
Cube	40.1	37.9	34.8	37.6
Octahedron	29.7	29.8	30.5	30
Dodecahedron	31.5	30.6	30.7	30.9

3.4.2 Effect of diamond orientations

The effect of diamond orientations on the retention capacity is studied in this section for all three particle shapes shown in Fig. 3.11. Based on the study in the previous section, two additional orientations of those three particle shapes are studied and shown in Fig. 3.14a and Fig. 3.15a. The diamond particle size and material properties are the same as those used in the previous section. As these particles are all regular polyhedron, these three orientations for all the particle shapes are obtained by rotating the particles to keep the vertex, edge and flat surface face toward upward respectively. Similar to the previous section, three different horizontal loading directions are also considered and applied by imposing a gradually increased displacement at the centre point of the exposed edge/face respectively, shown in Fig 3.14b and 3.15b.

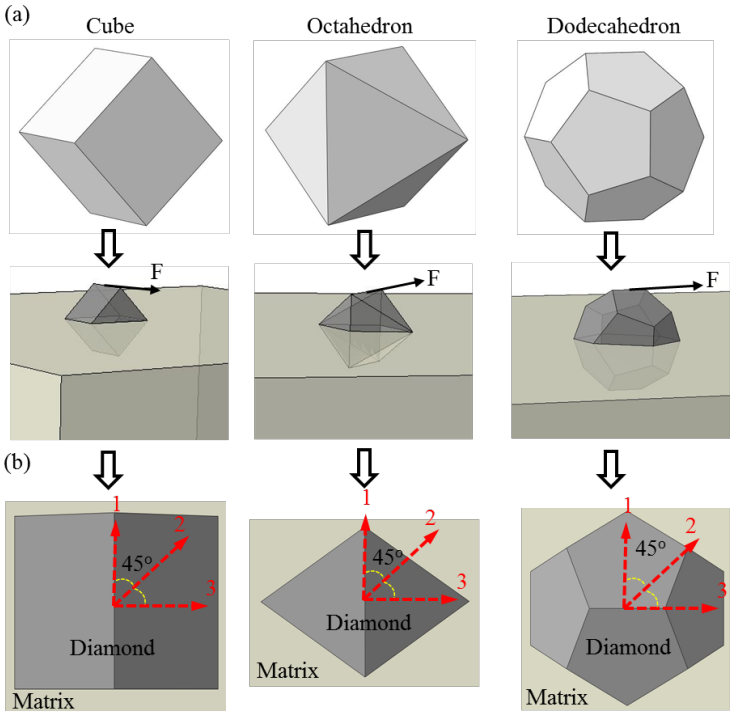

Fig. 3.14 Models for diamond particles with edge face toward upward: (a) different diamond shapes and (b) different horizontal loads from top view.

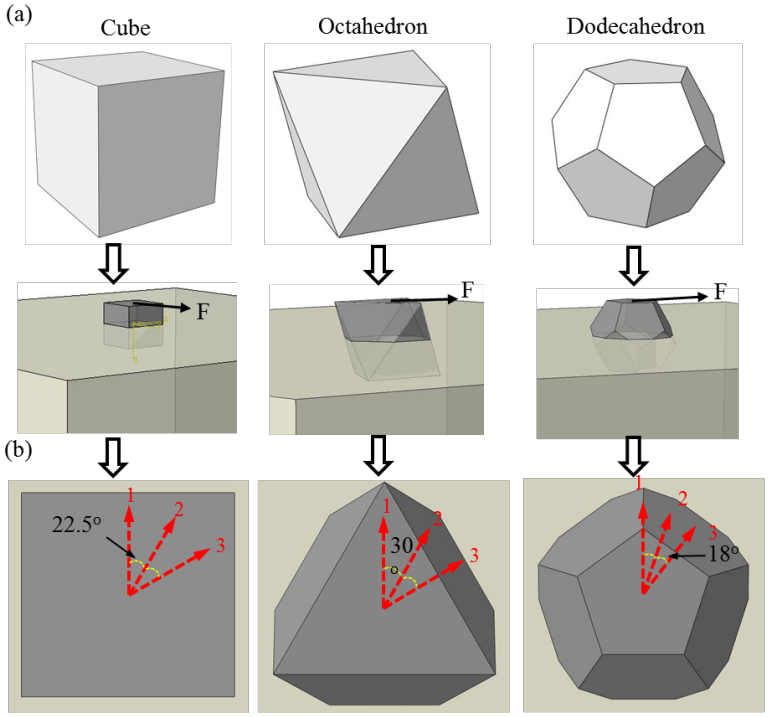

Fig. 3.15 Models for diamond particles with flat surface face toward upward: (a) Different diamond shapes and (b) Different horizontal loads from the top view.

Similar to the previous section, the critical forces corresponding to the interfacial failure initiation of all these cases obtained from the present analysis are reported in table 3.4. The table shows that the retention capacity of diamonds is greatly affected by the orientation and the shape of diamond particles, and the load direction has a relatively lower influence on the retention capacity. From the results, it can be seen that the cube and dodecahedron shaped particles achieved their highest retention capacities when they are having an orientation of "upward face" which correspond to a situation of the wear flat. However, the enhancement of diamond retention capacity with a wear flat situation is not desirable as the efficiency of the entire drilling process is also dependent on the sharpness of the cutting surface. In contrast, the octahedron shaped particle is the desirable shape as it has a relatively higher retention capacity with the orientation of "upward vertex" which is the sharp cutting surface for efficient cutting.

Table 3.4 Critical forces to initiate interface debonding of different diamond shapes with various orientations and loading directions.

Diamond shapes and load directions		Critical forces for interface failure of different diamond orientations		
		Upward vertex (N)	Upward edge (N)	Upward face (N)
Cube	P1	40.1	34.9	47.4
	P2	37.9	37.9	48.6
	P3	34.8	32.9	49.5
Octahedron	P1	29.7	31.3	23.0
	P2	29.8	29.1	22.6
	P3	30.5	29.5	22.6
Dodecahedron	P1	31.5	32.9	46.8
	P2	30.6	32.0	45.9
	P3	30.7	31.6	44.7

3.4.3 Effect of interfacial properties

The interfacial properties can be affected by several factors associated with the sintering process and metal matrix types. The cohesive zone parameters are characterised by six fracture property parameters in three different directions (Mode I, Mode II, and Mode III), which is discussed earlier. In order to investigate the effect of these interfacial parameters, twelve different cases having different values of these parameters (Table 3.5) are considered in the present study. For this purpose, the octahedron shaped diamond particle with its vertex facing toward upward is taken in this section by varying the values of those interfacial parameters. The reason to choose the octahedron diamond is due to its retention capacity is purely based on the interfacial adhesion which is proven in the previous section. The variation of critical forces corresponding to the initiation of interfacial debonding for all cases is simulated and reported in Table 3.5. It can be seen that the values of critical forces decrease steadily with the decrease of interfacial strength as well as the

fracture toughness values. The normal fracture energy has the most contribution to the interfacial adhesion as it leads the highest change of the value of critical force among all those parameters. The contribution of the fracture stresses is more than that of the fracture energies. Moreover, the results also indicate that the interfacial adhesion is mainly based on the Mode I fracture parameters.

Table 3.5 Twelve case studies of different interfacial parameters.

	Interfacial parameters						
	τ_n^0 MPa	τ_s^0 MPa	τ_t^0 MPa	G_{IC} mJ/mm^2	G_{IIC} mJ/mm^2	G_{IIIC} mJ/mm^2	Critical Force (N)
Case 1 (Original sample)	543	314	314	0.14	0.33	0.33	30.7
Case 2 (50% τ_n^0)	271.5	314	314	0.14	0.33	0.33	27.4
Case 3 (50% τ_s^0)	543	157	314	0.14	0.33	0.33	25.6
Case 4 (50% τ_t^0)	543	314	157	0.14	0.33	0.33	25.5
Case 5 (50% G_{IC})	543	314	314	0.07	0.33	0.33	24.9
Case 6 (50% G_{IIC})	543	314	314	0.14	0.165	0.33	29.2
Case 7 (50% G_{IIIC})	543	314	314	0.14	0.33	0.165	29.3
Case 8 (50% τ^0)	271.5	157	157	0.14	0.33	0.33	20.6
Case 9 (50% G_C)	543	314	314	0.07	0.165	0.165	24.4
Case 10 (50% Mode I)	271.5	314	314	0.07	0.33	0.33	23.6
Case 11 (50% Mode II)	543	157	314	0.14	0.165	0.33	25.3
Case 12 (50% Mode III)	543	314	157	0.14	0.33	0.165	25.4

3.5 Conclusions

A failure analysis of diamond impregnated bits is attempted by using the finite element method for the first time to simulate the interfacial failure mechanism between the matrix and diamond particles. This provides the vital understanding of diamond fall-out mechanism which is one of the significant failure modes of diamond bits. For this purpose, a single diamond particle along with a portion of the surrounding matrix in three-dimensional is developed and used as a representative part of diamond bits. The diamond is subjected to a tangential force at its tip which simulates the cutting force whereas the matrix is restrained at its far ends. 4-node linear tetrahedron elements are used for the diamond and matrix materials. A zero thickness surface based cohesive zone modelling technique is used to simulate the failure at the interface between the matrix and the diamond.

The performance of the proposed finite element model is investigated and validated by solving numerical examples and the results produced by the finite element model are compared with the results available in the literature. The performance of the model is found to be good in the majority of these test problems which include interfacial stress analysis of diamond impregnated bits and debonding simulations of a double cantilever beam and mixed-mode bending tests in three-dimensional models. Based on the confidence gained from the observation, the present model is used to conduct a parametric study for the critical force prediction of the interface failure initiation of diamond impregnated bits.

It has been observed that the shapes and orientations of diamond particles and interfacial properties have a significant influence on the retention capacity of diamond particles. As the efficiency of the entire drilling process is also dependent on the sharpness of the cutting surface, the octahedron shaped diamond particle is found to have a better performance for drilling because it has a relatively higher retention capacity when it is under sharp cutting face and a lower retention capacity when it is under blunt cutting face. It is also observed that the interface properties are the dominant parameters for the

retention ability of diamond particles as the value of critical force decreases steadily with the decrease of interfacial strength as well as the fracture toughness values, and the contribution of the Mode I properties is more than that of the Mode II and Mode III properties. For each individual interfacial parameter listed, the fracture energy in Mode I has the most contribution to the interfacial adhesion ability.

Acknowledgement

The work has been supported by the Deep Exploration Technologies Cooperative Research Centre whose activities are funded by the Australian Government's Cooperative Research Centre Programme. This is a DET CRC Document.

References for Chapter 3

SØRENSEN, B. F. & JACOBSEN, T. K. 2003. Determination of cohesive laws by the J-integral approach. *Engng Fract Mech,* 70**,** 1841-1858.

BARENBLATT, G. I. 1962a. Advances in Applied Mechanics. *Academic Press, New York***,** pp. 55.

BARENBLATT, G. I. 1962b. The mathematical theory of equilibrium cracks in brittle fracture. *Advances in applied mechanics,* 7**,** 55-129.

CAMANHO, P. P., DÁVILA, C. G. & DE MOURA, M. F. 2003. Numerical simulation of mixed-mode progressive delamination in composite materials. *Journal of Composite Materials,* 37**,** 1415-1438.

CAVALLI, M. N. 2003. Cohesive Zone Modelling of Structural Joint Failure. *Ph.D. Thesis, University of Michigan*.

CREWS, J. J. H. & R., R. J. 1998. A Mixed-Mode Bending Apparatus for Delamination Testing. NASA Langley Technical Report Server.

CUI, W. & WISNOM, M. R. 1993. A combined stress-based and fracture-mechanics-based model for predicting delamination in composites. *Composites,* 24**,** 467-474.

DE BORST, R. & ROTS, J. G. 1989. Occurence of Spurious Mechanisms in Computation of Strain-Softening Solids. *Engineering Computations,* 6**,** 272-280.

ELICES, M., GUINEA, G. V., GÓMEZ, J. & PLANAS, J. 2002. The cohesive zone model: advantages, limitations and challenges. *Engineering Fracture Mechanics,* 69**,** 137-163.

FIELD, J. E. 1986. Mechanical and physical properties of diamond. *Inst. of Phys.*

GONÇALVES, J. P. M., MOURA, M. F. S. F. D., CASTRO, P. M. S. T. D. &

MARQUES, A. T. 2000. Interface element including point-to-surface constraints for three-dimensional problems with damage propagation. *Engineering Computations,* 17**,** 28-47.

JAENSSON, B. O. & SUNDSTRÖM, B. O. 1972. Determination of Young's modulus and poisson's ratio for WC Co alloys by the finite element method. *Materials Science and Engineering,* 9**,** 217-222.

KONSTANTY, J. 2005a. Chapter 1 - Introduction. *In:* KONSTANTY, J. (ed.) *Powder Metallurgy Diamond Tools.* Amsterdam: Elsevier Science.

KONSTANTY, J. 2005b. Chapter 3 - Diamond tool design and composition. *In:* KONSTANTY, J. (ed.) *Powder Metallurgy Diamond Tools.* Amsterdam: Elsevier Science.

LEVIN, E. & GUTMANAS, E. Y. 1990. Solid-state bonding of diamond to Nichrome and Co-20wt% W alloys. *Journal of Materials Science Letters,* 9**,** 726-730.

LI, B., AMARAL, P. M., REIS, L., ANJINHO, C. A., ROSA, L. G. & FREITAS, M. D. 2010. 3D-modelling of the local plastic deformation and residual stresses of PM diamond–metal matrix composites. *Computational Materials Science,* 47**,** 1023-1030.

LIAO, Y. S. & LUO, S. Y. 1992. Wear characteristics of sintered diamond composite during circular sawing. *Wear,* 157**,** 325-337.

LIN, C.-S., YANG, Y.-L. & LIN, S.-T. 2008. Performances of metal-bond diamond tools in grinding alumina. *Journal of Materials Processing Technology,* 201**,** 612-617.

M. ALFANO, F. F., A. LEONARDI, C. MALETTA AND G. H. PAULINO 2007. Cohesive Zone Modeling of Mode I Fracture in Adhesive Bonded Joints. *Key Engineering Materials,* 348-349**,** 13-16.

MILLER, D. & BALL, A. 1990. Rock drilling with impregnated diamond microbits—An experimental study. *International Journal of Rock Mechanics*

and Mining Sciences & Geomechanics Abstracts, 27**,** 363-371.

MILLER, D. & BALL, A. 1991. The wear of diamonds in impregnated diamond bit drilling. *Wear,* 141**,** 311-320.

PAONE, J. & MADSON, D. 1966. *Drillability Studies: Impregnated Diamond Bits*, Department of the Interior, Bureau of Mines.

RINDERKNECHT, S. & KRÖPLIN, B. 1997. A computational method for the analysis of delamination growth in composite plates. *Computers & Structures,* 64**,** 359-374.

ROMANSKI, A. 2010. Factors affecting diamond retention in powder metallurgy diamond tools. *Archives of Metallurgy and Materials,* 55**,** 1073-1081.

SCOTT, P. M., NICHOLAS, M. & DEWAR, B. 1975. The wetting and bonding of diamonds by copper-base binary alloys. *Journal of Materials Science,* 10**,** 1833-1840.

SØRENSEN, B. F. 2002. Cohesive law and notch sensitivity of adhesive joints. *Acta Mater,* 50**,** 1053-1061.

SUH, C.-M., BAE, K.-S. & SUH, M.-S. 2008. Wear behavior of diamond wheel for grinding optical connector ferrule — FEA and wear test —. *Journal of Mechanical Science and Technology,* 22**,** 2009-2015.

TADA, H. 1985. The stress analysis of cracks handbook. *Paris productions incorporated*.

TURON, A., DÁVILA, C. G., CAMANHO, P. P. & COSTA, J. 2007. An engineering solution for mesh size effects in the simulation of delamination using cohesive zone models. *Engineering Fracture Mechanics,* 74**,** 1665-1682.

WANG, Y. H., ZANG, J. B., WANG, M. Z., GUAN, Y. & ZHENG, Y. Z. 2002. Properties and applications of Ti-coated diamond grits. *Journal of Materials Processing Technology,* 129**,** 369-372.

XUEFENG, T. & SHIFENG, T. 1994. The wear mechanisms of impregnated diamond bits. *Wear,* 177**,** 81-91.

ZHAI, J. & ZHOU, M. 2000. Finite element analysis of micromechanical failure modes in a heterogeneous ceramic material system. *International Journal of Fracture,* 101**,** 161-180.

ZHOU, Y., FUNKENBUSCH, P. D. & QUESNEL, D. J. 1997. Stress distributions at the abrasive-matrix interface during tool wear in bound abrasive grinding—a finite element analysis. *Wear,* 209**,** 247-254.

Chapter 4

Numerical simulation on the failure of impregnated diamond bit

(Journal Paper 3)

J. Xu, A.H. Sheikh and C. Xu

School of Civil, Environmental and Mining Engineering, the University of Adelaide, Australia

Publication:

J. Xu, A.H. Sheikh, C. Xu. (2016). Numerical simulation on the failure of impregnated diamond bit. *Advances in Engineering software*, Submitted for review: August 2016.

Statement of Authorship

Title of Paper	Numerical simulation on the failure of impregnated diamond bit
Publication Status	☐ Published ☐ Accepted for Publication ☑ Submitted for Publication ☐ Unpublished and Unsubmitted work written in manuscript style
Publication Details	J. Xu, A.H. Sheikh, C. Xu. (2016). Numerical simulation on the failure of impregnated diamond bit. *Advances in Engineering Software*, Submitted on 29/08/2016

Principal Author

Name of Principal Author (Candidate)	Jiayi Xu
Contribution to the Paper	Undertook literature review, developed analytic procedure and numerical models, performed analysis on different parameters and prepared manuscript.
Overall percentage (%)	80%
Certification:	This paper reports on original research I conducted during the period of my Higher Degree by Research candidature and is not subject to any obligations or contractual agreements with a third party that would constrain its inclusion in this thesis. I am the primary author of this paper.
Signature	Date 30/08/2016

Co-Author Contributions

By signing the Statement of Authorship, each author certifies that:

i. the candidate's stated contribution to the publication is accurate (as detailed above);

ii. permission is granted for the candidate in include the publication in the thesis; and

iii. the sum of all co-author contributions is equal to 100% less the candidate's stated contribution.

Name of Co-Author	Abdul Hamid Sheikh
Contribution to the Paper	Supervised development of numerical models, helped manuscript preparation, reviewed and corrected draft of the manuscript.
Signature	Date 30/8/2016

Name of Co-Author	Chaoshui Xu
Contribution to the Paper	Supervised development of work, helped to evaluate and edit the manuscript.
Signature	Date 10-09-2016

Please cut and paste additional co-author panels here as required.

Abstract

A finite element model is used to analyse the failure mechanisms of impregnated diamond bits to assess the diamond retention ability of these diamond drilling tools. In this approach, a zero thickness surface based cohesive zone modelling technique is used to simulate the interfacial failure between diamond particles and the matrix, and the extended finite element method (XFEM) is used to predict the initiation and propagation of cracks in the matrix. Both two-dimensional and three-dimensional modelling assessments are conducted in this study. For the validation of the model, two numerical examples are solved using the proposed method. The solutions are compared with published results and a good agreement between them is observed. Different values of interfacial parameters and matrix fracture properties are considered in this study to investigate their influences on the failure mechanisms of the diamond-matrix system. Different shapes of diamond particles are also considered to assess their effects on the critical forces for the initiation of interfacial debonding and matrix failure.

***Keywords*:**

Impregnated diamond bit; Extended finite element method; Cohesive zone model; Interfacial debonding; Metal matrix cracking

4.1 Introduction

Diamond cutting tools have been widely used since the invention of synthetic diamonds in the 1950s (Paone and Madson, 1966, Busch and Hill, 1975). Recently, the rotary drilling bit has become one of the most commonly used tools in the underground exploration and mineral extraction field (Kumar et al., 2015). Three different types of diamond drill bits (polycrystalline diamond compact (PDC) bit, surface-set diamond (SD) bit and impregnated diamond (ID) bit) have proven to be economically advantageous for rock drilling. Diamond particles are widely used in cutting tools not only due to the diamonds' hardness but also because of their high strength, high wear resistance, low friction coefficient and high thermal conductivity. Therefore, when used as an abrasive, diamonds have many obvious advantages over other common abrasives, including their high grinding efficiency, low grinding force, long lifespan and low comprehensive cost. ID drilling bits are usually composed of a base metal body mounted with several impregnated diamond segments at the cutting face, and the segments are usually formed from well-mixed diamond particles and metal powder through the sintering process (Li et al., 2010). The matrix material is a multi-phase alloy consisting of a skeleton such as tungsten carbide (WC), which has high wear resistance, and bonding metals such as cobalt (Co), copper (Cu), tin (Sn), nickel (Ni), and so forth. The skeleton material has the most effect on the wear resistance of the matrix and the interfacial properties of the diamond-matrix system (Hsieh and Lin, 2001, Lin et al., 2008, Tze-Pin et al., 1992, Ding et al., 1998). During the drilling operation, when the cutting surface of the bit slides over a rock due to the rotation of the bit, the embedded diamond particles near the cutting surface are partially exposed due to the gradual wear of the matrix material and these exposed diamonds do the cutting or drilling of the rock. The matrix is expected to hold the freshly exposed sharp diamonds firmly and, at the same time, it should wear at a rate compatible with that of diamonds so that the worn diamonds can fall out to allow new diamonds to be exposed, continuously (Xuefeng and Shifeng, 1994). This is known as having the ability to self-sharpen. However, the drilling performance of these bits is still

quite volatile and inconsistent due to a lack of fundamental understanding of the micro-mechanisms of both the matrix and the interface between the diamond and the matrix. The major issues that manufactures are currently facing with using impregnated diamond bits are ineffective matrix to diamond wear rates and premature diamond fall-out failure rates (Konstanty, 2005).

The failure mechanisms of ID bits, such as micro-cracking of the matrix and interfacial debonding, are complex and system-dependent processes which are affected by the properties of the matrix, the interfacial strength as well as the size and shape of the diamond particles (Chalkley and Thomas, 1969, Konstanty, 1999). Initially, some experimental studies (Miller and Ball, 1990, Miller and Ball, 1991, Xuefeng and Shifeng, 1994) on impregnated diamond bits were conducted where the wear mechanisms of these bits were investigated. However, these minor failures do not typically constitute full structural failure and do raise difficulties in the direct detection and measurement of the growth of these failures using normal experimental technologies. With the help of finite element analysis, these problems can be eliminated by using a combination of the cohesive zone method (CZM) and the extended finite element method (XFEM) techniques to simulate the interfacial failure and matrix cracks respectively. Although CZM and XFEM techniques have been used extensively to simulate different aspects of fracture of various engineering problems, they have not yet been applied to impregnated diamond drilling bits in order to assess the drilling conditions and visualise the failure mechanisms. The fundamental concept of the CZM technique is based around the fracture process zone, which is characterised by either the cohesive law or the traction separation law for de-cohesion of atomic lattices, as proposed by Barenblatt (1962), which is suitable for interfacial debonding analysis. The XFEM method, originally proposed by Belytschko et al. (1999), is a numerical technique that extends the conventional finite element method (CFEM) approach by extending the solution space for solutions to differential equations with discontinuous functions. It is a powerful and effective numerical technique suited to simulate initiation and propagation in the matrix.

Although some researchers (Romanski, 2010, Li et al., 2010, Suh et al., 2008) have conducted micromechanical modelling of the ID bits to analyse the stress distribution of a single diamond particle along with a portion of the surrounding matrix under a tangential load, no one has yet paid any attention to the modelling of realistic, accurate, failure mechanisms for this system. The ability to predict this critical damage build-up in an FEM model is of prime importance to understanding the fracture behaviours of ID bits. Therefore, the matrix crack and matrix-diamond interface failure are modelled by incorporating the XFEM and CZM techniques in combination for the first time in this study. This will help the industry to understand the wear mechanisms of impregnated diamond bits due to matrix failure or diamond pull-out more accurately which will be of benefit to the future design of these bits. Moreover, there is a need for investigating the effect of different parameters such as protrusions, shapes and orientations of the diamond particle on the bit's retention capacity. Such novel research is undertaken in this study.

4.2 Model formulation and material properties

4.2.1 Geometry of the model and its finite element meshing

The failure of ID bits is investigated by taking a single diamond particle, which is partially embedded within the matrix, and placing it subject to a tangential load (Fig. 4.1a). The dimension of the portion of the surrounding matrix is adequate to dissipate the stresses produced by the forces acting on the diamond particle. For the justification of the above model, it is assumed the diamond particles are uniformly distributed throughout the matrix and the diamond concentration is low enough that the stress of adjacent diamond particles at one point would not influence those at another. The design of ID bits avoids non-uniform distribution of diamond grits, a feature which would be responsible for localised stress concentrations, leading to premature failure

of the bit. A 2-dimensional finite element model is developed for this portion, and the finite element model (Fig. 4.1b) is drawn as a mirror image (upside down) of the actual object, as shown in Fig. 1b. The Figure also shows the finite element mesh where a finer mesh is used in the regions of interest, which is at the diamond part of the bit along with the vicinity of the interface between the diamond and the matrix, while a coarse mesh is used in the regions away from the interface with a gradual transition placed between the two in order to improve computational efficiency. Mesh convergence studies are performed for all models in this study in order to ensure a converged solution. Both horizontal and vertical thrust forces are considered and the results indicate that the fall-out of the diamond particle due to interfacial debonding is primarily facilitated by the tangential cutting force as the additional vertical forces do not affect the result significantly. A displacement is imposed at the tip of the protruding part of the diamond particle and the cutting force is predicted in the form of a resisting force with respect to the imposed displacement. Thus, the critical load for the interfacial debonding could also be determined in this way.

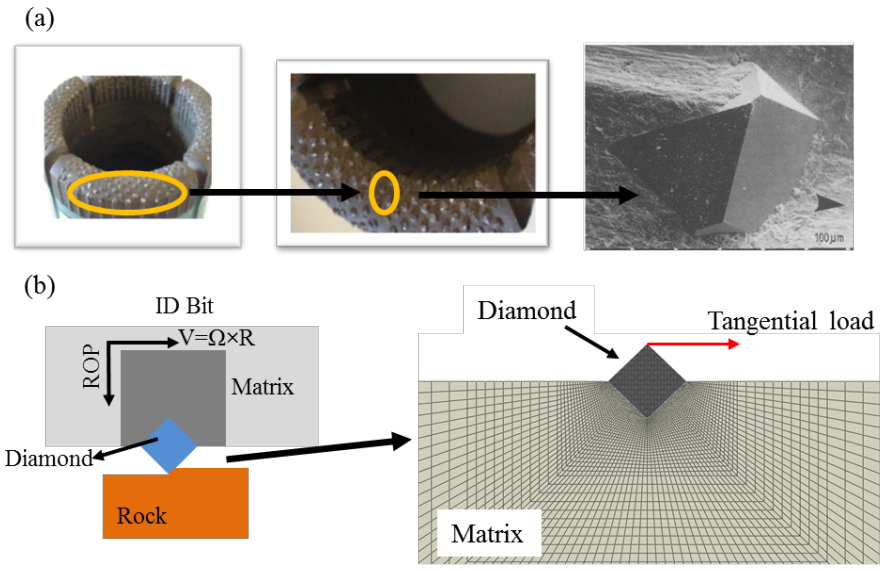

Fig. 4.1 Micromechanical model of a diamond impregnated bit: (a) SEM micrograph of an ID bit and (b) skeleton drawing of an ID bit and a finite element model of a single diamond particle embedded in the matrix.

The shape of synthetic diamond particles can be treated as regular polygons (2D model) in most cases, as the shape of synthetic diamond grits can be controlled for ID bits. A square geometry has typically been used by different investigators for simplicity, a geometry which is also used in most of the cases in the present study. According to the literature (Xuefeng and Shifeng, 1994, Li et al., 2010), the size of the diamond particles varies from 0.01 to 0.5 mm in diameter and a diameter of 0.5 mm is taken as the diamond particle size in this study for all the cases. The size taken for the surrounding matrix is about 20 times larger than that of the diamond, which is large enough to ensure that the stresses are zero near the boundaries (the edges of the darkened areas of the matrix in Fig. 4.1b) of the matrix. In the present study, a well-regarded finite element code ABAQUS 6.12 is used for reliable numerical modelling of the diamond-matrix system. Four nodes of bilinear plane strain quadrilateral elements are used to model both the diamond and the matrix parts.

4.2.2 Material model of the matrix and diamonds and their properties

In the present study, the diamonds are treated as elastic and isotropic materials, where the modulus of the elasticity is taken from the literature (Zhou et al., 1997, Li et al., 2010, Suh et al., 2008) as E = 1100 GPa, whereas the Poisson's ratio is ν = 0.1 for these diamond particles, as diamonds behaves like a brittle material. It is assumed that the applied load is stable and no impact force will cause the fracture of diamonds due to their high fracture resistance. Due to its high specific strength, stiffness and wear resistance, a Tungsten-carbide cobalt (WC-Co) alloy is taken as the metal matrix, with an elastic modulus of 600 GPa and a Poisson's ratio of 0.2, both of which were determined experimentally by Jaensson et al. (Jaensson and Sundström, 1972). It should be noted that the matrix alloy used here is a kind of cemented carbide material, which is a hard metal that can be treated as elastic material. Moreover, elastic-plastic material properties are used to model the matrix in some sample test cases where no significant effect of plasticity is observed.

4.2.3 Cohesive zone model for the diamond-matrix interface

For the analysis of the zero-thickness interface between the diamond and the matrix of ID bits, the concept of a cohesive zone modelling approach (Elices et al., 2002, M. Alfano, 2007) is most appropriate and is adopted in the present study, as it can quantitatively predictive analyses for interfacial fractures of adhesively bonded composite joints (Sørensen, 2002, B.F. Sørensen and Jacobsen, 2003). The interface has two possible modes of failure: they are Mode I (the opening mode) due to the tensile stress acting normal to the interface and Mode II (the sliding mode) due to shear stress parallel to the interface and perpendicular to the crack front. Fig. 4.2 shows the global (x-y) and local (n-s) coordinate system of the interface of the developed model. The relative displacement in global and local coordinate systems of the interface nodes between two elements is also shown in Fig. 4.2.

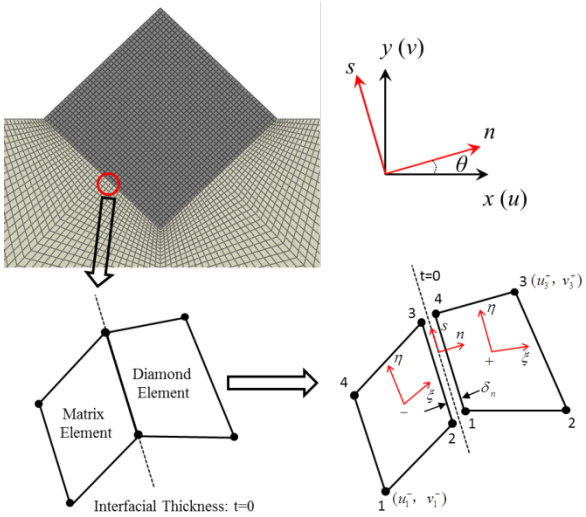

Fig. 4.2 Detail of an interface for the cohesive zone method.

The formulation of this approach is based on the traction-separation relationship, which is shown in Fig. 4.3, where OA shows the elastic response of the interface having a high stiffness of *K* and AB represents the interfacial damage in the form of a linear softening law. The damage is characterised by

the damage parameter (d) as shown in Fig. 4.3, which helps to represent the irrecoverable damage of the interface through pure elastic unloading with reduced stiffness. The separation at failure δ^f is obtained from the ultimate stress τ^0 (a material property of the interface) and the interfacial fracture toughness G_c (another material property), which is the area of the triangle OAB. The use of fracture energy helps to make the analyses mesh-insensitive.

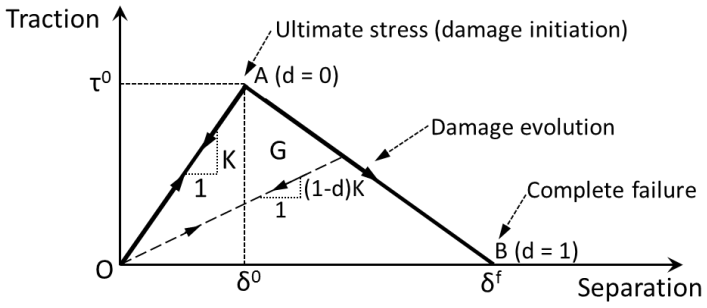

Fig. 4.3 A typical bilinear traction-separation relationship.

The traction separation law (Fig. 4.3) mentioned above is used in the present study, where the separation indicates the relative displacements at the interface and the tractions are simply the interfacial stresses. The relative displacement vector $\{\Delta\}$ in global coordinates (x-y) at any point in the interface of deformed configuration can be expressed as:

$$\{\Delta\}=\begin{Bmatrix}\bar{u}\\ \bar{v}\end{Bmatrix}=\begin{Bmatrix}u^+\\ v^+\end{Bmatrix}-\begin{Bmatrix}u^-\\ v^-\end{Bmatrix}=\sum_{i=1}^{4}N_i(\xi=-1,\eta)\begin{Bmatrix}u_i^+\\ v_i^+\end{Bmatrix}-\sum_{i=1}^{4}N_i(\xi=1,\eta)\begin{Bmatrix}u_i^-\\ v_i^-\end{Bmatrix} \quad (4.1)$$

where u^+ and u^- are the displacement components at the two sides of an interfacial point in the global x-direction whereas v^+ and v^- are the displacements in the global y-direction. u_i^+ and u_i^- are the corresponding displacements at the i-th node of the element (Fig. 4.3) used to model the materials on the two sides of this interfacial point and N_i are the shape functions of these elements. The coordinates of an element can be written as

$x = \sum_{i=1}^{4} N_i x_i$ and $y = \sum_{i=1}^{4} N_i y_i$ based on the isoparametric formulation, where x_i and y_i are the nodal coordinates of the element. Thus, the normal and tangential components of $\{\Delta\}$ with respect to the relative displacements in local coordinate system $\{\delta\}$ (Liao and Luo, 1992) can be obtained as:

$$\{\delta\} = \begin{Bmatrix} \delta_n \\ \delta_s \end{Bmatrix} = [Q]\{\Delta\} \tag{4.2}$$

where $[Q]$ is the transformation matrix from the global to a local coordinate system. The damage introduces nonlinearity in the system that requires an incremental/ iterative procedure for solving the governing equations. As the damage is an irreversible process, the solution technique is dependent on the loading history. Thus, there is a need for storing the maximum values of these relative displacements (δ_n^{max} , δ_s^{max}), which occurred before any increment/iteration and they are updated in that increment/iteration as follows:

$$\text{If } \delta_n > \delta_n^{\max} \Rightarrow \delta_n^{\max} = \delta_n \text{ otherwise } \delta_n^{\max} = \delta_n^{\max} \tag{4.3}$$

$$\text{If } |\delta_s| > \delta_s^{\max} \Rightarrow \delta_s^{\max} = |\delta_s| \text{ otherwise } \delta_s^{\max} = \delta_s^{\max} \tag{4.4}$$

For pure Mode I or Mode II criteria, the interfacial normal and shear tractions (τ_n and τ_s) can be related to the maximum value of these relative displacements using the interfacial constitutive properties in the form of traction-separation laws (Fig. 4.2) as:

$$\begin{aligned} \tau_n &= K_n \delta_n \text{ if } \delta_n^{\max} \le \delta_n^0 \\ \tau_n &= (1 - d_n) K_n \delta_n \text{ if } \delta_n^0 < \delta_n^{\max} < \delta_n^f \\ \tau_n &= 0 \text{ if } \delta_n^{\max} \ge \delta_n^f \end{aligned} \tag{4.5}$$

$$\begin{aligned} \tau_s &= K_s \delta_s \ \text{ if } \delta_s^{\max} \le \delta_s^0 \\ \tau_s &= (1-d_s) K_s \delta_s \ \text{ if } \delta_s^0 < \delta_s^{\max} < \delta_s^f \\ \tau_s &= 0 \ \text{ if } \delta_s^{\max} \ge \delta_s^f \end{aligned} \tag{4.6}$$

For the bilinear traction separation law (Fig. 4.3), the damage parameters for these two modes of fracture may be written as:

$$d_n = \frac{\delta_n^f \left(\delta_n^{\max} - \delta_n^o\right)}{\delta_n^{\max}\left(\delta_n^f - \delta_n^o\right)}, \ d_s = \frac{\delta_s^f \left(\delta_s^{\max} - \delta_s^o\right)}{\delta_s^{\max}\left(\delta_s^f - \delta_s^o\right)} \tag{4.7}$$

The above equations (5) and (6) can only be used if the two modes of failure are independent, that is, have no coupling between them. However, a mixed-mode fracture is more likely to occur at the matrix diamond interface due to the varying drilling conditions of the impregnated diamond bits, thus, the two modes of failure will be coupled, as mentioned earlier. In that situation, the damage onset and its propagation may occur before reaching the ultimate stress of Mode I (τ_n^0) and Mode II (τ_s^0). Under the mixed mode failure scenario, a quadratic failure criterion proposed by Cui et al. (Cui and Wisnom, 1993) for the prediction of damage initiation seems to be most suitable and is used in the present study. It is expressed as:

$$\left(\frac{\langle \tau_n \rangle}{\tau_n^0}\right)^2 + \left(\frac{\tau_s}{\tau_s^0}\right)^2 = 1 \tag{4.8}$$

Similarly, the power law [33] is used for the mixed mode damage evolution of the interface, which is expressed in terms of energy release rates (G_I and G_{II}) and their critical values (i.e., fracture toughness for these two modes) as:

$$\left(\frac{G_I}{G_{IC}}\right)^2 + \left(\frac{G_{II}}{G_{IIC}}\right)^2 = 1 \tag{4.9}$$

where $G_I = \int_0^{\delta_n^{max}} \tau_n d\delta_n$, $G_{II} = \int_0^{\delta_s^{max}} \tau_s d\delta_s$ and $G_{IC} = \int_0^{\delta_n^f} \tau_n d\delta_n$, $G_{IIC} = \int_0^{\delta_s^f} \tau_s d\delta_s$.

In a mixed mode failure analysis, the two modes of the traction-separation relationship are combined and expressed in terms of an equivalent traction-separation relationship having a similar bilinear shape, which helps to implement the mixed-mode damage model conveniently. This combined traction-separation relationship will have the same initial stiffness (*K*), whereas the separation at the onset of damage initiation δ_m^0 and the separation at complete failure δ_m^f (subscript *m* indicates a mixed-mode fracture) can be obtained from Equations (8) and (9) respectively (Camanho et al., 2003). In that case, the two components of the separation obtained in any incremental/iterative steps are to be combined to have a single resultant component δ_m as:

$$\delta_m = \sqrt{\delta_n^{\,2} + \delta_s^2} \tag{4.10}$$

The material properties required for defining the interfacial behaviour in the present study are the fracture toughness values G_{IC} and G_{IIC} for the two modes and the corresponding ultimate stresses τ_n^0 and τ_s^0. It has been proved experimentally as well as theoretically (Zhai and Zhou, 2000, Cavalli, 2003) that these material parameters should be taken for the weaker material, which is the metal matrix in the present case, providing that the matrix is adequately connected to the diamond. Thus, the material properties of tungsten carbide cobalt (the matrix) are taken as the interfacial material parameters which are: τ_n^0 = 543 MPa, τ_s^0 = 314 MPa, G_{IC} = 0.14 mJ/mm^2 and G_{IIC} = 0.33 mJ/mm^2.

4.2.4 Extended finite element model for the metal matrix

The extended finite element method (XFEM) has been used for the simulation of crack initiation and propagation problems extensively in recent years. This technique was firstly proposed by Melenk et al. (1996), based on the concept of the partition of unity method, to add the enrichment functions into the standard finite element and allow simulation of initiation and propagation of a discrete crack without the requirement of a pre-defined crack and re-meshing. As mentioned earlier, XFEM is a numerical technique that extends the classical finite element method (FEM) approach by extending the solution space for solutions to different equations with discontinuous functions. XFEM was initially applied to model fractures in a material, which is very suitable for the modelling of matrix cracks in this study. The advantage of XFEM is that the finite element mesh does not need to be updated to track the crack path. The enriched Finite Element approximation (Elguedj et al., 2006) can be written as:

$$u(x) = \sum_{i=1}^{N} N_i(x)[u_i + H(x)a_i + \sum_{a=1}^{4} F_a(x)b_i^a] \tag{4.11}$$

where $N_i(x)$ is the standard finite element shape function that is associated with node i; u_i is the nodal displacement vector associated with the continuous part of the finite element solution. $H(x)$ is the discontinuous jump function across the crack surfaces and $F_a(x)$ is the elastic asymptotic crack tip functions. a_i and b_i^a are the associated nodal enriched degree of freedom vectors. Referring to Fig. 4.4, x is a sample integration point, x* is the closest point to x that is located on the crack surface, and n is the unit outward normal to the crack at x*. It also illustrates the discontinuous jump function across the crack surface, which is shown in Equation (12):

$$H(x) = \begin{cases} 1 & if\,(x - x^*).\mathrm{n} \geq 0, \\ -1 & otherwise \end{cases} \tag{4.12}$$

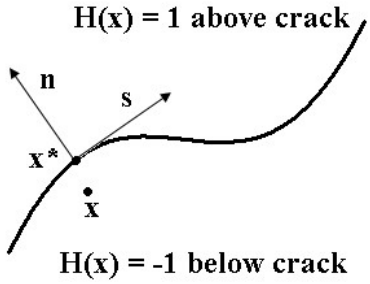

Fig. 4.4 Heaviside jump function.

The crack tip enrichment functions are suitable for stationary cracks only and account for crack tip singularity. The functions use displacement field basis functions for a sharp crack in an isotropic linear elastic material. The crack tip enrichment functions in isotropic elasticity $F_\alpha(x)=F_\alpha(r,\theta)$ are obtained from the asymptotic displacement fields, as shown in Eq 4.13:

$$[F_a(x), a = 1 \sim 4] = [\sqrt{r}\sin\frac{\theta}{2}, \sqrt{r}\cos\frac{\theta}{2}, \sqrt{r}\sin\theta\sin\frac{\theta}{2}, \sqrt{r}\sin\theta\cos\frac{\theta}{2}] \tag{4.13}$$

where (r,θ) represent the coordinate values at the crack tip from a polar coordinate system, as shown in Fig. 4.5:

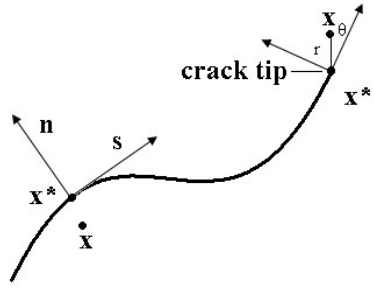

Fig. 4.5 The crack tip from a polar coordinate system.

In XFEM, the crack is located using the level set method (LSM). The level set method is a numerical scheme proposed by Osher and Sethian (Osher and Sethian, 1988) to model the motion of interfaces. The level set of a real value function is the set of all the points at which the function obtains a specified value. For example, the zero-valued level set of $f(x,y) = x^2 + y^2$ is a circle located at the origin. To describe the crack completely, two level set functions $\Phi(x)$ and $\Psi(x)$ are used, where the level set $\Phi = 0$ denotes the crack face and the intersection of $\Phi = 0$ and $\Psi = 0$ represents the crack front. Specifically, the nodal value of the function Φ is the signed distance from the crack surface to the node. The value of the function Φ is positive on one side of the crack and negative on the other. On the other hand, the nodal value of the function Ψ is the signed distance of the perpendicular surface that passes through the crack front and the sign is negative on the side towards the crack. The LSM is used to represent the crack location, including the location of crack tips. The XFEM is used to compute the stress and displacement fields necessary for determining the rate of crack growth. The LSM was first applied in XFEM by Stolarska et al. (2001) and Sukumar et al. (2000) to track moving discontinuity.

The damage modelling in the XFEM framework to simulate moving cracks is achieved by applying the cohesive segments method; the formulae and laws that govern the behaviour of XFEM-based cohesive segments for a crack propagation analysis are very similar to those used for surface-based cohesive method with traction-separation constitutive behaviour, shown in section 4.2.3. However, unlike the CZM, which requires that the cohesive surface aligns with the element boundaries and the crack paths need to be predefined, the XFEM-based cohesive damage mechanics can be used to simulate crack initiation and propagation along an arbitrary, solution-dependent path in the bulk materials. The damage properties such as initiation and evolution are specified in the material definition and the enriched element does not undergo damage under pure compression. Thus, the damage properties used for the

metal matrix are the maximum principle stress σ_{max} = 543 MPa, and fracture energy release rates G_{IC} = 0.14 mJ/mm^2 and G_{IIC} = 0.33 mJ/mm^2.

4.3 Validations

Due to the lack of available experimental test data for validation of the present model, the developed model cannot be directly validated or compared with experimental results. Moreover, although a few studies (Zhou et al., 1997, Suh et al., 2008) conducted some numerical simulations on the stress analysis of impregnated diamond bits, they did not consider the interfacial or matrix damage failure. Thus, in order to validate the present model with damage analysis, two example problems are modelled and analysed as indirect validation for the present model.

4.3.1 Validation of the interfacial damage model

The problem of a double cantilever beam (DCB), as shown in Fig. 4.6, is used in this section for an indirect validation of the interfacial damage model. The DCB, made of T300/977-2 carbon fibre reinforced epoxy laminate, is used for the present analysis, and the results are compared with the experimental test data reported by Morais et al. (2002). The laminate (3.96 mm) consists of 24 identical layers having 0^0 orientation and the following material properties: E_1 = 150.0 GPa, E_2 = 11.0 GPa, G_{12} = 6.0 GPa, ν_{12} = 0.25. Similar to the diamond-matrix system, a two dimensioned finite element model is developed for the DCB with the damage model based on the cohesive zone modelling technique at the interface (BC) between the two cantilever beams. Four interfacial parameters are used for the cohesive zone model. They are τ_n^0 = 45 MPa, τ_s^0 = 80 MPa, G_{IC} = 0.268 mJ/mm^2 and G_{IIC} = 0.4 mJ/mm^2. The load-displacement (P-δ) curve obtained in the present analysis is plotted in Fig. 4.7,

along with that reported by Morais et al. (2002), which shows that the numerical result has a reasonable correlation with the experimental results.

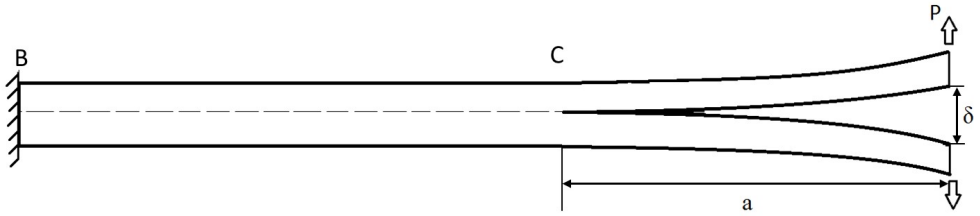

Fig. 4.6 Schematic drawing of a double-cantilever beam test.

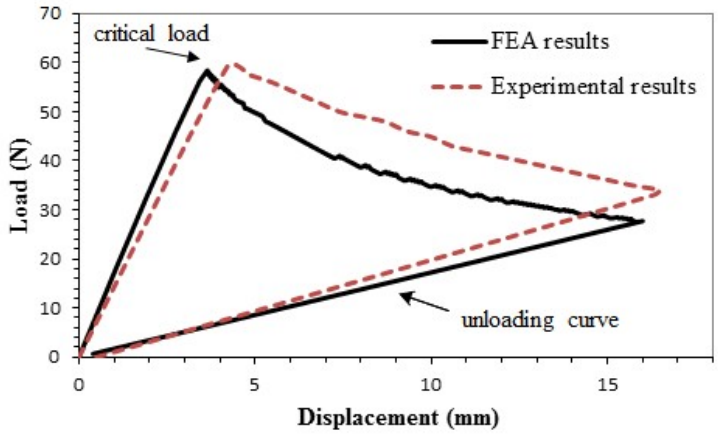

Fig. 4.7 Load-deflection curve of the double cantilever beam with delamination.

4.3.2 Validation of the extended finite element model

This example model verifies and illustrates the use of the extended finite element method (XFEM) in FEM to predict crack initiation and propagation due to stress concentration in a plate with a hole. The XFEM-based cohesive element method is used to analyse this problem and the geometry of the plate shown in Fig. 8 reveals that half of the plate is modelled, as it is in a symmetry condition. The thickness of the plate is 0.02 m. The material properties of the plate are as follows: E = 3.24 GPa and v = 0.3. The

maximum principal stress failure initiation criterion and energy-based damage evolution law are used to find their values as follows: σ_{max} = 22 MPa, G_{IC} = 2.87 J/m^2 and G_{IIC} = 2.87 J/m^2. Displacement loads are applied at the top and bottom edges to produce tensile stress, as shown in Fig. 4.8, and it also illustrates the deformed shape of the plate after the crack has occurred. The corresponding reaction forces versus displacements are plotted and compared with the experimental results reported by Tada et al. (1985), shown in Fig. 4.9. It can be seen from the results in Fig. 4.9 that a good agreement between the numerical predictions and the experimental results is obtained.

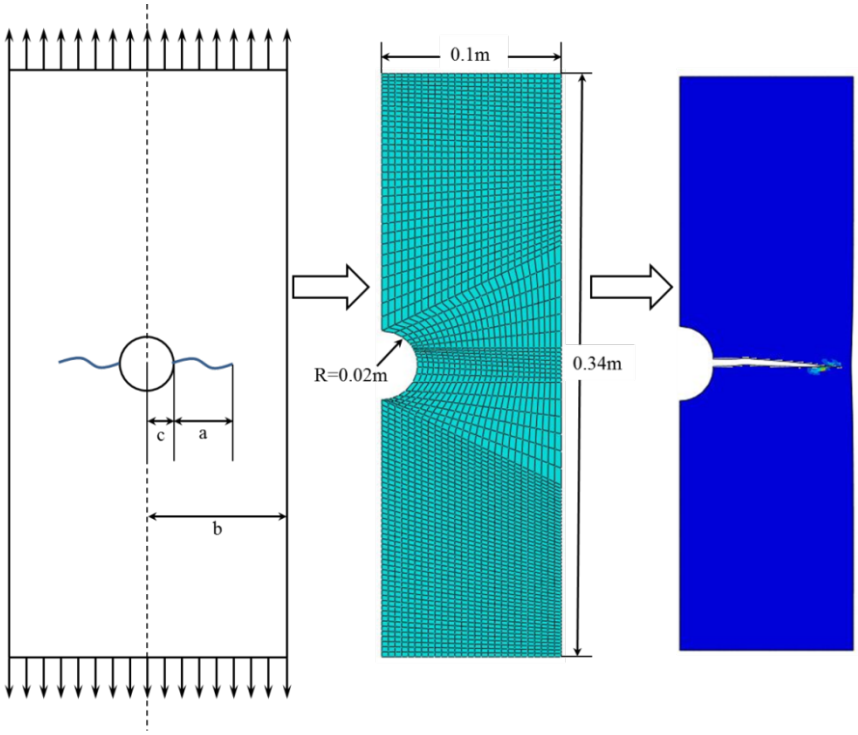

Fig. 4.8 Geometry of the plate specimen.

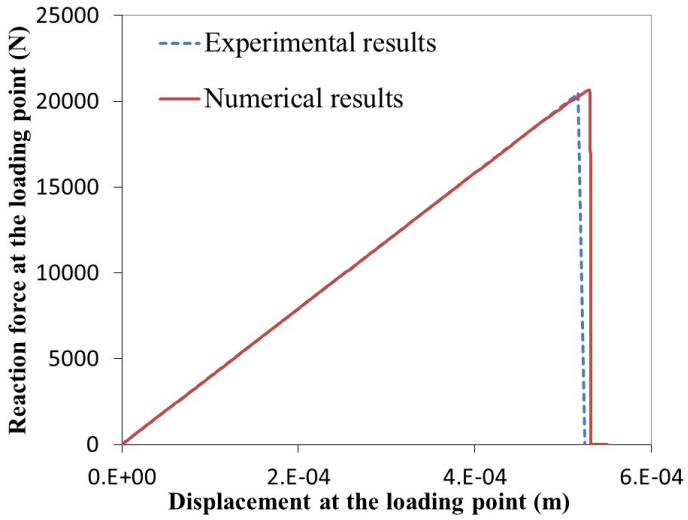

Fig. 4.9 Experimental and numerical results comparison for the plate specimen.

4.4 Results of the parametric study

A number of cases are investigated in the form of a parametric study in order to get a better understanding of different failure modes (matrix failure and interface debonding) of ID bits. The surface based CZM is used for interfacial fracture whilst XFEM is used for cracks propagating within the metal matrix. The analysis reported herein employed both of these models simultaneously to investigate a range of cases obtained by changing material properties (peak tractions and fracture energies of the interface and matrix) or geometric parameters (diamond shapes), which can help to understand the influence of this individual parameter on the retention capacity of diamond particles.

4.4.1 Effect of interfacial material properties – 2D

As the interfacial properties can be affected by several factors, such as the sintering process and the type of metal alloy used, it is essential to understand how these interfacial properties affect the retention capacity of the diamond

particles in the ID bits. The material properties, diamond particle size and mesh size used are same as those provided in Section 4.2 and kept unchanged to minimise their influence on the analysis results. Moreover, the orientation position and protrusion height are also kept constant (Fig. 4.1). As discussed earlier, the cohesive zone model is used for simulating the interface failure and the cohesive model is characterised by four parameters. In order to investigate the effect of these interface parameters, seven different cases having different values of these parameters (Table 4.1) are considered in the present study. The square shaped diamond particle (Fig. 4.1) with its vertex facing toward upward is used for all cases as it has no mechanical interlocking properties to influence the results. From Table 4.1, it can be seen that a proportional increase in the value of the interfacial parameters is proposed and two representative cases of different Mode I parameters are shown schematically in Fig. 4.10 (weak interface to strong interface).

Table 4.1 Seven case studies of different interfacial parameters.

	Interfacial parameters						
	τ_n^0 MPa	τ_s^0 MPa	G_{IC} mJ/mm^2	G_{IIC} mJ/mm^2	Initial failure	Failure initiation force (N)	Ultimate force (N)
Case 1	271.5	157	0.035	0.0825	Interface	31	31
Case 2	543	314	0.14	0.33	Interface	63	63
Case 3	814.5	471	0.315	0.7425	Interface	99	99
Case 4	950.2	549.5	0.429	1.01	Interface	114	114
Case 5	1086	628	0.56	1.32	Matrix	116	124
Case 6	1629	942	1.26	2.97	Matrix	108	163
Case 7	2172	1256	2.24	5.28	Matrix	110	230

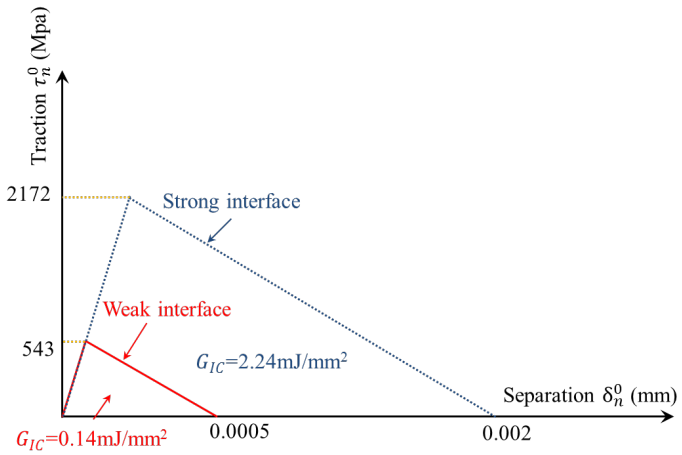

Fig. 4.10 CZM traction-separation laws of assumed strong and weak interfaces.

The forces produced at the diamond tip points due to the displacement imposed are analysed for each case shown in Table 4.1. The force-displacement variation curves for four representative cases are recorded and plotted in Fig. 4.11. The results show that the ultimate force for diamond particle fall-out increases with the increase of interfacial strength. The values of critical forces corresponding to the initiation of failure (either interfacial debonding or matrix crack) and ultimate forces for all cases are reported in Table 4.1. Among these cases, two different modes of initial failure (interfacial debonding and matrix crack) have occurred due to the effect of interfacial parameters. This is because in cases where the interface has relatively low cohesive parameters (a weak interface), the interface would lose its adhesion prior to the matrix failure, such as in Cases 1 to 4. In these cases, due to the weak interfacial bonding, the ultimate force is equal to the critical force for interfacial debonding. However, due to the relative strong interfacial strength for Cases 5, 6 and 7, matrix crack failure has occurred first with a force of 111 N, which is eventually followed by the failure of the interfacial debonding with different ultimate values (increasing with the increase of interfacial strength).

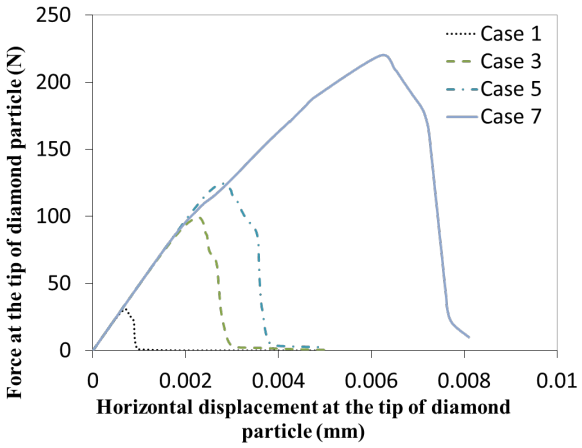

Fig. 4.11 Force-displacement variations at the tip of diamond particles for 4 cases with different interfacial parameters.

The distribution of maximum principal stress over the entire system of two representative cases (Cases 3 and 6) is presented in Fig. 4.12, and the failure mechanisms are also illustrated and compared. The Figure shows the occurrence of stress concentration near the tipping point (loading point) and the uppermost point of the diamond-matrix interface on the compression side (right side) in both cases. Fig. 4.12a represents the pure interfacial failure mode due to the use of weak interfacial bonding, where Fig. 4.12b shows the combined failure modes (matrix crack and interfacial failure) with the strong interface. Due to the strong interfacial adhesion, the required force at the tip of the diamond (the cutting force) is much higher than the weak interfacial strength case to pull out the diamond particle.

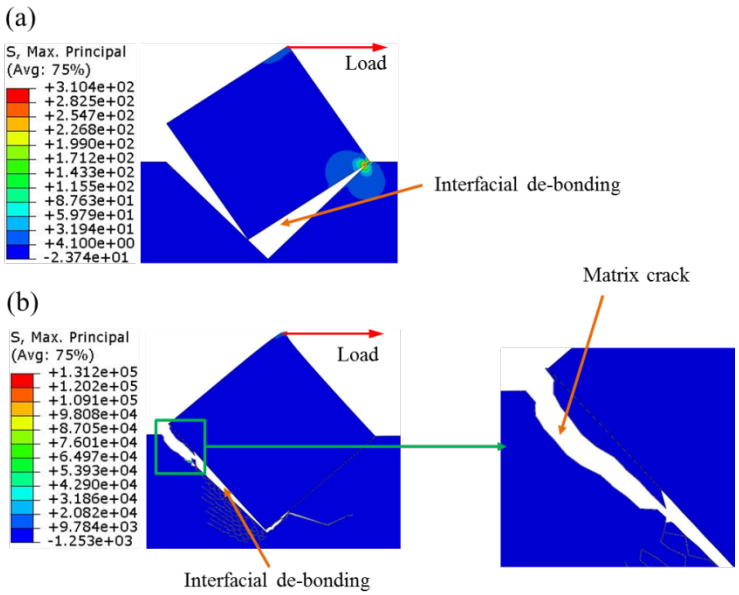

Fig. 4.12 Maximum principal stress contours and failure mechanisms illustration for the square shape ID bit with two cases: (a) weak interface (b) strong interface.

4.4.2 Effect of matrix fracture properties – 3D

A three-dimensional model, with a regular octahedron-shaped diamond particle having its vertex-face upward and half of the particle embedded in the matrix (Fig. 4.13a), is created to study the effect of matrix properties on the critical load to initiate damage in the ID bit. Similar to the above section, the size of the diamond particle is 0.5 mm in diameter, and the material properties used for the diamond and the interface are the same as those mentioned in Sections 4.2.2 and 4.2.3, where the Mode III (shear) material properties for the interface are assumed to be the same as for Mode II fracture properties. Finer meshes are applied in the region of interest, which is in the vicinity of the interface between the diamond and matrix as shown in Fig. 4.13b as the stress intensity will occur at the interface area and the debonding failure is expected to start in this area. A tangential displacement load is applied at the tip of the cutting face of the diamond particle.

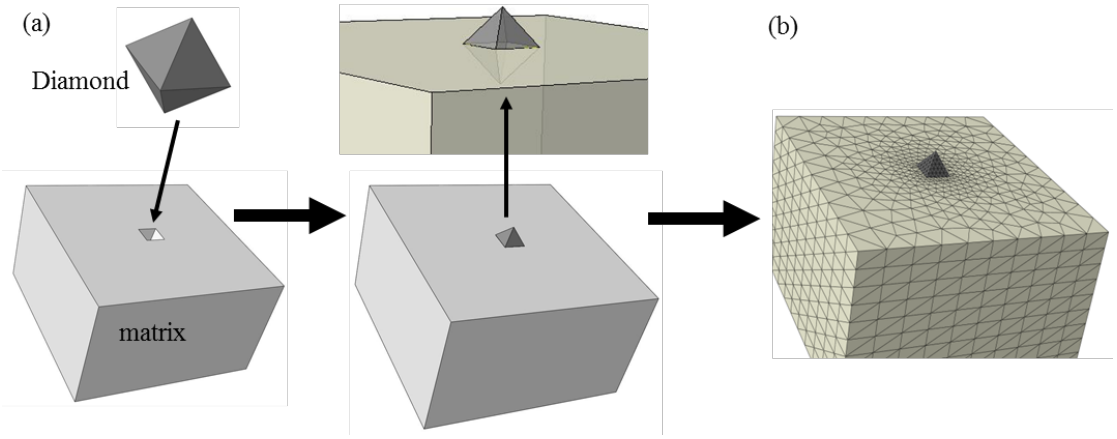

Fig. 4.13 3-D finite element model of the representative part of the ID bit: (a) Diamond & Matrix parts and (b) mesh configuration of the model.

The reason to use this shape of diamond particle is due to the diamond's retention ability and is based purely on the interfacial adhesion when the particle is in the orientation shown in Fig. 4.13. The maximum principal stress criterion is used for the damage initiation of the metal matrix, and an energy based damage evolution criterion is used for the crack propagation. Six different cases having different values of the matrix material parameters (Table 4.2) are considered in the present study. The table shows that a proportional decrease in the value of the matrix material parameters is presented from Case 1 to Case 6, and the critical loads to initiate interface failure and matrix crack are calculated and reported.

Table 4.2 Six case studies of different matrix material properties.

	Matrix fracture parameters				Critical loads (N)	
	τ_p^0 MPa	G_{IC} mJ/mm^2	G_{IIC} mJ/mm^2	G_{IIIC} mJ/mm^2	Matrix crack	Interface failure
Case 1	543	0.14	0.33	0.33	No crack	30.5
Case 2	488.7	0.1134	0.2673	0.33	29.5	31
Case 3	434.4	0.0896	0.2112	0.2112	29	31
Case 4	380.1	0.0686	0.1617	0.1617	28	31.6
Case 5	325.8	0.0504	0.1188	0.1188	26.4	30.9
Case 6	271.5	0.035	0.0825	0.0825	19.2	33

According to the results shown in Table 4.2, the matrix crack did not occur in the first case when the matrix and the interface had similar fracture properties. Only interfacial failure has occurred under the tangential cutting force of 30 N, and the distribution of the principal stress in the diamond-matrix system of Case 1, before the occurrence of the interfacial debonding, as illustrated in Fig. 4.14a. Fig 4.14b also shows the diamond particle pull-out failure (top view, side view and cut out view) after the occurrence of the complete de-bonding of the interface. Due to the value of the matrix parameters being reduced in the following cases, the matrix crack has occurred before the interfacial failure as the required force to initiate such failure has become lower than that of interfacial failure (around 31 N). It can be seen that the force for the matrix crack initiation decreases with the decrease of the matrix-fracture properties.

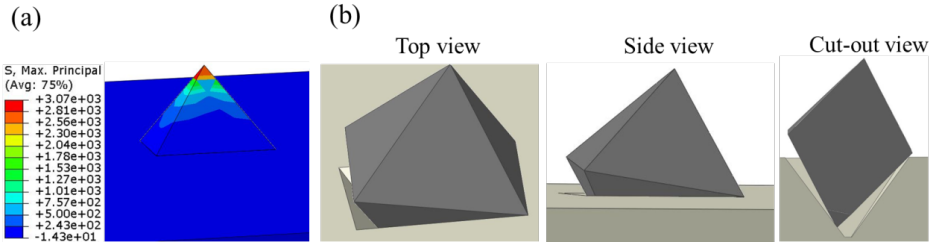

Fig. 4.14 3-D finite element model of the representative part of the ID bit: (a) Diamond and matrix parts and (b) mesh configuration of the model.

Since similar failure mechanisms were obtained for the following cases (Case 2 to Case 6), the visualized result of Case 6 is taken as an illustration example to illustrate the principal stress distribution after the initiation of matrix crack (Fig 4.15a) and the crack propagation through the matrix and interface (Fig. 4.15b). From the cut-out view in Fig 4.15b, we can see that the matrix crack is firstly initiated at the tension side and then propagated to the interface to cause interfacial failure, which is very similar to the failure process of the two-dimensional model shown in Section 4.4.1.

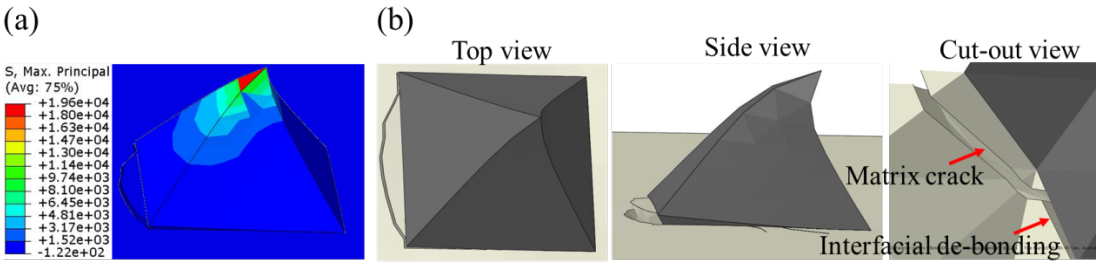

Fig. 4.15 3-D finite element model of the representative part of the ID bit: (a) Diamond and matrix parts and (b) mesh configuration of the model.

4.4.3 Effect of diamond shapes

The shape of the diamond grits plays an important role in the behaviour of abrasive cutting tools, and it has a significant effect on their retention capacity or failure mode in ID bits. Thus, the diamond particle shape is investigated in this section. Natural diamonds with irregular shapes are not suitable for ID bit use as they are mostly in round shape with limited cutting ability (Fig. 4.16a) (Sumiya et al., 1997). Particles with sharp cutting surfaces (vertex and edge) remove surface material much faster than round particles without sharp surfaces. Unlike natural diamonds, synthetic diamond particles are mainly produced using the Chemical Vapor Deposition (CVD) technique, which can help to produce regular shaped diamonds (Fig. 4.16b). Therefore, synthetic diamonds can be conveniently represented as regular polygons, as shown in Fig. 4.17. In this study, six regular polygonal shapes having a different

number of sides ranging from 4 to 12 are used to show their effects on different failure modes (interfacial and matrix failure). The force is applied to these systems by imposing a gradual horizontal displacement at the tip (top corner) of the diamond towards the right side. Similar to the previous section, the size of the diamond particles remains constant, r = 0.25 mm (radius of the circle circumscribing the polygons), for all the cases shown in Fig. 17. The protrusion height h = 0.25 is used and the vertex of each of the diamond particles is rotated to face upward to form a sharp cutting surface in all these cases. Same material properties, provided in Section 2, are used for both the diamond and the matrix parts. In order to simulate different failure modes for each case, two different interfacial parameters (weak interface and strong interface) are used in this section for each diamond shape. For the weak interface, τ_n^0 = 543 MPa, τ_s^0 = 314 MPa, G_{IC} = 0.14 mJ/mm^2 and G_{IIC} = 0.33 mJ/mm^2 were used as the interfacial property parameters, whereas a perfect interface (infinite interfacial strength created by applying tied interface connection instead of CZM) was used for the strong interface case.

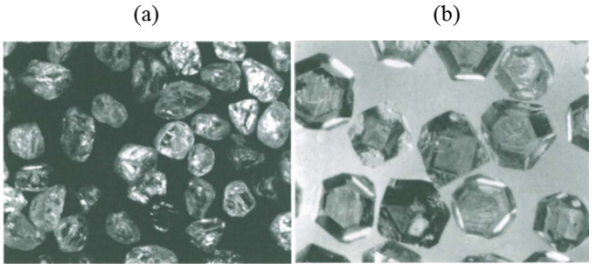

Fig. 4.16 Shape illustration of natural and synthetic diamonds: (a) natural diamond and (b) synthetic diamond.

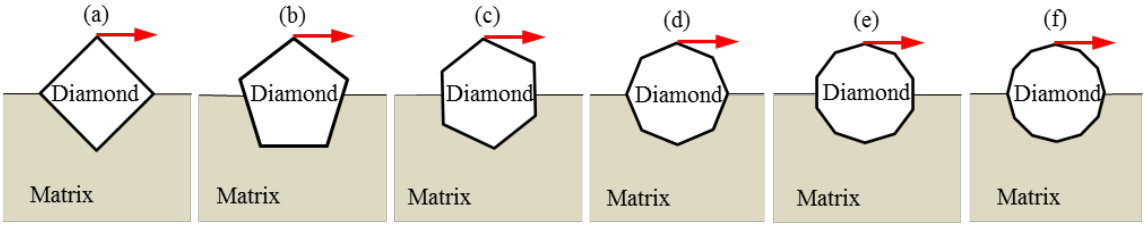

Fig. 4.17 Study of different diamond shapes: (a) square, (b) pentagon, (c) hexagon, (d) octagon, (e) decagon and (f) dodecagon.

The distribution of maximum principal stress over the entire system obtained after the initiation of failure for all diamond shape cases is presented in Fig. 4.18. The Figure shows the occurrence of stress concentrations near the tipping point (loading point) and the area around the diamond-matrix interface in all cases. The first column (a) in Fig. 4.18 represents the weak interface case for all diamond particle shapes, whilst the second column (b) represents the strong interface. According to the results, interfacial failure would occur prior to the occurrence of matrix failure when the interface and matrix have similar fracture parameters, which is called a weak interface. Under this condition, the shape of the diamond particle has little effect on its retention ability, with a change from the lowest critical force of 63 N for a square shaped particle to the highest critical force of 109 N for a hexagon shaped particle. For the strong interface, the square shaped particle has the lowest critical force to initiate the matrix crack at the tension side, where all the other shapes with strong interfaces require much higher critical forces, in the range between 440 N and 645 N.

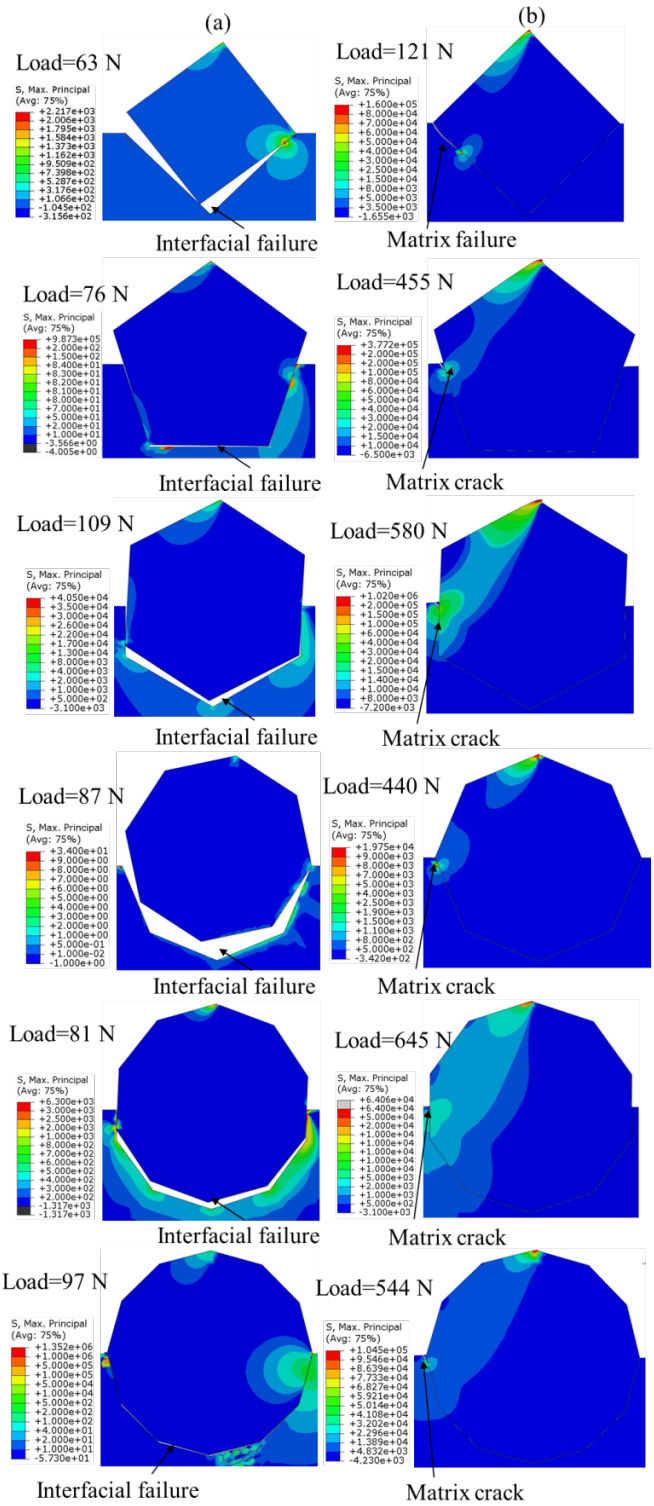

Fig. 4.18 Maximum principal stress distributions of different diamond shapes with different interface properties: (a) weak interface and (b) strong interface.

The critical values of the cutting force corresponding to the initiation of the interfacial failure or matrix crack for the different diamond shapes with the weak interface and strong interface are plotted in Fig. 4.19, respectively. The results indicate that the hexagon shaped diamond particle has the relatively strongest interfacial bonding ability among these differently shaped particles when the weak interface is applied. On the other hand, when the interface has strong binding strength, matrix failure would occur first in the vicinity of the interface at the tension side. The critical forces to initiate the matrix crack are much higher than those for weak interface failure. Hexagon and decagon shaped particles require relatively higher forces for matrix failure, where the critical force of the square shaped particle is much lower than for the other shapes (121 N).

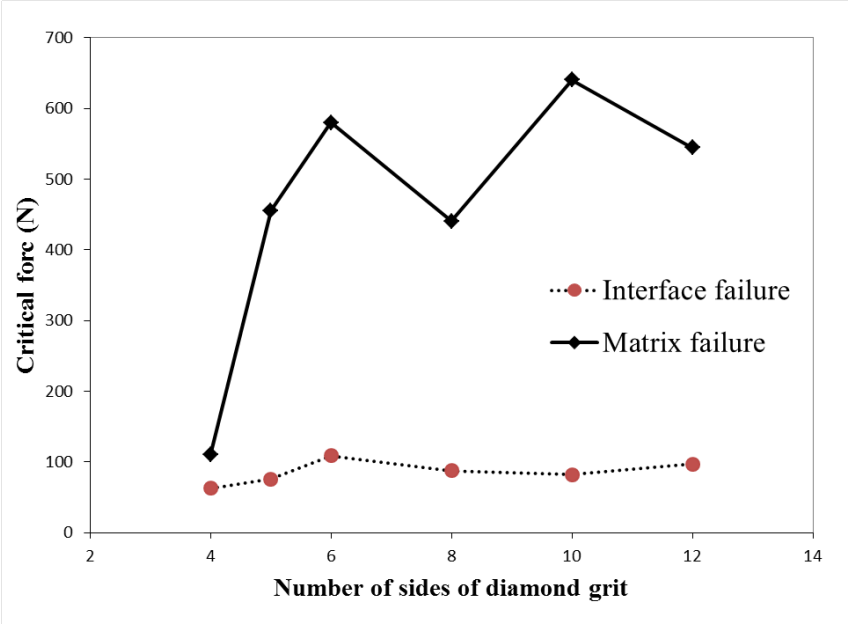

Fig. 4.19 Effect of diamond particle shape and interfacial strength on its retention capacity.

4.5 Conclusions

In this study, the failure mechanisms of impregnated diamond bits are investigated through the use of the finite element method. The present study has a focus on the interfacial failure mechanisms between the matrix and diamond particles, as well as the matrix crack failure. The developed model includes a single diamond partially embedded in a portion of the surrounding matrix, which is a representative part of diamond bits, and a zero thickness surface based cohesive zone model is used to simulate the interfacial failure, where the extended finite element model with cohesive damage is used to analyse the matrix crack initiation and propagation. This provides vital understanding of the diamond pull-out mechanism, which is one of the significant failure modes of diamond bits. A tangential displacement load is applied at the protruding tip of the diamond particle to simulate the cutting force during the drilling operation, and the surrounding matrix is restrained at its far ends. Both two-dimensional and three-dimensional models of the impregnated diamond bits are conducted and analysed in this study. The diamond-matrix system is simulated by the finite element modelling with 4-node plane strain quadrilateral elements in two-dimensional models and 4-node linear tetrahedron elements in three-dimensional models.

Numerical examples are developed and solved to validate the finite element model and investigate its performance by comparing the results with the results available in the literature. These example problems include the interfacial debonding analysis of a double cantilever beam and the fracture initiation and propagation simulation of a thin plate with a hole. An adequate performance of the model is found in this validation section, and therefore, the present model is used to conduct a parametric study for the critical force prediction of the initiation of the interfacial failure and matrix crack of the impregnated diamond bits.

Different shapes of the diamond particles and interfacial properties between the diamond and matrix have been investigated and their effects on the

retention capacity of the diamond particle of impregnated diamond bits are studied and compared. It has been observed that both parameters have a significant influence on the retention ability of the diamond particles and failure mechanisms of the ID bits. When the interface has relatively lower adhesion strength, the interface tends to de-bond prior to the occurrence of matrix failure. Under this circumstance, the critical forces for interfacial failure are relatively low and the shape of the diamond particles has little effect on its retention capacity. On the other hand, the matrix starts to crack in the vicinity at the tension side of the interface when the interface has a very high binding strength. At this point, the square shaped diamond particle has a much lower critical force for the initiation of matrix failure than the other shapes. As the efficiency of the entire drilling process is also dependent on the sharpness of the cutting surface, the hexagon shaped diamond particle is found to have a better performance for drilling due to its relatively higher retention capacity as well as its sharper cutting face. Moreover, the effect of the matrix-fracture parameters has also been studied by conducting a three-dimensional model and the result is similar to the two-dimensional model. When the matrix has relatively higher fracture properties, only interfacial failure would occur. However, if the weak matrix fracture properties were given in the model, the matrix crack would occur at the start and be followed by the pull-out (interfacial debonding) failure of the diamond particle. Finally, it is worth noting that the interfacial properties directly influence the ultimate force (diamond pull-out) of the diamond-matrix system, which the ultimate strength increases with the increase of the interfacial strength.

Acknowledgement

The work has been supported by the Deep Exploration Technologies Cooperative Research Centre, whose activities are funded by the Australian Government's Cooperative Research Centre Programme. This is a DET CRC Document.

References for Chapter 4

SØRENSEN, B. F. & JACOBSEN, T. K. 2003. Determination of cohesive laws by the J-integral approach. *Engng Fract Mech,* 70**,** 1841-1858.

BARENBLATT, G. I. 1962. Advances in Applied Mechanics. *Academic Press, New York***,** pp. 55.

BELYTSCHKO, T. & BLACK, T. 1999. Elastic crack growth in finite elements with minimal remeshing. *International Journal for Numerical Methods in Engineering,* 45**,** 601-620.

BUSCH, D. M. & HILL, B. S. 1975. *Concrete Drilling with Diamond Impregnated Bits*, De Beers Industrial Diamond Division.

CAMANHO, P. P., DÁVILA, C. G. & DE MOURA, M. F. 2003. Numerical simulation of mixed-mode progressive delamination in composite materials. *Journal of Composite Materials,* 37**,** 1415-1438.

CAVALLI, M. N. 2003. Cohesive Zone Modelling of Structural Joint Failure. *Ph.D. Thesis, University of Michigan*.

CHALKLEY, J. R. & THOMAS, D. M. 1969. The tribological aspects of metal bonded diamond grinding wheels. *Powder Metallurgy,* 12(24)**,** 582-597.

CUI, W. & WISNOM, M. R. 1993. A combined stress-based and fracture-mechanics-based model for predicting delamination in composites. *Composites,* 24**,** 467-474.

DE MORAIS, A. B., DE MOURA, M. F., MARQUES, A. T. & DE CASTRO, P. T. 2002. Mode-I interlaminar fracture of carbon/epoxy cross-ply composites. *Composites Science and Technology,* 62**,** 679-686.

DING, H., LI, Y., YANG, X., HAO, H. & JIN, Z. 1998. Design of a non-homogeneous diamond bit matrix. *Journal of Materials Processing Technology,* 84**,** 159-161.

ELGUEDJ, T., GRAVOUIL, A. & COMBESCURE, A. 2006. Appropriate Extended Functions for X-FEM Simulation of Plastic Fracture Mechanics. *Computer Methods in Applied Mechanics and Engineering,* 195**,** 501–515.

ELICES, M., GUINEA, G. V., GÓMEZ, J. & PLANAS, J. 2002. The cohesive zone model: advantages, limitations and challenges. *Engineering Fracture Mechanics,* 69**,** 137-163.

HSIEH, Y.-Z. & LIN, S.-T. 2001. Diamond tool bits with iron alloys as the binding matrices. *Materials Chemistry and Physics,* 72**,** 121-125.

JAENSSON, B. O. & SUNDSTRÖM, B. O. 1972. Determination of Young's modulus and poisson's ratio for WC Co alloys by the finite element method. *Materials Science and Engineering,* 9**,** 217-222.

KONSTANTY, J. 1999. Developing a better understanding of the bonding and wear mechanisms involved in using diamond impregnated tools. *In Proceedings of International Workshop on Diamond Tool Production, Turin, Italy***,** pp. 97-106.

KONSTANTY, J. 2005. Chapter 3 - Diamond tool design and composition. *In:* KONSTANTY, J. (ed.) *Powder Metallurgy Diamond Tools.* Amsterdam: Elsevier Science.

KUMAR, S., SINGH, I. V., MISHRA, B. K. & RABCZUK, T. 2015. Modeling and simulation of kinked cracks by virtual node XFEM. *Computer Methods in Applied Mechanics and Engineering,* 283**,** 1425-1466.

LI, B., AMARAL, P. M., REIS, L., ANJINHO, C. A., ROSA, L. G. & FREITAS, M. D. 2010. 3D-modelling of the local plastic deformation and residual stresses of PM diamond–metal matrix composites. *Computational Materials Science,* 47**,** 1023-1030.

LIAO, Y. S. & LUO, S. Y. 1992. Wear characteristics of sintered diamond composite during circular sawing. *Wear,* 157**,** 325-337.

LIN, C.-S., YANG, Y.-L. & LIN, S.-T. 2008. Performances of metal-bond diamond tools in grinding alumina. *Journal of Materials Processing Technology,* 201**,** 612-617.

M. ALFANO, F. F., A. LEONARDI, C. MALETTA AND G. H. PAULINO 2007. Cohesive Zone Modeling of Mode I Fracture in Adhesive Bonded Joints. *Key Engineering Materials,* 348-349**,** 13-16.

MELENK, J. M. & BABUSKA, I. 1996. The partition of unity finite element method: basic theory and applications. *Computer Methods in Applied Mechanics and Engineering,* 139**,** 289-314.

MILLER, D. & BALL, A. 1990. Rock drilling with impregnated diamond microbits—An experimental study. *International Journal of Rock Mechanics and Mining Sciences & Geomechanics Abstracts,* 27**,** 363-371.

MILLER, D. & BALL, A. 1991. The wear of diamonds in impregnated diamond bit drilling. *Wear,* 141**,** 311-320.

MOES, N., DOLBOW, J. & BELYTSCHKO, T. 1999. A finite element method for crack growth without remeshing. *International Journal for Numerical Methods in Engineering,* 46**,** 131-150.

OSHER, S. & SETHIAN, J. A. 1988. Fronts propagating with curvature dependent speed: algorithms based on Hamilton–Jacobi formulations. *Journal of Computational Physics,* 79**,** 12-49.

PAONE, J. & MADSON, D. 1966. *Drillability Studies: Impregnated Diamond Bits*, Department of the Interior, Bureau of Mines.

ROMANSKI, A. 2010. Factors affecting diamond retention in powder metallurgy diamond tools. *Archives of Metallurgy and Materials,* 55**,** 1073-1081.

SØRENSEN, B. F. 2002. Cohesive law and notch sensitivity of adhesive joints. *Acta Mater,* 50**,** 1053-1061.

STOLARSKA, M., CHOPP, D. L., MOES, N. & BELYTSCHKO, T. 2001. Modelling crack growth by level sets in the extended finite element method. *International Journal for Numerical Methods in Engineering,* 51**,** 943-960.

SUH, C.-M., BAE, K.-S. & SUH, M.-S. 2008. Wear behavior of diamond wheel for grinding optical connector ferrule — FEA and wear test —. *Journal of Mechanical Science and Technology,* 22**,** 2009-2015.

SUKUMAR, N., MOES, N., MORAN, B. & BELYTSCHKO, T. 2000. Extended finite element method for three-dimensional crack modeling. *International Journal for Numerical Methods in Engineering***,** 1549-1570.

SUMIYA, H., TODA, N. & SATOH, S. 1997. Mechanical properties of synthetic type IIa diamond crystal. *Diamond and Related Materials,* 6**,** 1841-1846.

TADA, H. 1985. The stress analysis of cracks handbook. *Paris productions incorporated*.

TZE-PIN, L., HOOD, M., COOPER, G. A. & XIAOHONG, L. 1992. Wear and failure mechanisms of polycrystalline diamond compact bits. *Wear,* 156**,** 133-150.

XUEFENG, T. & SHIFENG, T. 1994. The wear mechanisms of impregnated diamond bits. *Wear,* 177**,** 81-91.

ZHAI, J. & ZHOU, M. 2000. Finite element analysis of micromechanical failure modes in a heterogeneous ceramic material system. *International Journal of Fracture,* 101**,** 161-180.

ZHOU, Y., FUNKENBUSCH, P. D. & QUESNEL, D. J. 1997. Stress distributions at the abrasive-matrix interface during tool wear in bound abrasive grinding—a finite element analysis. *Wear,* 209**,** 247-254.

Chapter 5

Conclusions

Diamonds have been widely used to make diamond tools for rock and metal machining operations such as drilling, sawing and grinding in mining, civil and many other engineering disciplines for many decades. Diamond tools can be loosely divided into three classes, namely impregnated, brazed, and electroplated tools, according to the manufacturing process. The impregnated diamond core bits, commonly used in the mineral exploration industry for hard rock drilling, consist of large numbers of diamond grits having a size in the order of 100 microns, commonly embedded in a metal matrix. The drill bit diamond segments are manufactured by mixing the diamond grits with the metal powders thoroughly and then processing the mixture under high temperatures and high pressure, known as the sintering process, to form solid segments. Thus the diamond bit segment is practically a particulate composite material where the metals act as the matrix for binding the diamond particles that are randomly distributed within the composite material. The diamond composite segments are attached to the steel core barrel by means of brazing or laser welding to form the final drill bit. Synthetic diamond manufacturing techniques have undergone a tremendous revolution over the past five decades. There are two commonly used methods for the production of synthetic diamonds: high-pressure high-temperature (HPHT) techniques and chemical vapor deposition (CVD) techniques. A CVD diamond refers to the manner of growing such diamonds from a gas phase. The CVD diamond is a major breakthrough in the low-pressure synthesis of polycrystalline diamonds. In operation, impregnated diamond bits have unique self-sharpening characteristics. Under ideal conditions, the matrix is expected to hold the

freshly exposed, sharp diamonds firmly and at the same time, the matrix should wear at a rate compatible with that of the diamonds so that the worn diamond can fall out to allow new diamonds to be exposed continuously. However, in some cases, diamonds are held by the matrix through mechanical interlocking, which gives a low interfacial strength and leads to a weak retention ability of the diamond bit. The lack of interfacial bonding between diamond particles and the surrounding metallic matrix results in the de-bonding of diamonds prior to reaching their full-service life, which is one of the most undesirable failure modes of a diamond bit. This premature loss of diamonds greatly impacts the tool's cutting efficiency and increases the cost of drilling operations as well as reducing the service life of the diamond bit. Thus, in order to improve the retention capacity of diamonds to avoid their premature fall-out, a great deal of effort has been made to establish a strong bond between the diamonds and the matrix by means of supportive chemical bonding. Consequently, the technique of metal-coating on diamonds has been invented and used to resolve the problems. Several investigations as to the stress distribution inside the impregnated diamond bits using numerical simulations have been carried out by researchers over the previous few decades. However, no modelling has been found on the interfacial failure of this system, which can predict the diamond pull out process realistically. Therefore, proper modelling of interfacial crack initiation and its propagation in impregnated diamond bits is necessary to understand the complex interaction process between the rock-diamond-matrix better, so that the design of such tools can be improved significantly.

The specific contributions of this research are summarised in Section 5.1. The limitations of this research and the recommendations for future work are presented in Section 5.2.

5.1 Research contributions

This thesis presents a micromechanical model, in both two dimensions and three dimensions, of a single diamond particle embedded inside the metal matrix in terms of the tangential cutting force applied to the cutting face of the diamond particle. An FEM modelling tool is employed to study the impregnated diamond bit's stress and strain distributions during the cutting process, incorporating of CZM (cohesive zone modelling) to simulate interfacial crack initiation and its propagation between the diamond particle and the surrounding metal matrix as it is the weakest component and the location of the critical failure mode during drilling operations. Moreover, the failure of the matrix has also been simulated using XFEM (extended finite element modelling) to model the crack's initiation and propagation in a metal matrix. Parametric studies are undertaken to investigate the effect of various features that can influence the retention capacity of the diamond particle. This includes the diamond's shape, orientation and load directions, as well as different interface properties. Based on the results, observations and in-depth analysis, the following overall conclusions can be drawn:

1. A two-dimensional FE model incorporating cohesive zone modelling, which is based on the traction-separation law, has been proposed to conduct fast and accurate predictions of interfacial debonding of impregnated diamond drill bits. The CZM is developed for modelling automatic crack propagation without any predefined cracks. In order to introduce the chemical bonding between the diamond particle and the metal matrix, tungsten coating of the diamond is used in this study, and therefore, a thin film of tungsten-carbide will be formed at the interface. As the interface properties could be affected by the coating material and sintering process, as well as the characteristics of the metal matrix and there is no valid experimental test available to measure the interface properties for impregnated diamond bits directly, the interface properties have been assumed to be the same as the properties of tungsten-carbide. In order to validate the proposed FE

model and examine its performance, a number of numerical examples have been simulated and tested, including the stress analysis of a single diamond particle embedded in the matrix under different matrix and diamond wear conditions, along with a double cantilever beam test. The results indicate that the modified FE model can efficiently and correctively cover a wide range of impregnated diamond bits for interfacial failure analysis. Therefore, having proved that the model has sufficient accuracy and reliable confidence, the proposed FE model has been applied to investigate the ways in which the diamond's shape, orientation, protrusion, and interface property affects the critical tangential load at the top tip of the diamond particle to initiate interface debonding. The hexagon shaped diamond has been found to be the best shape for drilling purposes due to its high retention capacity and cutting efficiency when its sharp corner has been orientated to do the cutting. In general, the diamond fall-out load decreases with the increasing protrusion of the diamond particle. Therefore, the matrix has to wear at a rate compatible with the rate of diamond loss. The interface fracture is dominated by Mode-I fracture properties.

2. A further developed FE model in three-dimensions has been proposed to simulate the diamond particle fall-out failure of the impregnated diamond drill bits with the incorporation of the cohesive zone method. The diamond particles developed in this study have been assumed to be a regular polyhedron with a constant diameter of 0.5 mm. The diamond was pre-treated with a tungsten coating to increase the binding between the diamond and the matrix. Two numerical example problems, a double cantilever beam test and a mixed-mode bending test, have been developed and solved by using the same computer techniques to validate the proposed model as well as to investigate its performance. As the obtained results have a good agreement with the experimental results, the present model can be recommended with confidence for the analysis of interface failure between the diamond

and the matrix of an impregnated diamond bit with reasonable accuracy and reliability. Parametric studies have been carried out to analyse the effect of different input parameters on the diamond particle's retention ability. It has been observed that the diamond's shape, orientation, and its interface properties have significant effects on the improvement of the diamond particle's retention ability under such circumstances. The diamond particle's shape and its orientation are found to have a more dominant influence than the load direction. The normal mode fracture energy has the greatest impact on the diamond's retention ability, and the Mode I fracture parameters are found to be the dominant influence on the particle's retention capacity.

3. Combined XFEM and SCZM for predicting matrix microcracking and interface debonding of ID bits is presented in this study. Both XFEM and SCZM are based on traction-separation law, represented by the maximum normal and shear strength and the normal and shear fracture energies. Tungsten carbide (WC) fracture properties were used in the models as the material properties of both the metal matrix and the interface. In general, regardless of how many sides the regular diamond polygon has (from a 4-sided square shape to a 12-sided dodecagon shape), the interface failure mode will always occur first when the same fracture properties are applied for the matrix and interface for all the half embedded diamond particles. There are two key reasons for the interface delamination that occurs before matrix failure. Firstly, the different material properties on the two sides of the interface (the diamond and the matrix) lead to a stress concentration region at the interface region. Moreover, the geometrical shape of the model leads the stress concentration at the interface to fall at the left hand side of the diamond's corner. Therefore, incorporation of the cohesive zone interface should correctly and accurately predict the failure mode of the ID bit. The square-shaped and pentagon-shaped diamond particles, with a lower number of sides, have poor retention abilities. In order to simulate the matrix failure mode, the perfect

interface (infinite strength) was applied as the interface properties for all the models with different diamond particle shapes. The critical loads to initiate micro cracks in the matrix that are computed are much higher than the loads to initiate interface failure. According to the results, the decagon shaped particle requires the highest force to initiate matrix failure, whilst the square shaped diamond has the lowest retention ability among all the models.

5.2 Limitations and future perspectives

Based on the results, it should be stressed that there are some limitations in this work, as well as a potential axis for further research. The following points are recognised to be the limitations of this research:

1. For the two-dimensional and three-dimensional FE modelling of impregnated diamond drill bits, the geometry of the model is limited to regular shaped diamond particles, which could pose restrictions on the interpretation of the simulation results when making links with laboratory tests of impregnated diamond bits. As the real diamond particle shape is irregular in most cases, a further developed numerical model considering more realistic diamond sizes and shapes is expected to provide more reliable results.

2. The present research is limited to one type of metal matrix composite as the binding material of the diamond particles; however, cobalt-base, iron-base, copper-base and tin-base alloys have also been widely used as a base matrix material for diamond-impregnated tools over the years. As the prime role of the metal matrix is to hold the diamond particle firmly during operation and it should also wear simultaneously with the diamond particle to allow the embedded diamond particle to protrude out, different matrices can be used when drilling different rock types. Therefore it is necessary to take into account more types of matrix than the tungsten-base alloy alone for the analysis of

impregnated diamond bits. The material properties of different types of metal matrix should first be observed through the experimental tests. Due to the variations in the matrix material properties, the interface properties should also be varied. There is currently no valid method available to test the interface properties directly, thus, a proper experimental test method for the determination of the interface properties between diamonds and a range of matrices should be proposed in a future study.

3. The uncertainty of the design variables of impregnated diamond bits is not considered in the present study, however, the material manufacturing deviations during the sintering process may cause micro-cracks or flaws either in the matrix or at the interface. This may lead to the premature failure of the diamond-impregnated bits. Therefore, robust design and reliability based on an optimisation design are very important for the cutting efficiency and service life of impregnated diamond bits in any future work.

4. In the present research, only a static tangential load is considered and applied to the cutting face of the diamond particle. However, the real drilling conditions of the impregnated bits are more complex, with the forces acting on the diamond bit varying due to the vibrations caused by the uneven surface of the rocks. Therefore, a more realistic loading condition of the impregnated diamond bit, based on experimental determination of potential parameters, should be considered in the numerical simulation in any future research. Dynamic loading conditions and impact loads could also be considered, along with diamond particle failure, as the diamond is a brittle material, which can easily crack under impact loads.
5. As the drilling operation can create heat at the cutting surface between the bit and rock, the temperature at the bit surface can reach as high as some 700 degrees. This may lead to material property changes in the drill bit as the majority portion of the bit consists of metals. Therefore,

the thermal effect and the thermal conductivity of the bit should be considered during future numerical simulations.

Appendix

Copy of Paper 1 (as published)

J. Xu, A.H. Sheikh, C. Xu. (2016). Interfacial failure modelling of diamond bits made of particulate composites. *Composite Structures*, Vol. 115, pp. 145-159.

Composite Structures 155 (2016) 145–159

Contents lists available at ScienceDirect

Composite Structures

journal homepage: www.elsevier.com/locate/compstruct

Interfacial failure modelling of diamond bits made of particulate composites

J. Xu, A.H. Sheikh *, C. Xu

Deep Exploration Technologies Cooperative Research Centre, School of Civil, Environmental and Mining Engineering, University of Adelaide, Adelaide, SA 5005, Australia

ARTICLE INFO

Article history:
Received 4 January 2016
Revised 15 July 2016
Accepted 27 July 2016
Available online 29 July 2016

Keywords:
Diamond impregnated bits
Particulate composite materials
Diamond pull out
Interface de-bonding
Cohesive zone modelling
Finite element modelling

ABSTRACT

The failure analysis of diamond impregnated bits, which are found as particulate composite materials consist of diamond particles randomly distributed within a metal matrix, is conducted to study the pull out behaviour of diamond grits for an assessment of diamond retention capacity of these drilling bits. The finite element technique is used to model the diamond-matrix system where a zero thickness surface based cohesive zone modelling technique is used to simulate the failure at the interface between the matrix and the diamond particle. For the validation of the model, few numerical examples are initially solved and the results produced by the model are compared with the published results which show a good performance of the model. Finally, a parametric study is conducted to show the effects of shapes, orientations and protrusions of diamond particles as well as interface properties on the retention capacity of diamond particles.

1. Introduction

Since the invention of synthetic diamonds dated back to 1950s, these diamonds have been increasingly used as impregnated diamond tools for drilling, grinding, sawing and similar activities of hard materials such as rock, concrete, metal and glass. The popularity of diamond impregnated tools is due to various advantages such as low friction coefficient, high stiffness and thermal conductivity as well as high bulk modulus exhibited by these tools [1,2]. The impregnated diamond bits are commonly used in the mineral exploration industry for drilling hard rocks. A segment of these bits is made with particulate composite material consist of large numbers of diamond particles having a size of the order of 100 μm which are evenly distributed within a metal matrix. The diamond grits are thoroughly mixed with metal powders and the mixture is processed under high temperature and pressure, known as sintering process, to form these solid bit segments. The materials commonly used for this metal matrix are cobalt, copper, tin, tungsten, and nickel due to their optimal mechanical and thermal properties [3–5]. During the drilling operation, when the cutting surface of the bit slides over a rock due to rotation of the bit, the embedded diamond particles near the cutting surface are partially exposed due to gradual wear of the matrix material and these exposed diamonds do the cutting or drilling of the rock. The matrix is expected to hold the freshly exposed sharp diamonds firmly and at the same time, it should wear at a rate compatible with that of diamonds so that the worn diamond can fall out to allow new diamonds to expose continuously [6]. This is one of the major advantages of impregnated diamond bits, which is known as their self-sharpening ability. The de-bonding of diamonds prior to reaching their full service life is one of the most undesirable failure modes of these bits. This premature loss of diamonds greatly impacts the tool's cutting efficiency and increase the cost of drilling operation [7].

In order to study the mechanical properties of particulate composites, Huang et al. [8] conducted an experimental test to evaluate the Elastic Moduli of polyester resin matrix composites with hollow glass spheres inclusions as reinforcements and the results have been compared with the theoretically calculated elastic moduli. Tagliavia et al. [9] have investigated the mechanical properties of syntactic forms reinforced with spherical hollow particles under tensile loading where the effect of particle-matrix de-bonding and particle wall thickness on the elastic modulus of the reinforced foam has been shown. Tagliavia et al. [9] have developed a model which they used along with the finite element analysis to undertake this research. Shams et al. [10] have developed another model and made a study, which is very similar to Tagliavia et al. [9]. However, the behaviour of these particulate composite materials [8–10] will be quite different from the diamond impregnated bits as the most effective particles are partially exposed from the matrix in

* Corresponding author.
E-mail address: abdul.sheikh@adelaide.edu.au (A.H. Sheikh).

http://dx.doi.org/10.1016/j.compstruct.2016.07.075
0263-8223/

the present case whereas these are embedded within the matrix for these materials [8–10].

The retention of diamond grits by the matrix is a complex and system-dependent process which is affected by the properties of the matrix, interfacial materials as well as the size, shape and orientation of diamond particles [11,12]. A poor adhesion at the interface between the matrix and diamond particles leads to premature fall out of diamond grits while resisting the interfacial stresses developed during the operation of the bits. A majority of literature has identified that the premature interface failure is one of the major issues limiting the performance of diamond bits. In some cases, diamonds are mostly hold by the matrix through mechanical interlocking which gives a low interfacial strength. In order to improve the retention capacity of diamonds, many attempts have been made to establish a strong bond between the matrix and diamonds by adding some alloy which reacts with carbons present in diamonds to form chemical bonding in the form of metal-carbide elements at the interface [13,14]. Initially, iron, tungsten and nickel alloys are added into the metal matrix formation which not only helps to improve the strength, toughness and hardness of the matrix but also enhances the interfacial strength as these metals have a strong atomic bonding affinity for carbons. However, it has been proved that a severe diamond surface degradation is often observed by the formation of too thick carbide layers due to adding more chemically reactive materials into the metal matrix powder [7]. Also for an industrial scale of production, it is almost impracticable to prevent the graphitization of diamonds under high temperature which is required when the matrix material includes these reactive alloys. Consequently, the technique of metal-coated diamonds has been invented which not only protects the diamonds from oxidization, but also increases their retention capacity [12]. Tungsten has been widely used as a coating material for diamond grits, and it helps to form a thin film of tungsten carbide at the interface that acts as a strong chemical bond between the matrix and diamonds [7]. Besides using tungsten as coating material, some other metals such as Ti-coating are also used which improves the interfacial bonding strength significantly [4].

Initially, some experimental studies [6,15,16] on impregnated diamond bits were conducted where the wear mechanisms of these bits were investigated. Also, the wear modes have also been classified into four distinct types where the pull out of diamonds is one of these failure modes, which has an importance influence on the efficiency of these bits. However, no one made any attempt to quantify these failure mechanisms in terms of displacements, forces or some other mechanical parameters so far. The first attempt towards modelling the behaviour of these diamond bits is due to Zhou et al. [17] who conducted stress analysis of a single diamond particle along with a portion of the surrounding matrix as a representative part of these bits using a 2-dimensional finite element model without considering any failure or damage at the interface between the matrix and diamonds. This may be defined as a micro-mechanical modelling of the bits where the diamond is subjected to a horizontal cutting force only at its cutting tip. Zhou et al. [17] plotted the variation of normal stress along the interface for different levels of matrix wear and these stress distributions were taken as the measure of interface de-bonding failure. Suh et al. [18] conducted a similar study on diamond impregnated grinding wheel where they calculated the von Mises stress along the interface where they also studied the effect of unsymmetrical matrix wear with respect to the diamond particle. In a slightly different study, Li et al. [19] tried to predict the plastic deformation and residual stresses within the matrix near the diamond particle which are produced due to the sintering process where a 3-dimensional finite element simulation of the micro-mechanical model were used. It is interesting to note that no one has paid any attention so far on the modelling of interface failure of this system which can predict the diamond pull out process more realistically. This is a problem of interfacial crack propagation which is a complex process but a proper modelling of this process is necessary for a better understand of these diamond tools and their design.

A satisfactory solution of the above problem can be achieved by using the concept of fracture mechanics which can be implemented through finite element modelling. In this context, the Virtual Crack Closure Technique (VCCT) [20] became quite popular which is based on Linear Elastic Fracture Mechanics (LEFM). Although valuable information related to onset and stability of a crack can be obtained by using this technique (VCCT), it is not convenient for modelling crack propagation as VCCT requires re-meshing to advance the crack front when the energy release rate reaches its critical value [21]. Moreover, the VCCT requires the information of a pre-defined initial crack. These problems can be eliminated by using the cohesive zone modelling (CZM) technique which is becoming very popular in recent years for modelling automatic crack propagation in many engineering problems. However, this technique needs the information of the crack propagation direction in advance. Incidentally this is predefined in the present problem which is simply the interface between the matrix and diamonds. Similarly, there are many other problems such as delamination in multi-layered composite laminates, bond failure of reinforcing bars or externally bonded plates in concrete structures, delamination in adhesively bonded joints, matrix-inclusions de-bonding in any composite materials and similar situations where the direction of crack propagation is known [22–24].

Actually, the delamination problem in multilayered composite structures has drawn a significant attention in recent past which has helped to develop this modelling technique (CZM) so well that it can be used with full confidence. The fundamental idea of the CZM technique is based on the concept of fracture process zone which is characterise by the cohesive law or traction separation law for the de-cohesion of atomic lattices as proposed by Barenblatt [25]. According to this model, the traction across the interface between the two materials is increased elastically at the beginning with the separation of these two materials until the traction reaches its critical value. This traction is then decreased with further increase of the separation and eventually disappears according to some principles of damage mechanics.

The CZM technique, which has been successfully applied to various problems, should to be most suitable for the present problem but it has not been exploited so far. Thus the matrix-diamond interface failure is modelled by finite element and CZM techniques in combination for the first time in this study. This will help to understand the wear mechanism of impregnated diamond bits due to diamond pull out more accurately that can benefit the design of these bits. Moreover, there is a need for investigating the effect of different parameters such as protrusions, shapes and orientations of the diamond particle on its retention capacity which is undertaken in this research as this has not been studied previously.

2. Numerical model

2.1. Geometry of the model and its finite element meshing

Similar to the previous investigations [17,18], the failure of diamond impregnated bits is modelled by taking a single diamond particle which is partially embedded within the matrix and cuts the rock with its exposed part during the drilling operation (Fig. 1a). The model also includes a portion of the surrounding matrix that holds the diamond particle (Fig. 1a) where the dimension of this portion of matrix (within the dotted lines) is adequate

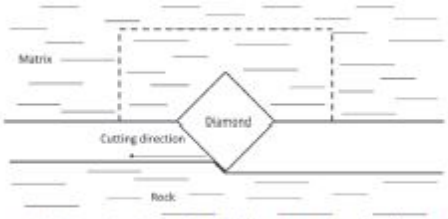

(a) Schematic draw of the drilling operation of a diamond impregnated bit

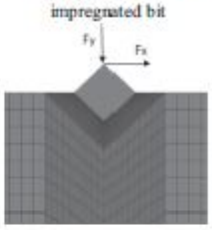

(b) Finite element model of the representative part of the diamond impregnated bit

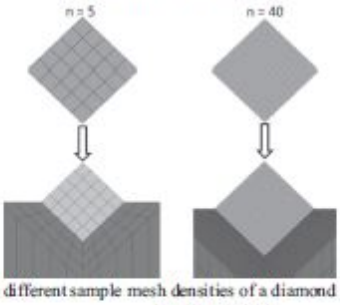

(c) Two different sample mesh densities of a diamond particle and its surround matrix

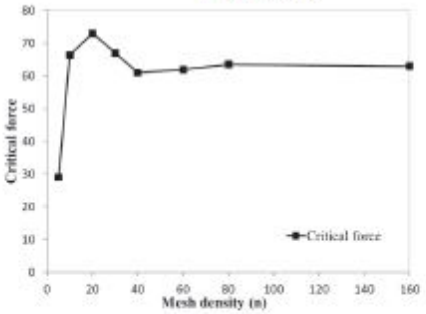

(d) Critical force versus n (mesh size)

Fig. 1. Finite element model of a diamond impregnated drill bit.

to dissipate the stresses produced by the forces acting on the diamond particle. For the justification of the above model, it is assumed that diamond particles are evenly distributed within the matrix and having adequate gaps between them so that stresses around these particles do not affect each other. This is true for most of the diamond bits as they are designed to have adequate service lives by avoiding non-uniform distribution of diamond grits which is responsible for localised stress concentration leading to premature failure of these bits. In order to predict the failure and stresses within the representative portion of the diamond bit mentioned above (Fig. 1a), a 2-dimensional finite element modelling of this portion (Fig. 1b) is undertaken. For the convenience of representing the problem, the finite element model (Fig. 1b) is drawn as a mirror image (upside down) of the actual object. Although the model considered both horizontal and vertical forces to simulate cutting force (F_x) and vertical thrust force (F_y) on the bit, the results indicate that the fall-out of the diamond particle due to interfacial de-bonding are primarily facilitated by tangential cutting force and the additional vertical force do not affect the result much. Moreover, the magnitude of the cutting force is unknown and it changes during the cutting process. This problem is addressed by the displacement control technique where the displacement is imposed at the tip of the protruded (exposed) part of the diamond particle. The finite element model has predicted the cutting in the form of resisting force with respect to the imposed displacement. This has also determined the critical load for the interfacial de-bonding of the diamond particle.

Although the natural diamond particles are highly irregular in shape (either round and/or few sharp edges and corners), the shape of synthetic diamond grits, used in impregnated diamond bits, are controlled and these can be treated as regular polygons (2D model) in most cases. A square geometry has typically been used by different investigator for simplicity which is also used in most of the cases of the present study. The typical size of synthetic diamond particles varies from 0.01 to 0.5 mm [6,19] and this is taken as 0.5 mm in the present simulation. The size taken for the surrounding matrix is about 20 times larger than that of the diamond which is large enough to ensure that the stresses are zero near the boundaries (dotted lines in Fig. 1a) of the matrix. In the present study, a well-regarded finite element code ABAQUS 6.12 is used for a reliable numerical modelling of the diamond-matrix system. Four nodes bilinear plane strain quadrilateral elements are used to model both diamond and matrix. The mesh convergence study is performed for all examples to ensure a converged solution but the details are not shown. A sample representative case of the finite element model of the system with meshing is shown in Fig. 1b. A finer mesh is used for the regions of interest, which is the diamond particle and the portion of matrix at the vicinity of the interface, while a coarse mesh is used for the portion of matrix away from the interface with a gradual transition in order to improve the computational efficiency. The detail of the mesh convergence study of this problem is illustrated by taking 8 different mesh densities. The mesh divisions used for the diamond particle is defined as $n \times n$ and the value of n is taken as 5, 10, 20, 30, 40, 60, 80 and 160 in the present study. Fig. 1c shows two sample cases corresponding to $n = 5$ and $n = 40$. The values of the critical load obtained from these eight mesh densities are plotted in Fig. 1d, which shows that the results converged well as the mesh density increased. It can be seen that a mesh density corresponding to $n = 40$ is adequate to obtain accuracy result in this case.

2.2. Material model of the matrix and diamonds and their properties

Since diamonds behaves like a brittle material, they are treated as elastic and isotropic materials. In the present study, the modulus of the elasticity is taken as $E = 1100$ GPa whereas the Poisson's ratio $v = 0.1$ for these diamond particles [17–19]. The Tungsten-carbide cobalt (WC-Co) alloy is used as the matrix material which is having high wear resistance and hardness characteristics. The mechanical properties of WC-Co is significantly influenced by the content of cobalt as well as the tungsten-carbide grain size before sintering [26]. The modulus of elasticity and Poisson's ratio of WC-Co alloy are taken as 600 GPa and 0.2 respectively which were experimentally determined by Jaensson et al. [27] for low cobalt contained alloy. It is worth to note that WC-Co alloy is a kind of cemented carbide material and due to the high proportion of tungsten-carbide content, the matrix behaves as a hard metal

and it is treated as elastic material in the present study. In order to ensure that, elastic-plastic material properties are used to model the matrix in some sample test cases where no significant effect of plasticity is observed.

2.3. Failure model for the diamond-matrix interface

The traditional continuum based approach is not computationally attractive for modelling the interfacial failure in the present study as the thickness of the interface is very small which needs a very fine mesh to capture the sudden variation of displacements and stresses within this small distance. In this situation, the concept of cohesive zone modelling approach [23,28] is most appropriate which is adopted in the present study. This modelling approach assumes that the interface has no thickness and the formulation is based on traction separation relationship instead of stress strain relationship. A typical traction separation ($\tau - \delta$) relationship is shown in Fig. 2 where OA shows the elastic response of the interface having a high stiffness of K and AB represents the interfacial damage in the form of a linear softening law. The damage is characterized by the damage parameter (d) as shown in Fig. 2 which helps to represent the irrecoverable damage of the interface through pure elastic unloading with reduced stiffness.

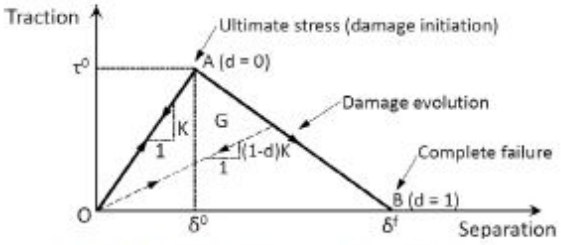

Fig. 2. A typical bilinear traction-separation relationship.

The separation at failure δ^f is obtained from the ultimate stress τ^0 (a material property of the interface) and the interfacial fracture toughness G_c (another material property) which is the area of the triangle OAB. The use of fracture energy helps to make the analyses mesh insensitive.

As the present problem is based on 2D analysis, an interface may have two possible modes of failure: 1) Mode I or opening mode due to tensile stress acting normal to the interface and 2) Mode II or sliding mode due to shear stress parallel to the interface. Thus the traction separation law (Fig. 2) mentioned above will be used for both these modes of failure which will have coupling that will be discussed later. In the present case, the separation indicates the relative displacements between the diamond and the matrix at their interface whereas the tractions are simply the interfacial stresses. These relative displacements $\{\Delta\}$ at any point of the interface may be expressed as:

$$\{\Delta\} = \begin{Bmatrix} \bar{u} \\ \bar{v} \end{Bmatrix} = \begin{Bmatrix} u^+ \\ v^+ \end{Bmatrix} - \begin{Bmatrix} u^- \\ v^- \end{Bmatrix} = \sum_{i=1}^{4} N_i(\xi = -1, \eta) \begin{Bmatrix} u_i^+ \\ v_i^+ \end{Bmatrix} - \sum_{i=1}^{4} N_i(\xi = 1, \eta) \begin{Bmatrix} u_i^- \\ v_i^- \end{Bmatrix} \quad (1)$$

where u^+ and u^- are the displacement components at the two sides of an interfacial point in the global x-direction whereas u_i^+ and u_i^- are the corresponding displacements at the ith node of the elements (Fig. 3) used to model the materials on the two sides of this interfacial point and N_i are the shape functions of these elements. This is similarly applicable to v^+ and v^- which are the displacement components in the global y-direction.

The normal and tangential components of these relative displacements $\{\delta\}$ are in local coordinate system n-s (Fig. 3) which can be obtained from their global counterparts $\{\Delta\}$ using the coordinate transformation.

According to the isoparametric formulation, the coordinates of an element can be written as $x = \sum_{i=1}^{4} N_i x_i$ and $y = \sum_{i=1}^{4} N_i y_i$ where

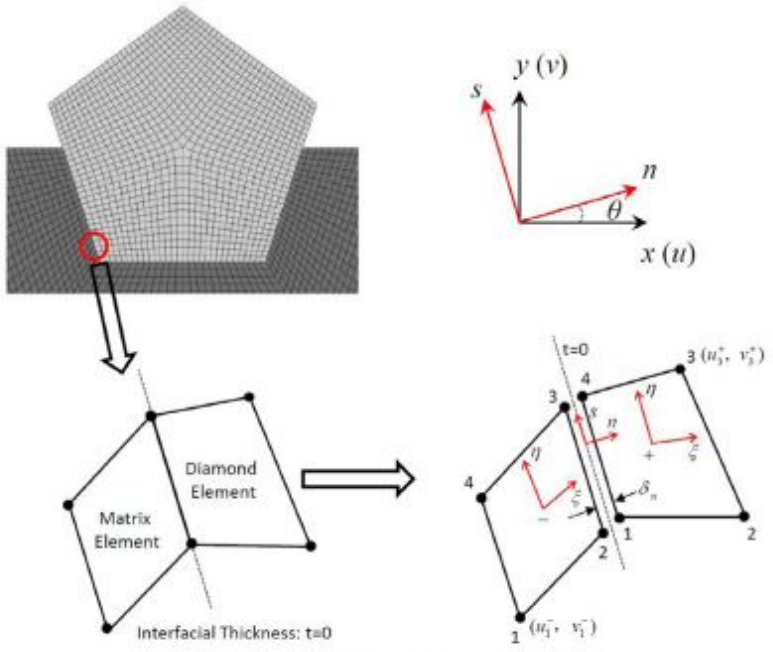

Fig. 3. Detail of an interface for cohesive zone modelling.

x_i and y_i are the nodal coordinates of the element. With these, the vectors along the curvilinear coordinate system ξ and η can be obtained as:

$$\{V\}_\xi = \begin{Bmatrix} \frac{\partial x}{\partial \xi} \\ \frac{\partial y}{\partial \xi} \end{Bmatrix} = \sum_{i=1}^{4} \frac{\partial N_i}{\partial \xi} \begin{Bmatrix} x_i \\ y_i \end{Bmatrix} \tag{2}$$

$$\{V\}_\eta = \begin{Bmatrix} \frac{\partial x}{\partial \eta} \\ \frac{\partial y}{\partial \eta} \end{Bmatrix} = \sum_{i=1}^{4} \frac{\partial N_i}{\partial \eta} \begin{Bmatrix} x_i \\ y_i \end{Bmatrix} \tag{3}$$

The above vectors may be taken at any point on the interface after substituting as $\xi = +1$ or $\xi = -1$ depending on the location of the element (i.e., negative or positive side of the interface). In order to keep the presentation simple, the + or − superscripts are avoided in this section. It should be noted that the vectors $\{V\}_\xi$ and $\{V\}_\eta$ may not be orthogonal to each other in all cases as the elements will not always have a rectangular shape (Fig. 3). However, the vector $\{V\}_\eta$ will always follow the interfacial direction which aligns with the mode II or shear failure. In order to get the vector $\{V\}_n$ along the normal direction of the interfacial and laying in $\xi - \eta$ plane for the modelling of mode I failure, it is convenient to have the vector perpendicular to the $\xi - \eta$ (or x-y) plane first and it can simply be obtained as:

$$\{V\}_z = \frac{(\{V\}_\xi \times \{V\}_\eta)}{\|\{V\}_\xi \times \{V\}_\eta\|}. \tag{4}$$

As the above equation gives a normalized unit vector $\{V\}_z$ perpendicular to the $\xi - \eta$ plane, $\{V\}_\eta$ can be normalized to have the tangential unit vector $\{V\}_s$ which may be utilized to get the unit normal vector $\{V\}_n$ as follows.

$$\{V\}_s = \frac{\{V\}_\eta}{\|\{V\}_\eta\|} \tag{5}$$

$$\{V\}_n = \{V\}_s \times \{V\}_z \tag{6}$$

Once $\{V\}_n$ and $\{V\}_s$ are obtained, the transformation matrix $[Q]$, which correlates the local coordinate system s-n of the interface (Fig. 3) with the global coordinate system x-y, can be simply formed as

$$[Q] = \begin{bmatrix} \{V\}_n^T \\ \{V\}_s^T \end{bmatrix} = \begin{bmatrix} \cos\theta & \sin\theta \\ -\sin\theta & \cos\theta \end{bmatrix} \tag{7}$$

where θ is the orientation of the normal to the interface as shown in Fig. 3. By using the above transformation matrix $[Q]$ and the interfacial relative displacements $\{\Delta\}$ expressed in global coordinates in Eq. (1), these relative displacements can be expressed in local coordinates as:

$$\{\delta\} = \begin{Bmatrix} \delta_n \\ \delta_s \end{Bmatrix} = [Q]\{\Delta\} \tag{8}$$

The damage introduces nonlinearity in the system that requires an incremental/iterative procedure for solving the governing equations. As the damage is an irreversible process, the solution technique dependent on the loading history. Thus there is a need of storing the maximum values of these relative displacements ($\delta_n^{\max}$, $\delta_s^{\max}$) which occurred before any increment/iteration and they are updated in that increment/iteration as follows:

$$\text{If } \delta_n > \delta_n^{\max} \Rightarrow \delta_n^{\max} = \delta_n \text{ otherwise } \delta_n^{\max} = \delta_n^{\max} \tag{9}$$

$$\text{If } |\delta_s| > \delta_s^{\max} \Rightarrow \delta_s^{\max} = |\delta_s| \text{ otherwise } \delta_s^{\max} = \delta_s^{\max} \tag{10}$$

The interfacial normal and shear tractions (τ_n and τ_s) can be related to the maximum value of these relative displacements using the interfacial constitutive properties in the form of traction separation laws (Fig. 2) as:

$$\begin{aligned} &\tau_n = K_n\delta_n \text{ if } \delta_n^{\max} \leqslant \delta_n^0 \\ &\tau_n = (1-d_n)K_n\delta_n \text{ if } \delta_n^0 < \delta_n^{\max} < \delta_n^f \\ &\tau_n = 0 \text{ if } \delta_n^{\max} \geqslant \delta_n^f \end{aligned} \tag{11}$$

$$\begin{aligned} &\tau_s = K_s\delta_s \text{ if } \delta_s^{\max} \leqslant \delta_s^0 \\ &\tau_s = (1-d_s)K_s\delta_s \text{ if } \delta_s^0 < \delta_s^{\max} < \delta_s^f \\ &\tau_s = 0 \text{ if } \delta_s^{\max} \geqslant \delta_s^f \end{aligned} \tag{12}$$

For the bilinear traction separation law (Fig. 2), the damage parameters for these two modes of fracture may be written as:

$$d_n = \frac{\delta_n^f(\delta_n^{\max} - \delta_n^0)}{\delta_n^{\max}\left(\delta_n^f - \delta_n^0\right)}, \quad d_s = \frac{\delta_s^f(\delta_s^{\max} - \delta_s^0)}{\delta_s^{\max}\left(\delta_s^f - \delta_s^0\right)} \tag{13}$$

The above Eqs. (11) and (12) can be used if the two modes of failure are independent having no coupling between them. However, due to the varying drilling conditions of the impregnated diamond bits, the matrix-diamond interface is more likely to have a mixed-mod fracture where the two modes of failure will be coupled as mentioned earlier. In that situation, the damage onset and its propagation may occur before reaching the ultimate stress of mode I (τ_n^0) and mode II (τ_s^0). Under mixed mode failure scenario, a quadratic failure criterion proposed by Cui et al. [29] for the prediction of damage initiation seems to be most suitable which is used in the present study and it is expressed as:

$$\left(\frac{\langle\tau_n\rangle}{\tau_n^0}\right)^2 + \left(\frac{\tau_s}{\tau_s^0}\right)^2 = 1 \tag{14}$$

Similarly, the power law [33] is used for the mixed mode damage evolution of the interface which is expressed in terms of energy release rates (G_I and G_{II}) and their critical values (i.e., fracture toughness for these two modes) as:

$$\left(\frac{G_I}{G_{IC}}\right)^2 + \left(\frac{G_{II}}{G_{IIC}}\right)^2 = 1 \tag{15}$$

where $G_I = \int_0^{\delta_n^{\max}} \tau_n d\delta_n$ and $G_{II} = \int_0^{\delta_s^{\max}} \tau_s d\delta_s$.

In a mixed mode failure analysis, the traction separation relationship (Fig. 2) for the two modes are combined and expressed in terms of an equivalent traction separation relationship having a similar bilinear shape which helps to implement the mixed-mode damage model conveniently. This combined traction separation relationship will have same initial stiffness (K) whereas the separation at the onset of damage initiation δ_m^0 and the separation at complete failure δ_m^f (subscript m indicates mixed-mode fracture) can be obtained from Eqs. (14) and (15) respectively [30]. In that case, the two components of the separation obtained in any incremental/iterative are to be combined to have single resultant component δ_m as

$$\delta_m = \sqrt{\delta_n^2 + \delta_s^2} \tag{16}$$

With the above equations, the stiffness matrix of the interface can be derived using Virtual Work Principles following the unusual steps of finite element technique. It should be noted that the Newton-Cotes integration technique is used to evaluate the interfacial stiffness matrix following the full integration scheme in order to have better results as recommended by Goncalves and

de Borst [31,32]. Thus the material properties required for defining the interfacial behaviour in present study are the fracture toughness values G_{IC} and G_{IIC} for the two modes and the corresponding ultimate stresses τ_n^0 and τ_s^0. It has been proved experimentally as well as theoretically [33,34] that these material parameters should be taken for the weaker material which is the metal matrix in the present case if the matrix is adequately connected to the diamond. Thus, the material properties of tungsten carbide cobalt (matrix) are taken as the interfacial material parameters which are:

$\tau_n^0 = 543$ MPa, $\tau_n^0 = 314$ MPa, $G_{IC} = 0.14$ mJ/mm^2 and $G_{IIC} = 0.33$ mJ/mm^2.

3. Validation of the numerical examples

Although some researchers studied the behaviour of diamond impregnated bits experimentally [5,16,35] as well as numerically [17,18] but there is no experimental test data available for validation of the present model as no one attempted to quantify the failure mechanism as mentioned earlier. On the other hand, the available numerical results [15,16] cannot be used for a complete validation of the present models because these studies did not consider the interfacial damage. These studies [15,16] used a linear finite element model to evaluate the diamond-matrix interfacial stresses which were taken as a simple measure of interfacial debonding. However, these numerical results [15,16] are utilised for a partial validation of the present model taking a perfect diamond-matrix interface. The interface damage model used in the present analysis is indirectly validated with the test data of a double cantilever beam (DCB) [24].

3.1. Validation of the model with perfect diamond-matrix interface considering different levels of matrix and diamond wear

This problem is picked up from the paper of Zhou et al. [17] who applied a constant cutting force ($P = 2.5$ N) on the diamond particle having a square geometry with 0.015 mm sides (Fig. 4a) and the analysis was carried out taking the modulus of elasticity as 1141 GPa and 110 GPa for the diamond and the matrix (bronze) respectively. The problem seems to be hypothetical in regards to the particle size and the magnitude of cutting force but this is used only for the purpose of validation. The same loading, material properties and geometric dimensions are used in the present finite element model and the analysis is carried out for different levels of matrix wear (Fig. 4a). For the representation of results with respect to the meshing used in the present analysis (diamond has a regular/structured meshing with a division of 12 × 12), the matrix wear is defined as "0" (initial condition or basic case) when one-fourth of the diamond height is exposed or protruded out of the matrix whereas this is "6" when six layers of matrix elements of the basic case are removed to have half protrusion of the diamond particle (Fig. 4a). These elements are removed incrementally at the rate of two layers at a time that has simulated seven different levels of matrix wear ranging from "0" to "12" with an increment of 2. The finite element mesh used for three sample cases of matrix wear is shown in Fig. 4a where the entire portion of the matrix considered in the present model is not shown for the convenience of presentation.

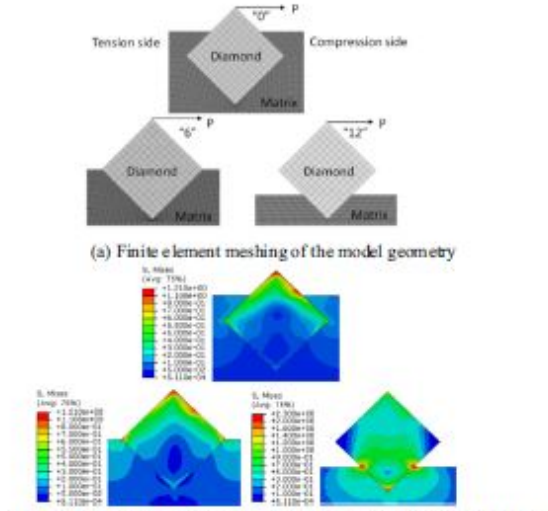

(a) Finite element meshing of the model geometry

(b) Distribution of the Von-Mises stress over the entire body found in the present FE analysis

Fig. 4. Finite element analysis for different level of matrix wear.

Similar to Zhou et al. [17], the cutting force is applied on the left side of the diamond particle's exposed edge where total force (2.5 N) is equally distributed at the six nodes starting from the top corner of the diamond. The variations of Von-Mises stress over the entire system predicted by the present finite element model are illustrated as stress contours in Fig. 4b. It could be noted that higher values of this stress component are concentrated at the tension side of the diamond-matrix interface near the exposed surface of the matrix. As Zhou et al. [17] presented their results in the form of distribution of the normal stress (σ_n) along the diamond-matrix interface; the normal stress (σ_n) at any point of the interface, which acts perpendicular to the interfacial plane, is computed by transforming the stresses (σ_x, σ_y, σ_{xy}) at that point obtained in the present analysis. For this purpose, the elements along the interface, which are within the diamond particle, are selected and the stresses at their gauss points are utilised. It should be noted that the number of gauss point of an element is one which is at its centroid for the type of element used in the present model. Based on these calculations, the variation of normal stress (σ_n) found along the interface on the tensile side of the diamond particle is plotted in Fig. 5. For the convenience of presentation, the distance along the interface, which is the horizontal axis of Fig. 5, is shown in terms of element numbers of the diamond particle where the number assigned to the lower corner element is 0 and the number incremented by one while moving along the interface on the tensile side following the direction of the arrow as shown. The figure shows that the matrix wear has a significant effect on the variation of interfacial normal stress. For the initial condition of the matrix wear ("0"), the maximum value of the normal stress is about 0.8 MPa which is found at element #17. For the highest level of matrix wear ("12"), the maximum/peak normal stress is found to be 1.25 MPa which indicates that it increases with the increase of the level of matrix wear. The figure shows the occurrence of a second peak stress when matrix wear is severe (e.g., second peak stress at element #7 and element #5 for matrix wear corresponding to "10" and "12" respectively). It also illustrates a significant variation of the stress distribution at the exposed surface of the matrix. Moreover, the present results are found to have very good agreement with those reported by Zhou et al. [17].

In order to study the effect of plastic deformation of the matrix (metal) on the final results, a typical elastic-plastic material model based on von Mises yield criterion with isotropic hardening and associated flow rule is used to the matrix (bronze). A bi-linear stress-strain curve with a yield stress of 70 MPa, ultimate stress of 220 MPa and maximum plastic strain of 5% is used for the

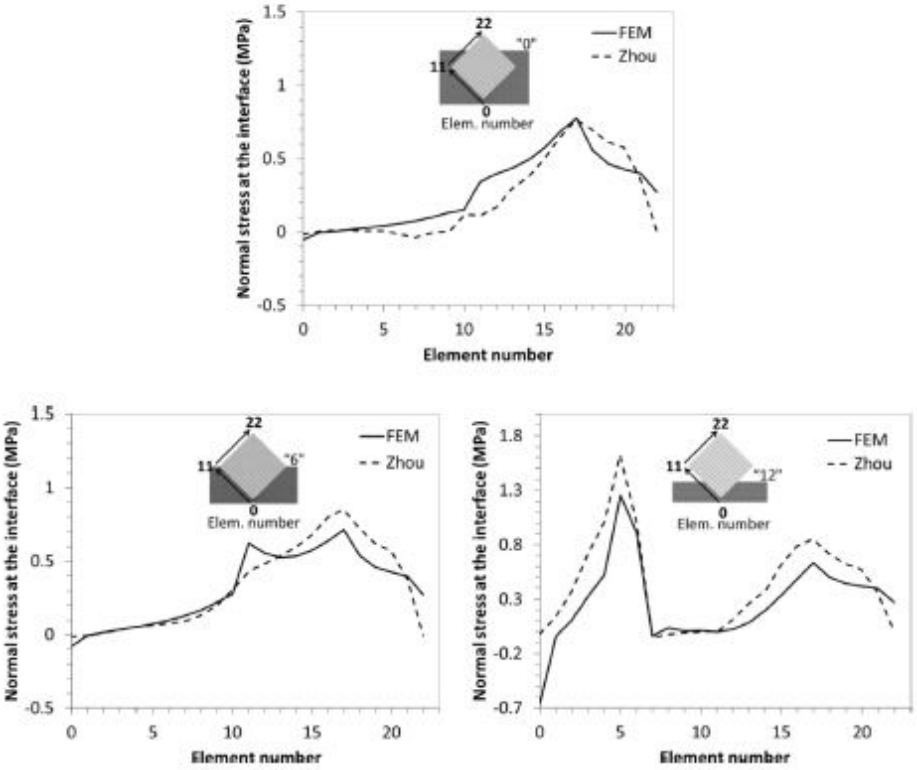

Fig. 5. Variation of normal stress along the interface as element centre stress in the diamond.

material. The comparison of the results obtained from these two models (one with elastic material model for the matrix and the other with elastic-plastic material model) has not shown any significant difference. Thus the elastic material model for representing the behaviour of matrix seems to be adequate for the present problem and it is followed in this paper.

A similar investigation was carried out by Suh et al. [18] who used 0.000231 N of the cutting force and 0.02 mm for the diameter of the square shaped diamond particle. The elastic modulus used [18] for the matrix and diamond are 7 GPa and 1171 GPa respectively. Moreover, they have presented their results in the form of von Mises stress instead of normal stress along the tension side of the diamond matrix interface. Using these geometric and material properties, the present finite element models are developed for two different levels of diamond wear which are defined as "1" and "9". Fig. 6a shows these two sample cases where a number (e.g., "1") indicates the number of elements from the unworn top corner to the worn horizontal plane of the diamond particle along one of its exposed edges. These numbering system is based on the meshing used in the present analysis (diamond has a mesh with division of 15 × 15). Since the value of the normal force has not been mentioned in the paper, it is assumed a value of 0.00231 N of normal force (ten times larger than the horizontal cutting force) is applied at the horizontal worn surface of the diamond. The variation of the von Mises stress over the entire diamond-matrix system predicted by the present model is shown in Fig. 6b for these two cases of diamond wear.

For both cases of diamond wear as mentioned above, the variation of von Mises stress along the diamond-matrix interface obtained in the present analysis is plotted in Fig. 7. In this case,

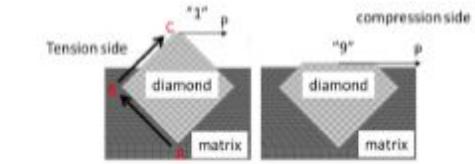

(a) Finite element meshing of the model geometry

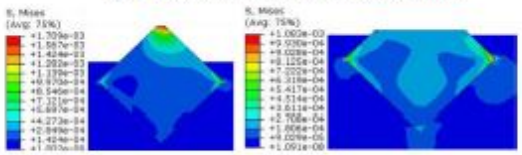

(b) Distribution of the Von-Mises stress over the entire body found in the present FE analysis

Fig. 6. Finite element analysis for different level of diamond wear.

the von Mises stress is calculated at the nodes along the interface of the tension side of the diamond where these nodes are taken from the bottom corner "A" of the diamond to the top corner "C" (Fig. 6(a)). With respect to the meshing used in the present analysis (mesh division of diamond: 15 × 15), "A" is defined as 0, "C" is defined as 30 (no wear) and the diamond left corner "B" is defined as "15". Fig. 7 shows that there are some discrepancies between the present results and those reported by Suh et al. [18]. One of the probable reasons behind the discrepancy between these results

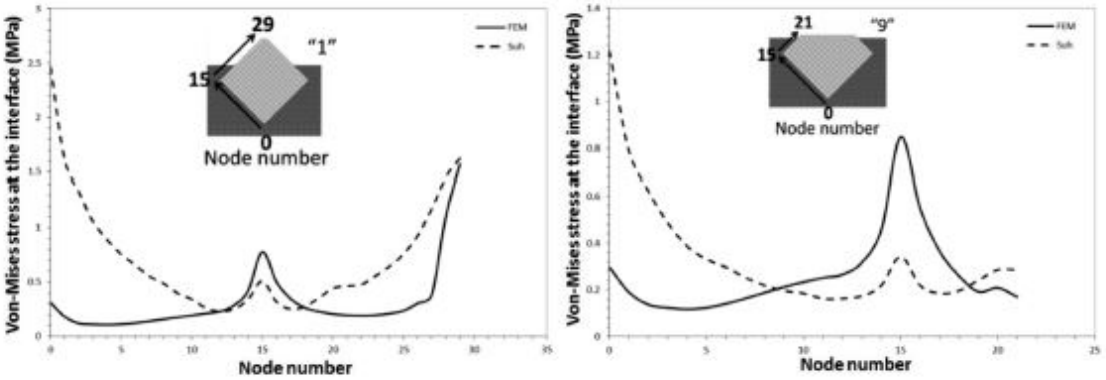

Fig. 7. Variation of Von-Mises stress along the interface node as a function of particle wear.

is the magnitude of the applied normal force which is not reported by Suh et al. [18] and a value of this force is guessed in the present analysis. Assuming a value of the friction coefficient in the range of 0.1, the value of the normal force is taken in the range of 10 times of the cutting force. Moreover, Suh et al. [18] obtained a higher stress near the root (Point A, Fig. 6a) compared to that at the left corner (Point B, Fig. 6a) which is not expected physically. The left corner of the diamond particle is most vulnerable and it should capture more stresses compared to other parts which are experience consistently in all cases of the present study.

3.2. Validation of the interfacial damage model with a double cantilever beam

As there is no data available for the validation of diamond-matrix interfacial damage as mentioned earlier, the problem of a double cantilever beam (DCB) as shown in Fig. 8 is used in this section for an indirect validation of the interfacial damage model. This problem (DCB) is commonly used in laminated composite structures and some other areas for the same purpose. The experimental test data reported by Morais et al. [24] for a DCB made of T300/977-2 carbon fibre reinforced epoxy laminate is used for the present analysis. The laminate (3.96 mm) consists of 24 identical layers having 0° orientation and the following material properties: E_1 = 150.0 GPa, E_2 = 11.0 GPa, G_{12} = 6.0 GPa, ν_{12} = 0.25. Similar to the diamond-matrix system, a two dimensioned finite element model is developed for the DCB (Fig. 8) with the damage model based on cohesive zone modelling technique at the interface (BC) between the two cantilever beams. The load-displacement (P-δ) curve obtained in the present analysis is plotted in Fig. 9 along with that reported by Morais et al. [22] which shows that the numerical result has a reasonable correlation with the experimental results.

In order to validate the crack propagation under mixed–mode loading condition of the developed model, the experimental test data reported by Crews et al. [36] for a mixed-mode bending (MMB) test apparatuses (Fig. 10) made of AS4/PEEK carbon-fibre reinforced composite is used for the present analysis. Table 1

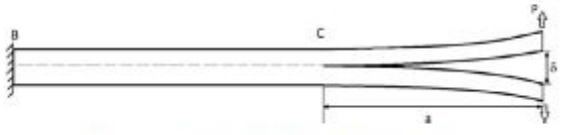

Fig. 8. Schematic draw of double-cantilever beam test.

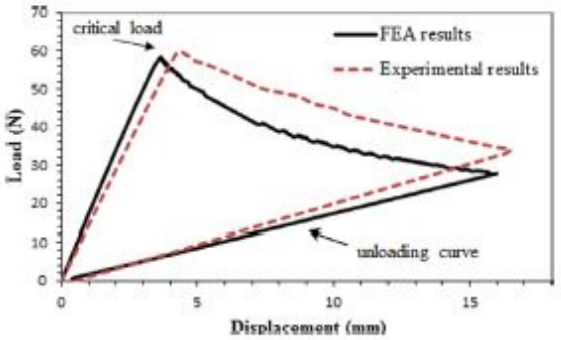

Fig. 9. load-deflection curve of the double cantilever beam with delamination.

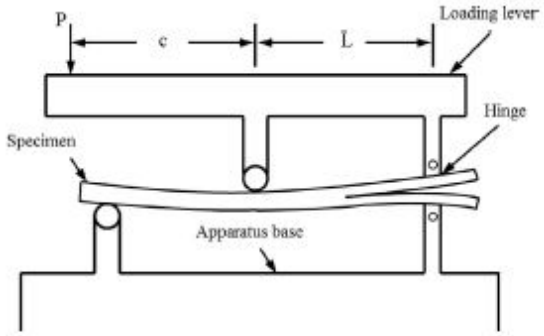

Fig. 10. Illustration of mixed-mode bending test.

shows the dimension and material properties of the MMB specimens (Fig. 10).

In this study, five different G_{II}/G_T ratios have been simulated and compared with the experimental results, which are shown in Table 2. It can be seen that a good agreement between the numerical predictions and the experimental results is obtained.

4. Parametric study

With initial confidence gained from the validation of the proposed modelling technique carried out in the previous section, the method is applied for the interfacial failure modelling of diamond-matrix system in this section. As there is no published

Table 1
Dimension and properties for MMB test specimen.

Specimen Dimension				
L (Length)		W (Width)	T (Thickness of one arm)	
102 mm		25.4 mm	1.56 mm	
Mechanical Material Properties				
E_{11}	$E_{22} = E_{33}$	$G_{12} = G_{13}$	G_{23}	$\nu_{12} = \nu_{13}$
122.7 GPa	10.1 GPa	5.5 GPa	3.7 GPa	0.25
ν_{23}	G_{IC}	G_{IIC}	T	S
0.45	0.969 kJ/m^2	1.719 kJ/m^2	80 MPa	100 MPa

Table 2
Numerical and experimental comparison of maximum loads of MMB test.

G_{II}/G_T	P_{max} (numerical, N)	P_{max} (experimental, N)	Error (%)
0% (DCB)	165.83	147.11	12.7
20%	106.75	108.09	1.2
50%	298.64	275.35	8.4
80%	483.06	518.66	6.9
100% (ENF)	845.75	733.96	15.2

result available for this problem, a large number of cases are investigated in the form of parametric study. The specific parameters used in this study include diamond shapes, diamond orientations, diamond protrusion levels and interface material properties. In order to have an understanding of the effect of an individual parameter, the value of that parameter is varied while the values of other parameters are kept unchanged.

4.1. Effect of diamond shapes

The previous studies [37,38] have observed experimentally that the shape of diamond grits has a significant effect on their retention capacity or pull out rate. Thus the diamond shape is an important parameter which is investigated in this section. As mentioned earlier, the diamond bits use synthetic diamond particles which are produced by the chemical vapor deposition (CVD) technique [39]. This mechanized process (CVD) helps to produce regular shaped diamonds that can be conveniently represented as polygons as shown in Fig. 11. In this study, seven regular polygonal shapes having different number of sides ranging from 4 to 18 are used to show their effects on diamond retention capacity. The finite element meshing used for modelling all these diamond-matrix system is also shown in Fig. 11a. A size of r = 0.25 mm (radius of the circle circumscribing the polygons) is taken for all these polygonal shapes. The portion of these diamonds above the exposed surface of the matrix is defined as protrusion height which is taken as 0.25 mm for all these cases (i.e., the centre of the particles lies along the exposed surface of the matrix). The material properties used are same as those provided in Section 2. The force is applied to these systems by imposing a gradual horizontal displacement at the tip (top corner) of the diamond towards right side. The distribution of equivalent von Mises stress over the entire system obtained at the onset of interface failure is presented in Fig. 11b. The figure shows the occurrence of stress concentration near the tip point (loading point) and the upper most point of the diamond-matrix interface on the compression side (right side) in all cases. The stress concentration at this interfacial point is observed as the diamond is still having contact with the matrix at this point. As the interface has completely de-bonded at this

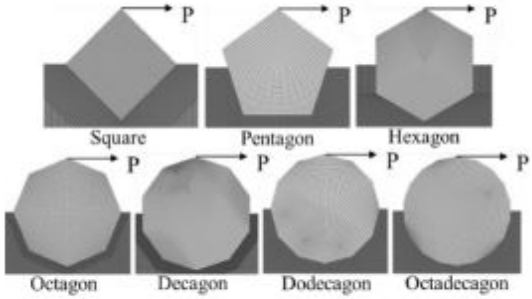

(a) Finite element meshing of the model geometry for different diamond shapes same circumcircle radius.

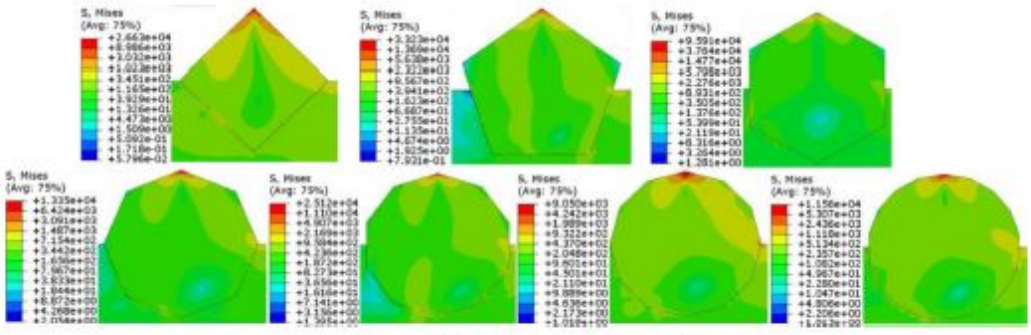

(b) Von-Mises stress distributions of different diamond shapes

Fig. 11. Models for different diamond particle shapes with same radius and protrusion height.

stage, the chemical bond between the diamond and matrix is lost which should lead to the fall out of diamonds. However, it is observed that stress concentrations are still present around one corner of the left (or tension) side of the interfaces for hexagon, decagon and octadecagon shaped diamonds. This ensures a contact between the matrix and diamonds at these corners, which prove additional restrain in the form of mechanical interlocking to have better retention ability. Thus the diamond particles having hexagon, decagon and octadecagon shapes are supposed to have relatively higher retention capacity.

The forces produced at the diamond tip points due to the displacement imposed at these points are captured. The force-displacement variation for two representative cases (square and hexagon shaped particles) is plotted in Fig. 12. It shows that the force is increased up to its peak value linearly and dropped down sharply for both cases where this pick force may be defined as the critical load of the initiation of interfacial de-bonding. The interfacial cracks are observed after reaching this critical load which cased this sudden reduction of the cutting force. For the square particle, the force is dropped to zero steadily after reaching its critical value of 61 N, which indicates that the particle has completely lost its retention capacity. In contrast, a relatively higher value of the peak force (86.5 N) is produced for the hexagonal particle which is due to its additional mechanical interlocking with the matrix. Moreover, the force started increasing again after reaching a value of 14.6 N and this is also due to the mechanical interlocking which didn't allow the particle to move out from the matrix freely. This is similarly observed in the case of decagon and octadecagon shaped particles. The orientation of the interface near the exposed surface of the matrix on the left (tension) side plays an important role on this addition mechanical interlocking found in the abovementioned cases. The critical load of interface failure is an important parameter to a designer as it indicates the retention capacity provided by the interface which is the primary focus of the present study.

The critical values of the cutting force corresponding to the initiation of the interface failure for each of the case studies are plotted in Fig. 13. The results have an anticipated trend where the hexagon, decagon and octadecagon particles have relatively higher retention ability due to the additional mechanical bonding as explained above. Among the different shapes studied here, the hexagon particle is found to have the highest retention capacity (86.5 N). For the particles, predominantly hold by the interfacial adhesion bonding with minimum mechanical interlocking, the critical force is found to increase with the increase of number of sides. For such cases, the square particle has the lowest value of critical force (61.2 N) whereas the dodecagon shaped particle has the highest value (85 N). It seems the orientation of the particles will play an important role on the mechanical interlocking which will influence the diamond retention capacity.

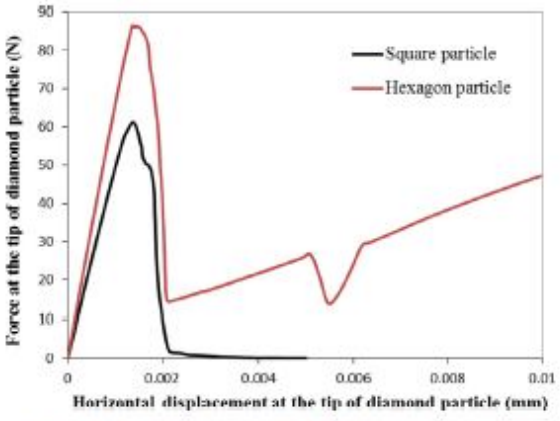

Fig. 12. Force-displacement variation at the tip of diamond particles.

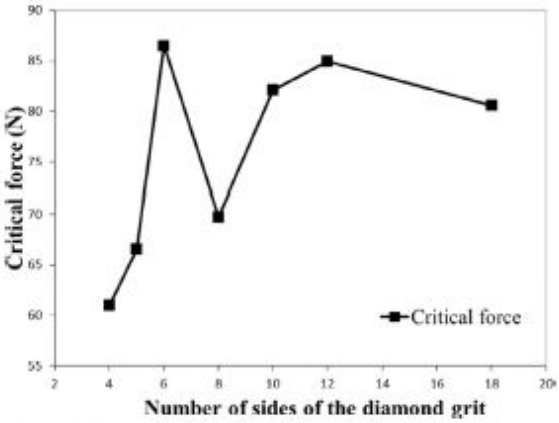

Fig. 13. Effect of diamond shape on its retention capacity with the same circumcircle radius.

In order to show the variation of crack opening at the critical point with respect to the cutting force, one of the cases considered in the above study (Fig. 11) is taken as the sample example, which is shown in Fig. 14a. It is observed that the left corner (point B, Fig. 14a) is the critical point having a maximum crack opening. This result is plotted in Fig. 14b, which shows that the cutting force reached its maximum value (61 N) when the crack opening at the critical point became 0.00026 mm.

Although it is more realistic to apply distributed load on the cutting edge of the diamond particle to simulate the real drilling

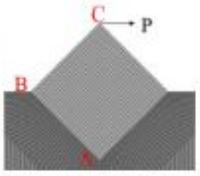

(a) Square shaped diamond particle

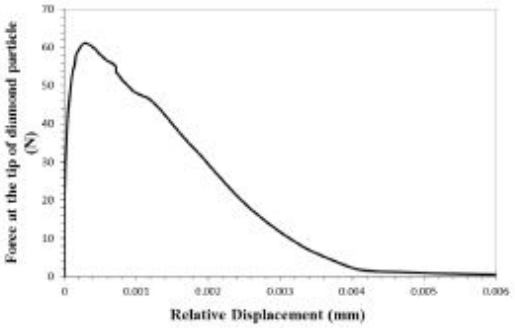

(b) Relative displacement jump verses load.

Fig. 14. Results of displacement jump with respect to the cutting force for square shaped diamond particle at point B.

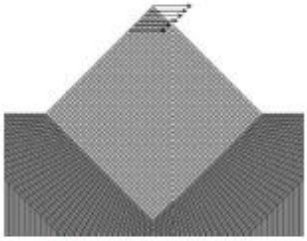

Fig. 15. Distributed load applied on the diamond of the model.

process, it is observed in the present study that the load distribution has no effect on the retention capacity of the diamond particle when compared with the point load. In order to demonstrate this, one of the cases of the problem considered in Fig. 11 (square shaped diamond particle) is taken as a sample case which is reanalysed with a distributed loading as shown in Fig. 15 where other parameters (used in Section 4.1) are kept unchanged. The maximum force to cause the diamond de-bonding failure is about 62 N for the case of distributed load whereas this is 61 N for the case of point load. Therefore, a concentrated load is applied for the purpose of simplicity. This cutting force is induced by imposed a horizontal displacement in order to mimic the actual drilling scenario.

The problem studied above (Fig. 13) with a constant circumcircle radius of diamond particles (Fig. 11) is reinvestigated with a constant volume fraction taking same area (0.125 mm^2) for all diamond particle shapes (Fig. 11). In this situation, the circumcircle radius of regular polygons is decreased with the increase of the number of their sides. Keeping other parameters unchanged, the problem is reanalysed and the critical values of the cutting force corresponding to the initiation of the interface failure obtained for the different shapes are plotted in Fig. 16. It shows that the values of this critical load found in the present scenario (Fig. 16) are reduced for all diamond shapes except the first case (square shape) compared to those obtained earlier (Fig. 13). Similar to the previous scenario, the hexagon shaped diamond particle has the highest retention capacity in the present situation (constant volume fraction) and it is 80.8 N now. However, the octagon shaped particle has the lowest retention capacity in the present scenario and it is 49 N.

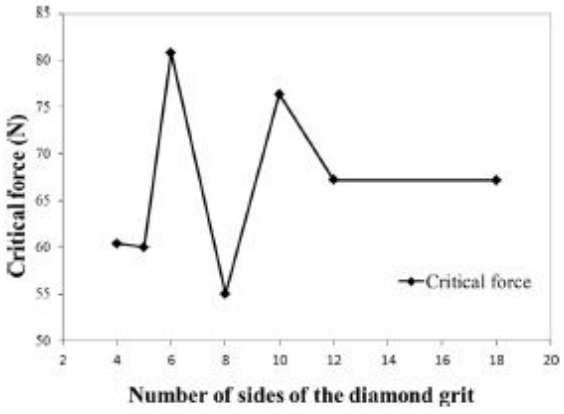

Fig. 16. Effect of diamond shape on its retention capacity with the same volume fraction.

4.2. Effect of diamond orientations

The effect of orientation of the diamond particles on their retention capacity is studied in this section for all seven particle shapes shown in Fig. 11a. The diamond particle size and material properties are same as those used in the previous section. For all these particle shapes, four different orientations are studied which are obtained by rotating the particles about their centres which are held at their initial position. In order to get the four orientations, the particles are rotated with an equal increment which is one fourth of the angle between the radial lines passing through two adjacent corners as shown in Fig. 17a. It should be noted that this angle is different for the different shapes (e.g., 90°/4 = 22.5° for the square particle whereas 60°/4 = 15° for the hexagonal particle) and its value decreases with the increase of the number of sides of the particles. Fig. 17a also shows the position of all these cases where the force or rather the horizontal displacement is imposed gradually. The finite element meshing of the diamond-matrix system for a sample particle shape (square) is shown in Fig. 17b for its four different orientations. Similarly, the results are shown as equivalent von-Mises stress in Fig. 17c which are obtained at the instant of interface failure (at the onset of the peak value of the cutting force).

The critical forces corresponding to the interface failure of all these cases obtained from the present analysis are reported in Table 3. The table shows that the retention capacity of diamonds is greatly affected by the orientation of diamond grits. For the different particle shapes, the variation of retention capacities of these grits due to their orientations is shown in terms of its highest and lowest values in Fig. 18. It can be seen from this figure that the square and decagon shaped particles achieved their highest retention capacities when they are having an orientation of 45° and 18° respectively which correspond to a situation of wear flat when a flat edge is utilized for cutting. The orientation has the highest influence for the square shaped diamond whereas this is lowest for the dodecagon shaped particle. However, the enhancement of diamond retention capacity with a wear flat situation is not desirable as the efficiency of the entire drilling process is also dependent on the sharpness of the cutting surface. Thus the four orientations are divided into two categories entitled as sharp and blunt where the blunt category (last column) corresponds to wear flat scenario which is not acceptable even it gives a higher diamond retention capacity. It is interesting to note that the hexagon shaped diamond particle has a relatively higher retention capacity when it has an orientation of 0° (sharp cutting surface) and a lower retention capacity for an orientation that makes the cutting surface blunt.

4.3. Effect of diamond protrusion (particle wear and matrix wear)

The wear of diamond bits is a complex process and it depends on a number of parameters associated with different operating conditions encountered while cutting different types of rocks. The material properties of diamond and matrix used in this section are same as those provided in Section 2. The metal matrix is likely to wear faster while cutting soft rocks consists of coarser loosely cemented particles. In contrast, it would wear slower while cutting hard rocks consist of finer particles. As a result of these, different protrusion levels of diamond grits (heights of the exposed part of the particles) can be obtained during the cutting operation. Since the protrusion of diamond grits depends on the diamond wear as well as the matrix wear, the effect of both these wear mechanisms is studied. In order to assess the contribution of the individual mechanisms, they are incorporated in the present numerical model separately as shown in Fig. 19. A regular quadrilateral shaped diamond particle with a symmetric orientation and symmetric matrix/diamond wear is taken to avoid the influence of other parameters on the effect of diamond protrusions.

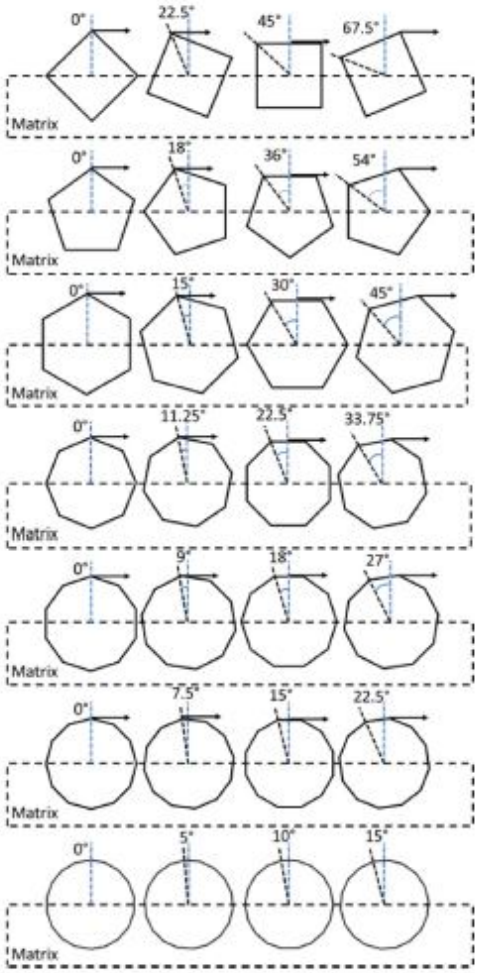

(a) Orientations of the diamond particles having different shapes

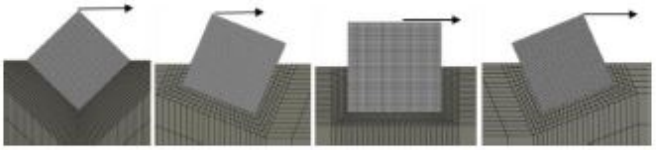

(b) Finite element meshing of the square shaped particle for different orientations

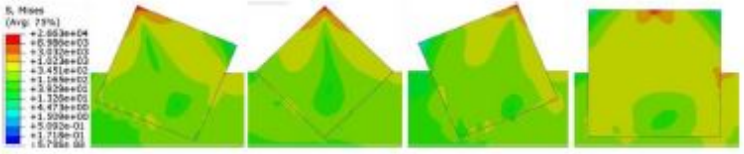

(c) Von-Mises stress distribution of the system having the square particle

Fig. 17. Diamond particles with different orientations.

In the present study, thirteen different cases of protrusion levels are considered where seven cases are due to the diamond wear (from 0.0197 mm to 0.25 mm of protrusion height) and six cases are due to matrix wear (from 0.0625 mm to 0.375 mm of protrusion height). The critical forces corresponding to the initiation of interface debonding for all these cases predicted by present numer-

Table 3
Critical forces for the onset of interfacial failure.

Cutting surface	Sharp			Blunt
Orientation (Square)	0°	22.5°	67.5°	45°
Interfacial Failure Force (N)	61.2	60.1	44.9	100
Orientation (Pentagon)	0°	18°	54°	36°
Interfacial Failure Force (N)	66.5	42	70.1	67.8
Orientation (Hexagon)	0°	15°	45°	30°
Interfacial Failure Force (N)	86.5	48.1	66.7	72.9
Orientation (Octagon)	0°	11.25°	33.75°	22.5°
Interfacial Failure Force (N)	68.4	63.6	60.5	89.8
Orientation (Decagon)	0°	9°	27°	18°
Interfacial Failure Force (N)	88.3	81.9	64.6	100.8
Orientation (Dodecagon)	0°	7.5°	22.5°	15°
Interfacial Failure Force (N)	82.3	79.1	81.6	84.4
Orientation (Octadecagon)	0°	5°	15°	10°
Interfacial Failure Force (N)	80.6	56.2	60.7	62.3

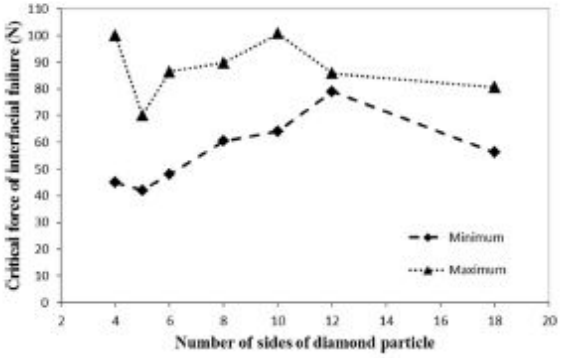

Fig. 18. Effect of orientations and shapes of diamonds on their retention capacity.

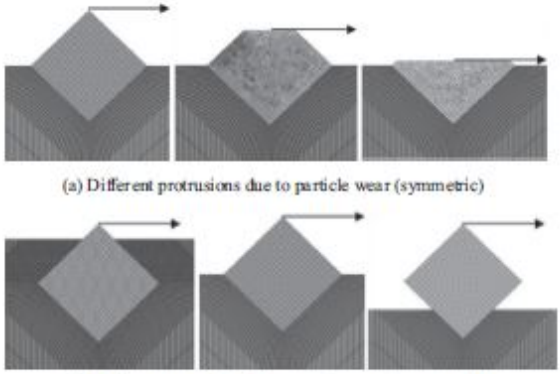

(a) Different protrusions due to particle wear (symmetric)

(b) Different protrusions due to matrix wear (symmetric)

Fig. 19. Interface failure influenced by (a) diamond wear and (b) matrix wear.

ical model are shown in Fig. 20. The results indicate that the critical force decreases with the increase of protrusion height in all cases as expected. In most of these cases, the critical force is same as the ultimate force required for the complete pull out of the diamond grit except the cases of lower level of matrix wear (up to 0.25 mm) where the load carrying capacity of the particle increases steady after the initiation of interface deboning. This is due to a strong mechanical interlocking provided the matrix which holds the particle in its position and does not allow a complete pull out of the particle. Moreover, Fig. 20 shows that the critical force

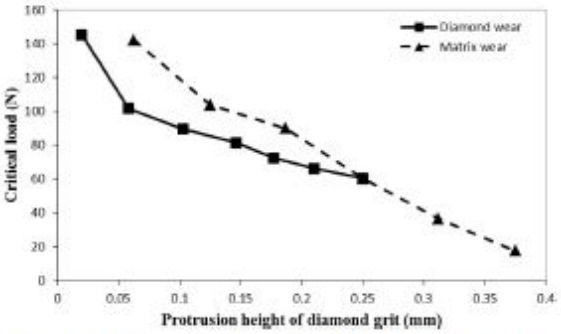

Fig. 20. Effect of diamond/matrix wear on critical load for interface failure.

for the matrix wear is relatively higher than that of diamond wear when protrusion level is up to 0.25 mm and same for both types of wear. The numerical results are reasonably intuitive which indicates that if the matrix wear rate is too high compare with the diamond wear rate, the diamond will have premature fall out before utilising the full capacity of the diamond which will significantly affect the efficiency of the diamond bit.

4.4. Multiple diamond particles and their interactions

In order to study the interaction of neighbouring particles, a typical example of a diamond bit consists of five diamond particles having identical shapes and protrusions as shown in Fig. 21 is considered in this section. The material properties of the matrix as well as diamonds, and their sizes and loading are same as those used in Section 4.3. The diamonds are having equal spacing (S) which is varied from 1 mm to 8 mm to show the effect of this spacing on the retention capacity of these diamond particles. The critical loads corresponding to the interface failure of these diamond particles (Fig. 21) obtained for four different values of their spacing (S) are presented in Table 4. The results clearly show that the interaction between the particles is reduced once the spacing between the particles is increased.

4.5. Effect of interface properties

The interface properties can be affected by several reasons associated with the sintering process and type of metal matrix. As discussed earlier, the cohesive zone model is used for simulating the interface failure and the cohesive model is characterized by four parameters. In order to investigate the effect of these interface parameters, four different cases having different values of these parameters (Table 5) are considered in the present study. For this purpose four different shapes of the diamond particle are used which are square, pentagon, hexagon and decagon (Fig. 11a).

The variation of critical force corresponding to the initiation of interface failure with respect to the number of sides of the diamond particles is plotted in Fig. 22 for the four different combinations of the interfacial properties (Table 5). It can be seen from the figure that the value of critical force decreases steadily with the decrease of interfacial strength as well as the fracture toughness values. However, the contribution of the Mode I properties is more than that of the Mode II properties. This difference is specifically quite big for square and pentagonal shape of the diamond grit. The figure shows that the highest critical force is found for all the particle shapes when the value of all interface properties is higher (Case 1, Table 5) whereas the lowest critical force is found when the value of all interface properties is lower (Case 4, Table 5).

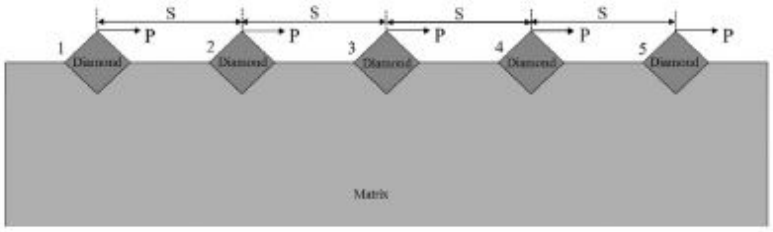

Fig. 21. Multiple diamond particles with equal spacing (S).

Table 4
Variation of critical load with respect to spacing between diamonds.

	Critical Load P (N)				
	Diamond 1	Diamond 2	Diamond 3	Diamond 4	Diamond 5
Case 1 (S = 1 mm)	42.8	65.1	63.7	62.2	75.9
Case 2 (S = 2 mm)	50.4	49.3	60.5	66.1	66.2
Case 3 (S = 4 mm)	62.3	62.2	61	63.1	66
Case 4 (S = 8 mm)	59.5	60.2	60.8	61.4	61.2

Table 5
Four study cases of different interfacial parameters.

	Mode I		Mode II	
	Ultimate stress	Fracture stress	Ultimate stress	Fracture stress
	(τ_n^0) (MPa)	(G_{IC}) (mJ/mm^2)	(τ_n^0) (MPa)	(G_{IIC}) (mJ/mm^2)
Case 1	543	0.14	314	0.33
Case 2	271.5	0.07	314	0.33
Case 3	543	0.14	157	0.165
Case 4	271.5	0.07	157	0.165

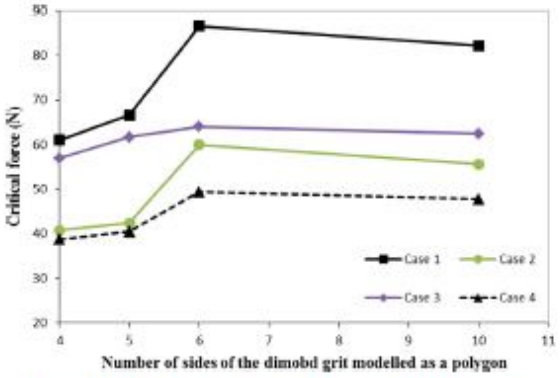

Fig. 22. Effect of interface properties on the critical load for interface failure.

Thus, the interface properties are dominant parameters for the retention ability of diamond particles.

5. Conclusions

In this paper, a failure analysis of diamond impregnated bits found in the form of particle composite materials is attempted for the first time. The present study has a focus on the interfacial failure mechanism between the matrix and diamond particles. This provides the vital understanding of diamond pull out mechanism which is one of the significant failure modes of diamond bits. For this purpose, a single diamond particle along with a portion of the surrounding matrix is used as a representative part of diamond bits. The diamond is subjected to a tangential force at its tip which simulates the cutting force whereas the matrix is restrained at its far ends. The finite element modelling is used to simulate the diamond matrix system where 4 node plane strain quadrilateral elements are used for the diamond and matrix materials. A zero thickness surface based cohesive zone modelling technique is used to simulate the failure at the interface between the matrix and the diamond.

In order to validate the finite element model and investigate its performance, numerical examples are solved and the results produced by the finite element model are compared with the results available in literature. The performance of the model is found to be good in majority of these test problems which include interfacial stress analysis of diamond impregnated bits, and de-bonding simulations of a double cantilever beam and mixed-mode bending tests. Based on the confidence gained from the observation, the present model is used to conduct a parametric study for the critical force prediction of the interface failure initiation of diamond impregnated bits.

It has been observed that the shapes, orientations and protrusions of diamond particles, and interfacial properties have significant influence on the retention capacity of diamond particles. As the efficiency of the entire drilling process is also dependent on the sharpness of the cutting surface, the hexagon shaped diamond particle is found to have a better performance for drilling because it has a relatively higher retention capacity when it is under sharp cutting face. The results also indicate that the critical force decreases with the increase of protrusion height in all cases. It is also observed that the interface properties are the dominant parameters for the retention ability of diamond particles as the value of critical force decreases steadily with the decrease of interfacial strength as well as the fracture toughness values, and the contribution of the Mode I properties is more than that of the Mode II properties.

Acknowledgements

The work has been supported by the Deep Exploration Technologies Cooperative Research Centre whose activities are funded by the Australian Government's Cooperative Research Centre Programme. This is DET CRC Document 2016/890.

References

[1] Busch DM, Hill BS. Concrete drilling with diamond impregnated bits: De Beers Industrial Diamond Division; 1975.
[2] Paone J, Madson D. Drillability studies: impregnated diamond bits: Department of the Interior, Bureau of Mines; 1966.
[3] Hsieh Y-Z, Lin S-T. Diamond tool bits with iron alloys as the binding matrices. Mater Chem Phys 2001;72:121–5.
[4] Lin C-S, Yang Y-L, Lin S-T. Performances of metal-bond diamond tools in grinding alumina. J Mater Process Technol 2008;201:612–7.
[5] Tze-Pin L, Hood M, Cooper GA, Xiaohong L. Wear and failure mechanisms of polycrystalline diamond compact bits. Wear 1992;156:133–50.
[6] Xuefeng T, Shifeng T. The wear mechanisms of impregnated diamond bits. Wear 1994;177:81–91.
[7] Konstanty J. Chapter 3 – diamond tool design and composition. In: Konstanty J, editor. Powder metallurgy diamond tools. Amsterdam: Elsevier Science; 2005. p. 39–68.
[8] Huang JS, Gibson LJ. Elastic moduli of a composite of hollow spheres in a matrix. J Mech Phys Solids 1993;41:55–75.
[9] Tagliavia G, Porfiri M, Gupta N. Analysis of hollow inclusion–matrix debonding in particulate composites. Int J Solids Struct 2010;47:2164–77.
[10] Shams A, Porfiri M. Analysis of particle–matrix interfacial debonding using the proper generalized decomposition. Compos Struct 2014;111:602–18.
[11] Chalkley JR, Thomas DM. The tribological aspects of metal bonded diamond grinding wheels. Powder Metall 1969;12(24):582–97.
[12] Konstanty J. Developing a better understanding of the bonding and wear mechanisms involved in using diamond impregnated tools. In: Proceedings of international workshop on diamond tool production, Turin, Italy; 1999, pp. 97–106.
[13] Scott PM, Nicholas M, Dewar B. The wetting and bonding of diamonds by copper-base binary alloys. J Mater Sci 1975;10:1833–40.
[14] Levin E, Gutmanas EY. Solid-state bonding of diamond to Nichrome and Co-20wt% W alloys. J Mater Sci lett 1990;9:726–30.
[15] Miller D, Ball A. Rock drilling with impregnated diamond microbits—an experimental study. Int J Rock Mech Min Sci Geomech Abstr 1990;27:363–71.
[16] Miller D, Ball A. The wear of diamonds in impregnated diamond bit drilling. Wear 1991;141:311–20.
[17] Zhou Y, Funkenbusch PD, Quesnel DJ. Stress distributions at the abrasive-matrix interface during tool wear in bound abrasive grinding—a finite element analysis. Wear 1997;209:247–54.
[18] Suh C-M, Bae K-S, Suh M-S. Wear behavior of diamond wheel for grinding optical connector ferrule – FEA and wear test –. J Mech Sci Technol 2008;22:2009–15.
[19] Li R, Amaral PM, Reis L, Anjinho CA, Rosa LG, Freitas Md. 3D-modelling of the local plastic deformation and residual stresses of PM diamond–metal matrix composites. Comput Mater Sci 2010;47:1023–30.
[20] Turon A, Dávila CG, Camanho PP, Costa J. An engineering solution for mesh size effects in the simulation of delamination using cohesive zone models. Eng Fract Mech 2007;74:1665–82.
[21] Rinderknecht S, Kröplin B. A computational method for the analysis of delamination growth in composite plates. Comput Struct 1997;64:359–74.
[22] Grassi M, Zhang X. Finite element analyses of mode I interlaminar delamination in z-fibre reinforced composite laminates. Compos Sci Technol 2003;63:1815–32.
[23] Alfano FF M, Leonardi A, Maletta C, Paulino GH. Cohesive zone modeling of model fracture in adhesive bonded joints. Key Eng Mater 2007;348–349:13–6.
[24] de Morais AB, de Moura MF, Marques AT, de Castro PT. Mode-I interlaminar fracture of carbon/epoxy cross-ply composites. Compos Sci Technol 2002;62:679–86.
[25] Barenblatt GI. Advances in applied mechanics. New York: Academic Press; 1962. p. 55.
[26] Andrew W. Cemented Tungsten Carbides: Production, Properties and Testing; 1998. Norwich, NY, USA. 1998.
[27] Jaensson BO, Sundström BO. Determination of Young's modulus and poisson's ratio for WC-Co alloys by the finite element method. Mater Sci Eng 1972;9:217–22.
[28] Elices M, Guinea GV, Gómez J, Planas J. The cohesive zone model: advantages, limitations and challenges. Eng Fract Mech 2002;69:137–63.
[29] Cui W, Wisnom MR. A combined stress-based and fracture-mechanics-based model for predicting delamination in composites. Composites 1993;24:467–74.
[30] Camanho PP, Dávila CG, De Moura MF. Numerical simulation of mixed-mode progressive delamination in composite materials. J Compos Mater 2003;37:1415–38.
[31] Gonçalves JPM, Moura MPSFd, Castro PMSTd, Marques AT. Interface element including point-to-surface constraints for three-dimensional problems with damage propagation. Eng Comput 2000;17:28–47.
[32] de Borst R, Rots JG. Occurence of spurious mechanisms in computation of strain-softening solids. Eng Comput 1989;6:272–80.
[33] Zhai J, Zhou M. Finite element analysis of micromechanical failure modes in a heterogeneous ceramic material system. Int J Fract 2000;101:161–80.
[34] Cavalli MN. Cohesive zone modelling of structural joint failure [PhD Thesis], University of Michigan; 2003.
[35] Liao YS, Luo SY. Wear characteristics of sintered diamond composite during circular sawing. Wear 1992;157:325–37.
[36] Crews JJH, Reeder James R. A mixed-mode bending apparatus for delamination testing. NASA Langley Technical Report Server; 1998.
[37] Konstanty J. Powder metallurgy diamond tools. Elsevier Science & Technology Books; 2005.
[38] Romanski A. Factors affecting diamond retention in powder metallurgy diamond tools. Arch Metall Mater 2010;55:1073–81.
[39] Chou YK, Liu J. CVD diamond tool performance in metal matrix composite machining. Surf Coat Technol 2005;200:1872–8.